AFOSR-TR- 88-0990

(2)

BLAST INDUCED LIQUEFACTION OF SOILS LABORATORY AND FIELD TESTS

Research Grant AFOSR-85-0172

Wayne A. Charlie, Ph.D., P.E.
Principal Investigator

Geotechnical Engineering Program
Civil Engineering Department

Colorado State University

(2)

FINAL REPORT

BLAST INDUCED LIQUEFACTION OF SOILS LABORATORY AND FIELD TESTS

Research Grant AFOSR-85-0172

Wayne A. Charlie, Ph.D., P.E.
Principal Investigator

Prepared by

Colorado State University
Department of Civil Engineering
Geotechnical Engineering Program
Fort Collins, Colorado 80523

REPORT AUTHORS
W.A. Charlie, D.O. Doehring, G.E. Veyera, and H.A. Hassen

RESEARCH TEAM
A.A. Awad, J.M. Bolton, T.E. Bretz, L.W. Butler, M.A. Chouicha, W.A. Charlie, D.S. Durnford, H.A. Hassen, M.E. Hubert, P.J. Jacobs, W.A. Lewis, L.A. Schure, C.A. Smoot, F. Rwebyogo, E.B. Thompson and G.E. Veyera

Prepared for

Air Force Office of Scientific Research
Bolling Air Force Base, Washington, D.C.
AFOSR Program Managers
Major Steven C. Boyce, Ph.D., P.E.
Spencer T. Wu, Ph.D., P.E.
Col. Lawrence D. Hokanson, ScD, P.E.

July, 1988

page left blank

REPORT DOCUMENTATION PAGE

Form Approved OMB No. 0704-0188

1a. REPORT SECURITY CLASSIFICATION: UNCLASSIFIED	1b. RESTRICTIVE MARKINGS
2a. SECURITY CLASSIFICATION AUTHORITY	3. DISTRIBUTION/AVAILABILITY OF REPORT: Approved for Public Release; Distribution Unlimited
2b. DECLASSIFICATION/DOWNGRADING SCHEDULE	
4. PERFORMING ORGANIZATION REPORT NUMBER(S)	5. MONITORING ORGANIZATION REPORT NUMBER(S): AFOSR-TR- 88-0990
6a. NAME OF PERFORMING ORGANIZATION: Dept. of Civil Engineering, Colorado State University	6b. OFFICE SYMBOL (If applicable):
6c. ADDRESS (City, State, and ZIP Code): Fort Collins, Colorado 80523	7a. NAME OF MONITORING ORGANIZATION: AFOSR/NA
	7b. ADDRESS (City, State, and ZIP Code): Bldg. 410, Bolling AFB, DC 20332-6448
8a. NAME OF FUNDING/SPONSORING ORGANIZATION: AFOSR	8b. OFFICE SYMBOL (If applicable): NA
8c. ADDRESS (City, State, and ZIP Code): Bldg. 410, Bolling AFB, DC 20332-6448	9. PROCUREMENT INSTRUMENT IDENTIFICATION NUMBER: Grant No. AFOSR-85-0172
	10. SOURCE OF FUNDING NUMBERS: PROGRAM ELEMENT NO. 6.1102F; PROJECT NO. 2302; TASK NO. C1; WORK UNIT ACCESSION NO.

11. TITLE (Include Security Classification) (U)
Blast Induced Liquefaction of Soils: Laboratory and Field Tests

12. PERSONAL AUTHOR(S)
W.A. Charlie, D.O. Doehring, G.E. Veyera and H.A. Hassen

13a. TYPE OF REPORT	13b. TIME COVERED	14. DATE OF REPORT (Year, Month, Day)	15. PAGE COUNT
FINAL	FROM 1985 TO 1988	1988, July, 25	184

16. SUPPLEMENTARY NOTATION

17. COSATI CODES		
FIELD	GROUP	SUB-GROUP

18. SUBJECT TERMS (Continue on reverse if necessary and identify by block number)
Liquefaction, Porewater Pressure, Dynamic Testing, Blast Loading, Soil Mechanics, Laboratory Testing, Field Testing, Material Modeling, Explosive Loading, Saturated Sand. (JES)

19. ABSTRACT

Our field, laboratory and theoretical research indicate that the destruction potential of an explosion may be greatly magnified if detonated in water saturated granular soils. While blast-induced liquefaction may not necessarily damage a facility structurally, it may render it unusable. Empirical models are given that can be used to estimate liquefaction potential as a function of density, effective stress and applied compressive strain. One of the models uses an empirical scaling law for explosive loadings to predict the extent of porewater pressure increases in the field from buried, contained charges in saturated soils. A numerical analysis that considers the saturated soil as a two-phase medium is presented. The analysis accounts for the nonlinear, inelastic behavior of the soil skeleton and has shown that liquefaction is dependent upon the constrained modulus of the soil skeleton. Results agree with the experimental observations. (cont.)

20. DISTRIBUTION/AVAILABILITY OF ABSTRACT	21. ABSTRACT SECURITY CLASSIFICATION
☒ UNCLASSIFIED/UNLIMITED ☐ SAME AS RPT ☐ DTIC USERS	UNCLASSIFIED
22a. NAME OF RESPONSIBLE INDIVIDUAL: Major Steven C. Boyce	22b. TELEPHONE (Include Area Code): (202) 767-6963 / 22c. OFFICE SYMBOL: AFOSR/NA

DD Form 1473, JUN 86 — Previous editions are obsolete.

19. (Abstract Continued)

The results of our study indicate the following.

1. Liquefaction can be induced by single and multiple blasts.

2. Liquefaction can be induced at distances much greater than those associated with structural damage.

3. Long term increases in residual porewater pressures can be induced by compressive shock wave loadings when the peak particle velocity exceeds 0.075 m/s.

4. Liquefaction can be induced in loose saturated sand by a single compressive shock wave when the peak particle velocity exceeds 0.75 m/s.

5. Soils at higher initial effective stress and higher initial relative density require more energy to produce liquefaction.

6. Destruction potential of an explosive charge may be greatly magnified if detonated in water-saturated soils.

7. Liquefaction occurs because of compressive strain induced by the compression stress wave, but liquefaction occurs after the stress wave passes.

The possibility exists that an explosive detonated in a soil having a high liquefaction potential could cause damage disproportionate to the energy released. Documented occurrence of blast-induced liquefaction is available in the open literature. Although considerable work remains to be done in projecting this information into a comprehensive method of predicting liquefaction for actual or hypothetical blasts, the data indicate that residual porewater pressure increases should not occur in soils subject to strains of less than 0.005 percent.

ACKNOWLEDGEMENTS

The Air Force Office of Scientific Research (AFOSR), Bolling Air Force Base, Washington, D.C., sponsored this research (Grant No. AFOSR-85-0172; Program Managers Major Steven C. Boyce, Spencer T. Wu and Col. Lawrence D. Hokanson). Wayne A. Charlie, Associate Professor Civil Engineering and Geotechnical Engineering Program Leader at Colorado State University, Fort Collins, Colorado, was the Prinicipal Investigator. Donald O. Doehring, Professor of Earth Resources, Colorado State University, provided geological, statistical and quality control expertise. The laboratory and field research was conducted by the following graduate students for their M.S. and Ph.D. research: A.A. Awad, J.M. Bolton, T.E. Bretz, L.W. Butler, M.A. Chouicha, H. Hassen, M.E. Hubert, P.J. Jacobs, W.A. Lewis, L.A. Schure, F. Rwebyogo and G.E. Veyera. Eric J. Rinehart, DNA, Scott E. Blouin, ARA, Inc. and George E. Veyera, CRT, Inc., provided technical assistance and insight. Carol Smoot typed and helped organize this report.

page left blank

TABLE OF CONTENTS

Chapter			Page
ABSTRACT AND REPORT DOCUMENTATION			iii
ACKNOWLEDGEMENTS			v
TABLE OF CONTENTS			vii
LIST OF FIGURES			ix
LIST OF TABLES			xiii
I.	INTRODUCTION		
	A.	Blast Induced Liquefaction Threat	1
	B.	Definition of Liquefaction	2
	C.	Objectives of the Research	3
	D.	Organization of the Report	4
	E.	Conclusions	5
II.	LITERATURE REVIEW		
	A.	Introduction and Definition of Liquefaction	7
	B.	Blast Induced Porewater Pressure and Liquefaction	8
	C.	Factors Influencing Liquefaction	10
	D.	Laboratory Studies	11
	E.	Field Studies	12
	F.	Empirical Relationships	14
	G.	Analytical and Theoretical Methods	18
	H.	Summary	19
III.	LABORATORY SHOCK TESTS ON SAND		
	A.	Introduction	35
	B.	Test Equipment and Instrumentation	35
	C.	Physical Properties of the Soils	36
	D.	Variation of Parameters	38
	E.	Sample Saturation	40
	F.	Quartz Beach Sand (Monterey 0/30, California)	42
	G.	Quartz Beach Sand (Tyndall AFB, Florida)	44
	H.	Granitic River Sand (Poudre River, Colorado)	45
	I.	Granitic River Fine Sand and Gravel (Poudre Valley,Colorado)	46
	J.	Coral Beach Sand (Eniwetok, South Pacific)	48
	K.	Summary	49
IV.	LABORATORY SHOCK AND QUASI-STATIC TESTS ON SILT		
	A.	Introduction	61
	B.	Test Equipment and Procedure	62
	C.	Test Instrumentation	62
	D.	Physical and Index Properties of the Soils	63
	E.	Quasi-Static Tests	63
	F.	Shock Tests	65
	G.	Summary	66

V. FIELD EXPLOSIVE TESTS ON PLACED SAND
A. Introduction..... 81
B. Test Site..... 81
C. Instrumentation..... 82
D. Soil Properties..... 82
E. Soil Placement and Saturation..... 83
F. Test Procedure..... 83
G. Planar Stress Wave Tests..... 84
H. Spherical Stress Wave Test Results..... 85
I. Summary..... 87

VI. IN-SITU EXPLOSIVE TESTS ON ALLUVIAL SAND
A. Introduction..... 99
B. Test Site and Soil Properties..... 99
C. Instrumentation.....100
D. Explosives and Test Procedures.....100
E. Test Results.....101
G. Summary.....104

VII. ANALYSIS OF SHOCK AND EXPLOSIVE INDUCED LIQUEFACTION
A. Empirical.....117
B. Analytical.....118
C. Theoretical.....118

VIII. SUMMARY.....121

APPENDIX A LABORATORY SHOCK TESTS ON SAND
A.1 Monterey No. 0/30 Quartz Beach Sand.....134
A.2 Tyndall Quartz Beach Sand.....138
A.3 Poudre Valley Granitic Sand.....139
A.4 Poudre Valley Granitic Fine Sand and Gravel.....140
A.5 Eniwetok Coral Beach Sand.....141

APPENDIX B OVERVIEW OF RESEARCH GRANT
B.1 Research Objectives.....174
B.2 Significant Accomplishments.....174
B.3 Written Publications.....176
B.4 Presentations on AFOSR Research.....179
B.5 Professional Personal (associated with this research).....181
B.6 Graduate Students (associated with this research).....182
B.7 Consultations to Government Agencies.....183
B.8 New Discoveries and Inventions.....184

LIST OF FIGURES

Figure		Page
2.1	Liquefaction is evident from the geysering of water and sand (about 1 m high) through an instrument borehole in an explosion-produced crater (Dial Pack).....	20
2.2	Example of explosion-induced liquefaction. A large, 300 m diameter, shallow crater was produced with explosives (Dial Pack).....	20
2.3	Liquefaction during the unloading phase from a cycle of isotropic compressive loading. Source: Fragaszy et al., (1983).....	21
2.4	Liquefaction coefficient as a function of charge weight and distance (Studer and Kok, 1980).....	22
2.5	Porewater pressure ratio as a function of charge weight and distance from explosive centrifuge modeling experiments (Fragaszy et al., 1983).....	22
2.6	Liquefaction coefficient to be expected as a function of charge and distance (Kok, 1977).....	23
2.7	Porewater pressure ratio for Monterey No. 0/30 sand as a function of density and effective stress (Veyera, 1985)..	23
3.1	Cross-section of the confining pressure tube and the sample container (Veyera, 1985).....	51
3.2	Hardware arrangement.....	51
3.3	Experimental shock facility prepared for loading (view from momentum trap).....	52
3.4	Porewater pressure ratio for Monterey No. 0/30 sand as a function of density and effective stress.....	53
3.5	Porewater pressure ratio for Tyndall beach sand as a function of the strain.....	54
3.6	Porewater pressure ratio for Poudre Valley Sand as a function of the strain.....	55
3.7	Porewater pressure ratio as a function of the sum of the peak strains for all data of fine sand.....	56
3.8	Porewater pressure ratio as a function of the sum of the peak strains for all data of gravel.....	56
3.9	Porewater pressure ratio as a function of the sum of the peak strains, Poudre valley fine sand and gravel.....	57

3.10 Porewater pressure ratio for Eniwetok coral sand as a function of the strain, relative density and effective stress..... 57

3.11 Porewater pressure ratio as a function of the strain for the five soils tested (D_R = 50% and σ'_o = 100 kPa)..... 58

4.1 Grain size distributions for soils used in this study.... 67

4.2 Change in peak porewater pressure as a function of the change in confining pressure in terms of soil type, void ratio, and initial effective stress for all static tests. 68

4.3 Excess residual porewater pressure as a function of the change in confining pressure in terms of soil type, void ratio, and initial effective stress for all static tests. 69

4.4 Porewater pressure ratio as a function of the change in confining pressure in terms of soil type, void ratio, and initial effective stress for all static tests..... 69

4.5 Porewater pressure ratio as a function of the sum of the peak sample strain in terms of void ratio and initial effective stress for all Monterey No. 0/30 sand static tests..... 70

4.6 Porewater pressure ratio as a function of the sum of the peak sample strain in terms of void ratio and initial effective stress for all Monterey No. 0/30 sand static tests..... 70

4.7 Comparison of porewater pressure ratio for static tests as predicted by experimental analysis and Veyera (1985) equation for dynamic tests (Monterey No. 0/30 sand) utilizing D_R..... 71

4.8 Porewater pressure ratio as a function of the sum of the peak sample strain in terms of soil type, void ratio, and initial effective stress for 50% sand, 50% silt and Bonny silt static tests..... 72

4.9 Porewater pressure ratio as a function of the sum of the peak sample strain in terms of soil type, void ratio, and initial effective stress for 50% sand, 50% silt and Bonny silt static tests..... 72

4.10 Porewater pressure ratio as a function of the sum of the peak sample strains in terms of soil type and void ratio for dynamic tests..... 73

4.11 Porewater pressure ratio as a function of the sum of the peak sample strains in terms of soil type and void ratio for dynamic tests..... 73

5.1 Cross-section of explosive test pit and soil sample..... 88

5.2 Poudre Valley sand gradation curve..... 88

5.3 Stress-strain curves for uniaxial loading of Poudre Valley sand (arithmetic scale)..... 89

5.4 Stress-strain curves for uniaxial loading of Poudre Valley sand (logarithmic scale)..... 89

5.5 Typical pore pressure time history measured by the pressure transducers..... 90

5.6 Typical pore pressure ratio versus time for the piezometer response..... 90

5.7 Measured peak porewater pressure for the planar detonations (D_R = 89%, Hassen, 1988)..... 91

5.8 Measured porewater pressure ratio for planar detonations (D_R = 89%; Hassen, 1988)..... 91

5.9 Pore pressure ratio for spherical shots as a function of scaled distance (D_R = 89%, Bretz, 1988)..... 92

5.10 Pore pressure ratio for spherical shots as a function of scaled distance (D_R = 50%, Schure, 1988)..... 92

5.11 Pore pressure ratio for spherical shots as a function of scaled distance (D_R = 1%, Schure, 1988)..... 93

5.12 Comparison of pore pressure ratio for planar and spherical detonations (D_R = 89%; Bretz, 1988; Hassen, 1988)..... 93

5.13 Pore pressure ratio for spherical shots as a function of peak strain (D_R = 50%, Schure, 1988)..... 93

5.14 Pore pressure ratio for spherical shots as a function of peak strain (D_R = 1%, Schure, 1988)..... 93

6.1(a) North-South cross-section through borehole one (BH-1).... 106

6.1(b) East-west cross-section through boreholes one and two (BH-1 and BH-2)..... 106

6.2 Instrumentation layout, plan view, for detonations one through five which utilizes borehole one as the explosive detonation point..... 107

6.3 Instrumentation layout, plan view, for detonations six which utilizes borehole two as the explosive detonation point..... 108

6.4 Typical stress-time history recorded using the Signal-Conditioner-TDR instrumentation system..... 109

6.5 Peak compressive stress data for detonations one through six with the empirical equation representing the line of best through the data..... 109

6.6 Peak compressive stress data for the South Platte River sand island, the statistically best fit line through the measured field data and other equations given in the literature..... 110

6.7 Peak particle velocity data and the empirical equation representing the line of best fit through the field data. 111

6.8 Peak particle velocity data for the South Platte River filed site, the best statistically best fit line through the data and other equations given in the literature..... 112

6.9 Residual porewater pressure expressed as the dimensionless porewater pressure ratio, (PPR = u/σ'), vs. time after detonation number six, (9.1030 kg)..... 113

6.10 Peak residual porewater pressure data for all detonations and the empirical equation representing the line of best fit through the data..... 113

6.11 Calculated peak residual porewater pressure ratio at $t = o^+$ for all detonations and Equation 6.4..... 114

6.12 Statistically best fit equations for peak residual porewater pressure ratio predictions based on peak strain..... 114

LIST OF TABLES

Table		Page
2.1	Reference summary of published research on liquefaction of saturated cohesionless soil by impact loading.....	24
2.2	Reference summary of published research on liquefaction of saturated cohesionless soil by shock loading.....	25
2.3	Reference summary of published research on liquefaction of saturated cohesionless soil by centrifuge and triaxial	26
2.4	Reference summary of published research on liquefaction of saturated cohesionless soil by large scale explosives.	27
2.5	Reference summary of published research on liquefaction of saturated cohesionless soil for compaction purposes...	28
2.6	Reference summary of published research on liquefaction of saturated cohesionless soil pits away from blast.....	29
2.7	Reference summary of published research on liquefaction of saturated cohesionless soil for line explosives.....	29
2.8	Reference summary of published research on liquefaction of saturated cohesionless soil for small explosives.....	30
2.9	Table of constant for estimated radius of liquefaction (Ivanov, 1967).....	32
2.10	Empirical Equations Developed to Estimate Peak Stress in Water and Water Saturated Soil.....	33
2.11	Relationship between peak compressive strain, velocity, and peak stress generated by a compressive shock wave in a linear elastic media.....	34
3.1(a)	Stress Wave Propagation Parameters for Quartz Sand (G_s = 2.65).....	59
3.1(b)	Stress Wave Propagation Parameters for Coral Sand (G_s = 2.80).....	60
4.1	Physical Properties of Monterey No. 0/30 Sand, Bonny Silt and a 50-50 Mixture of These Soils.....	74
4.2	List of Symbols for Figures 4.2 to 4.11.....	68
4.3	Quasi-Static Test Results - Monterey No. 0/30 Sand, D_R = 0% Series.....	75

4.4 Quasi-Static Test Results - Monterey No. 0/30 Sand, D_R = 60% Series..... 76

4.5 Quasi-Static Test Results - 50% Sand, 50% Silt Mixture... 77

4.6 Quasi-Static Test Results - Bonny Silt..... 78

4.7 Dynamic Test Results - 50% Sand - 50% Silt Mixture and Bonny Silt..... 79

5.1 Index properties of the Poudre Valley sand..... 95

5.2 Peak residual pore pressure increase of Poudre Valley sand as a function of charge weight, distance, and soil density for planar tests (Hassen, 1988)..... 96

5.3 Peak residual pore pressure increase of Poudre Valley sand as a function of charge weight, distance, and soil density for spherical tests (Bretz, 1988)..... 97

5.5 Peak residual pore pressure increase of Poudre Valley sand as a function of charge weight, distance, and soil density for spherical tests (Schure, 1988)..... 98

6.1 Summarized laboratory test results for the upper 3.65 m sand layer..... 115

6.2 Summarized laboratory test results for the silt layer, intercepted at a depth of 3.65 m..... 115

6.3 Test sequence, charge type, weight and depth of explosive for the six detonations fired during the test program.... 116

I. INTRODUCTION

A. Blast Induced Liquefaction Threat

Blast-induced liquefaction of water saturated soils represents a threat to both military and civilian structures. Liquefaction can lead to catastrophic consequences including landslides, foundation failure, floatation of buried buoyant structures, ground subsidence, and failure of earthfill dams. Liquefaction may be the cause of the unusually broad, flat crater shapes and late-time low frequency ground motion observed in nuclear (NE) and high explosive (HE) tests in the Pacific and Canada, respectively.

At the International Workshop on Blast-Induced Liquefaction, McCracken (1978) stated that, "We within the United States Air Force now believe that blast-induced soil liquefaction could be a far more serious threat to both civilian and military targets than we have given it credit for in the past." The Dutch also consider liquefaction a serious threat as is evident by Kok's (1978) statement during a discussion on possible effects from the detonation of a 500,000 kilogram (500 kiloton) nuclear weapon. Kok stated that, "everything will be liquefied ... all the structures will fall to pieces." Rischbieter (1977) noted that the Netherlands are concerned because of their coastal plains lying below sea level and Switzerland is concerned because of their abundance of lake shore deposits consisting of post-glacial alluvium. In Norway, Kummeneje and Eide (1961) showed that excess porewater pressure and liquefaction could be induced by blasting. The Russians have conducted an extensive series of field explosive tests and have developed empirical methods to predict the extent of blast-induced liquefaction (Lyakhov, 1961; Ivanov,

1967; and Florin and Ivanov, 1961). One of the earlier references to liquefaction was in a paper by Terzaghi (1956) in which he stated that nearby blasting operations caused the 1935 failure of the SWIR II dam in Russia.

B. Definition of Liquefaction

In 1978, The American Society of Civil Engineers, Committee on Soil Dynamics, Geotechnical Engineering Division, defined liquefaction as,

> The act or process of transforming any substance into a liquid. In cohesionless soils, the transformation is from a solid state to a liquified state as a consequence of increased pore pressure and reduced effective stress.

Several other definitions of liquefaction exist in the literature. Basically, they all state that liquefaction is a condition caused by an increase in porewater pressure, thus, a decrease in effective stress and a loss of shear strength of a soil mass.

Liquefaction can be caused by several mechanisms which include any activity in saturated, cohesionless soil that cause the soil grains to form a more compact structure. This compaction results in an increase in porewater pressure which, in turn, leads to a decrease in effective stress and thus, liquefaction. Liquefaction can last for seconds, minutes, or hours and longer. Excess porewater pressure has been reported to last up to several days. Given sufficient time, gravity induced failures can occur.

Liquefaction effects take many forms. These include flow failures of slopes or earth dams, settlement or tipping of buildings and piers, collapse of retaining walls, lateral spreading of inclined ground, and

deformation of the ground surface. Water spouts and sand boils typically accompany liquefaction.

C. Objectives of the Research

The primary objective of our investigation was to systematically evaluate the behavior of saturated granular soils subjected to shock and explosive loadings. We conducted laboratory and field experiments to simulate the field loading of a soil element located near the detonation point of an explosive. Intense compressive loadings having millisecond rise times to peak stress occur in this region. The soil's porewater pressure response both during and after the passage of the stress wave was used to evaluate the liquefaction potential of the soil. Experimental measurements included the applied loading stress, peak particle velocity and the porewater pressure response.

A large number of parameters have been observed to affect the onset of liquefaction. Some are associated with the soil while others are related to the explosive itself. We investigated the effect of variations in the initial relative density, the initial effective stress, and soil type along with the intensity geometry and number of applied loadings.

Laboratory shock tests were conducted on two quartz beach sands (coarse and fine), a granitic river sand, a granitic river gravel, a coral beach sand, and a clayey silt. Field explosive tests were conducted on a granitic river sand, and an in-situ granitic river sand-gravel deposit. Our analysis of the data include an evaluation of the influence of several parameters on the peak and long-term porewater pressure response in the soil, the stress wave velocity, and the peak particle velocity. The results of these analyses are used to define liquefaction threshold limits

and develop empirical relationships for predicting porewater pressure increases in saturated, cohesionless soils. Our study has derived and documented several important relationships between soil properties and compressional stress wave loading. In the course of this work, we evaluated existing empirical predictive techniques including the relationships between scaled charge distance, peak particle velocity, and peak porewater pressure, versus porewater pressure response. We use theoretical relationships and analytical models to explain the observed behavior of our field and laboratory tests.

D. Organization of the Report

In Chapter II, we present a review of the literature on blast-induced liquefaction. Chapters III and IV present the results of laboratory shock tests on water saturated gravels, sands and clayey silts conducted by Veyera (1985), Hubert, (1986), Chouicha (1987) and Bolton (1988). Chapter IV also presents the results of laboratory high-pressure quasi-static tests on sand, clayey silt and sand-clayey silt mixtures conducted by Bolton (1988). Chapters V and VI present the results of field explosive tests on saturated sands conducted by Bretz (1988), Hassen (1988), Jacobs (1988), Schure (1988) and Allard (1988). Chapter VII presents empirical, analytical and theoretical analysis of shock and explosive induced liquefaction conducted by Veyera (1985), Awad (1988), Hassen (1988), Bretz (1988) and the authors of this report.

E. Conclusions

Our research indicates that the destruction potential of an explosion may be greatly magnified if detonated in water saturated granular soils. While blast-induced liquefaction may not necessarily damage a facility structurally, it may render it unusable. Blast-induced liquefaction can cause late time decreases in the soil's shear strength that produces damage disproportionate to the amount of explosive used and ground motions inconsistent with previous experience. For example, recent re-examinations of the events at the Pacific Proving Grounds, where nuclear explosives (NE) were detonated in the 1950's, and high explosive (HE) tests conducted at Suffield, Canada, suggest that liquefaction may be the primary factor causing the unusually broad, flat crater shapes.

The results of our study indicate the following.

1. Liquefaction can be induced by single and multiple explosive induced compressive wave loadings.
2. Liquefaction can be induced at distances from explosions much greater than those associated with structural damage.
3. Fairly long term increases in residual porewater pressures can be induced by compressive shock wave loadings when the peak particle velocity exceeds 0.075 m/s, the peak porewater pressure exceeds 250 kPa, or the peak strain exceeds 0.005 percent.
4. Liquefaction can be induced in loose saturated sands by a single compressive shock wave when the peak particle velocity exceeds 0.75 m/s, the peak porewater pressure exceeds 2,500 kPa, or the peak strain exceeds 0.05 percent.

5. Soils at higher initial effective stress and higher initial relative density require more energy to produce liquefaction.
6. Destruction potential of an explosive charge may be greatly magnified if detonated in water-saturated soils.
7. Liquefaction occurs because of compressive strain induced by the compression stress wave, but liquefaction occurs after the stress wave passes.
8. Liquefaction occurs because loading-unloading of the porewater is elastic but the soil skeleton is not.

An explosive detonated in a soil having a high liquefaction potential could cause damage disproportionate to the energy released. Documented occurrence of blast-induced liquefaction is available in the open literature. Although considerable work remains to be done in projecting this information into a comprehensive method of predicting liquefaction for actual or hypothetical blasts, the data indicate that residual porewater pressure increases should not occur in soils subject to strains of less than 0.005 percent. Transient and quasi-static tests indicate that residual porewater pressure increases and liquefaction are not strain-rate sensitive for sand but are strain-rate sensitive for silt.

II. LITERATURE REVIEW

This chapter summarizes the current state of knowledge about the nature and occurrence of blast-induced liquefaction from field observations, from laboratory tests, and from small-scale field tests. Empirical, analytical and theoretical aspects of liquefaction are reviewed.

A. Introduction and Definition of Liquefaction

The term liquefaction has been used to describe the state of a saturated, cohesionless soil. The manifestations of soil in a liquefied state are: sand boils, flow failures, low frequency ground oscillations, loss of bearing capacity, rise of buoyant buried structures and ground settlement. Indirect evidence of a liquefied soil include the measurement of excess porewater pressure and delayed failures (Committee on Earthquake Engineering, 1985).

Several definitions have been proposed for liquefaction. These include:

> Liquefaction- "Denotes a condition where a soil will undergo continued deformation at a low residual resistance stress or with no residual resistance due to the build up of high pore-water pressures which the effective confining pressure to a very low value; pore-water pressure build up leading to true liquefaction of this type may be due to either static or cyclic stress applications" (Seed, 1976).
>
> Initial Liquefaction- "Denotes a condition where, during the course of cyclic stress application, the residual pore-water pressure on completion of any full stress cycle becomes equal to the applied confining pressure; the development of initial liquefaction has no implication concerning the magnitude of the deformations which the soil might subsequently undergo; however it defines a condition which is a useful basis for assessing various possible forms of subsequent soil behavior" (Seed, 1976).
>
> Liquefaction- "The act or process of transforming any substance into a liquid. In cohesionless soil, the transformation is from a solid state to a liquefied state as a consequence of increased

porewater pressure and reduced effective stress. Liquefaction is thus defined as a changing of states which is independent of initiating disturbance that could be static, vibratory, sea wave, shock loading, or a change in ground water pressure. The definition also is independent of deformation or ground failure movements that might follow the transformation. Liquefaction always produces a transient loss of shear resistance but does not always produce a long-term reduction of shear strength" (Committee on Soil Dynamics, 1978).

Liquefaction-"Is a phenomenon where in a mass of soil loses a large percentage of its shear resistance, when subjected to undrained monotonic, cyclic or shock loading, and flows in a manner resembling a liquid until the shear stresses acting on the mass are as low as the reduced shear resistance" (Castro and Poulos, 1977).

Liquefaction- "This term is used to include all phenomena giving rise to a loss of shearing resistance or to the development of excessive strain as a result of transient or repeated disturbance of saturated cohesionless soils" (Committee on Earthquake Engineering, 1985).

The definition by Seed (1976) for initial liquefaction and that for liquefaction by the Committee on Soil Dynamics (1978) will be used for this report. In this way, blast-induced liquefaction can be evaluated by comparing the amount of porewater pressure increase that occurs after the passage of the explosive-induced compressive stress wave. The porewater pressure increase above the hydrostatic pressure, remaining after the passage of the compressive stress wave, will be referred to as the residual excess porewater pressure.

B. Blast-Induced Porewater Pressure and Liquefaction

Documentation of blast-induced liquefaction exists in the literature. Reviews of explosive induced liquefaction phenomena and experiences are given by Blouin (1978), Charlie et al. (1980, 1985), (Fragaszy et al. (1983)), Gilbert (1976), Marti (1978), Rischbieter (1977), Veyera (1985), and others. Fountains of water and sand boils

(Figure 2.1) have occurred and excess porewater pressure have been measured following HE explosive tests. Soils flowing towards and into blast craters (Figure 2.2) have significantly changed the crater profile and significant settlement outside the crater have occurred as a result of liquefaction.

Residual porewater pressure develops and liquefaction occurs because the stress-strain behavior of granular soil is nonlinear and inelastic. For undrained compressive loading of water saturated granular soils, the soil skeleton will deform inelastically while the porewater and mineral phase (i.e. soil grains) deform elastically. Upon unloading, some or all of the stress originally carried by the soil skeleton is transferred to the porewater pressure. The development of liquefaction under these circumstances is graphically expressed in Figure 2.3 (Fragaszy et al., 1983).

A single explosion produces a high frequency, high intensity compressional wave of very short duration. The motion radiates outward from the source, attenuating with distance. The duration, magnitude, and form of ground motion is a function of the charge size and shape, location of the charge with respect to the soil surface, and distance from the charge (Lyakhov, 1961). Compressive wave loading predominates near the explosive source and shear and surface wave loading predominates at large distances from the explosive surface (Melzer, 1978). For multiple explosive sources, the number and timing of the explosive sources also have a large influence on the duration and extent of the induced ground motion.

C. Factors Influencing Liquefaction

Observations by many investigators both in blasting and in earthquake research have led to the recognition of several significant factors related to the occurrence of liquefaction. These include:

Degree of Saturation. The presence of air in a soil decreases the soil's potential for liquefaction. Liquefaction has been proven difficult to induce in soils with a degree of saturation less than 100 percent (Florin and Ivanov, 1961; Van der Kogel et al., 1981; Studer., 1977; True, 1969).

Gradation, Particle Size and Shape. Cohesionless soils with a narrow band of gradation are generally considered easier to liquefy than soils with a wide band of gradation (Damitio, 1978; Klohn et al., 1981; Kummeneje and Eide, 1961; Rischbieter, 1977;). The roundness of the soil grains also seems to contribute to liquefaction; but angular sands have been liquefied under dynamic loading (Ivanov et al., 1981).

Compressibility. The tendency for volume decrease is a necessary condition for liquefaction. Both the compressibility of the soil skeleton and the fluids (gas and water) in the soil voids must be considered (Florin and Ivanov, 1961; Lyakhov, 1961; Studer and Kok, 1980; Van der Kogel et al., 1981).

Permeability and Drainage. The rate of dissipation of the porewater pressure is a function of the permeability of the soil, the drainage length, and drainage boundaries. Liquefaction is observed to occur mostly in soils which are prevented from draining rapidly (Florin and Ivanov, 1961; Kok, 1978; Damitio, 1978; Kurzeme, 1971).

Relative Density. Soils with a relative density of less than 65 percent are typically considered susceptible to liquefaction (Damitio, 1978; Florin and Ivanov, 1961; Kummeneje and Eide, 1961; Yamamura and Koga, 1974; Veyera, 1985). However, Veyera (1985) and Hubert (1986) have experimentally shown that shock-induced liquefaction can also be induced in soils at relative densities above 80 percent.

Overburden (Effective Stress). The effective stress of a soil increases as the overburden increases. Thus, the porewater must reach a higher pressure to overcome the effective stress and to liquefy the soil. Larger effective stresses also increase the soil skeleton's stiffness, further reducing the soil's potential for liquefaction (Florin and Ivanov, 1961; Rischbieter, 1977; Studer and Kok, 1980).

D. Laboratory Studies

A summary of laboratory studies of shock induced liquefaction is given in the following sections.

1. Impact Loading

A simplified way of producing liquefaction is by impacting a container filled with saturated sand. A primary drawback to this method is the lack of accuracy in estimating the impact force to generate liquefaction. Table 2.1 provides the summary of published tests by impact loading.

2. Shock Loading

Several approaches have been taken to liquefy a saturated material by shock loading. Colorado State University's shock device, designed by Charlie and Veyera (1985) under AFOSR funding, uses water to apply a compressive shock load. It is the only system in this country that is able to vary the initial effective stress over a wide range of values and record dynamic porewater pressure responses. Van der Kogel et al., 1981; Perry, 1972; Mason and Walter, 1968; True, 1969; Studer and Hunziker (1977) and several others have attempted to liquefy saturated sand by air blasts. See Table 2.2 for the summary of published results of tests by shock loading.

3. Centrifuge and Quasi-Static Triaxial Testing

Schmidt et al. (1981) and Fragaszy et al. (1983) modeled major military events by increasing the gravitational field in a centrifuge. The models were subjected to scaled charge weights of the actual test or

by compressed air. The Pacific Proving Ground Tests on the Eniwetok coral atoll were reproduced, resulting in liquefaction (Fragaszy et al., 1983).

Fragaszy and Voss (1986) tested a silica sand and the Eniwetok coral sand in a high pressure triaxial cell. Several cycles of quasistatic isotropic compressive loading produced liquefaction at low confining stresses. See Table 2.3 for the summary of published results of centrifuge and quasistatic tests.

E. Field Studies

A summary of field studies of explosive induced liquefaction is given in the following sections.

1. Large Explosives Tests

The detonation of up to several kilotons of HE explosions have been done by the military to investigate ground motion, structural response and crater formation. Little attention has been given to the generation of porewater pressure, except that in some instances, the observation of geysers, sand boils, and springs were observed and recorded indirectly indicating liquefied layers at some depth below the ground water table (Langley et al., 1972; Banister et al., 1976; Banister and Ellett, 1974). The location of the ground water table is a primary factor influencing the shape of the crater formed by an explosion. If the scaled depth of the ground water table is very deep or nonexistent, the crater will be in the form of a deep bowl. In cohesionless material with a small scaled distance to the water table, the craters tend to be very broad and shallow which may be caused by a liquefied state (Roddy, 1976; Nordyke,

1976; Melzer, 1978; Blouin, 1978). See Table 2.4 for the summary of published results for tests using large HE.

2. Explosive-Induced Compaction

The ability to compact loose saturated deposits through the use of explosives has been recognized for several decades. The stabilization of submerged slopes and construction sites by explosive densification provides an economical method of developing naturally unsuitable locations in areas near water. The general procedures for compacting large areas involves simultaneous detonation or delayed detonation of small buried charges in a grid pattern (Mitchell and Katti, 1981; Kok, 1978a; Queiroz et al., 1967; Obermeyer, 1980; Klohn et al., 1981). Densification is measured by the amount of settlement in the treated area, which can vary from 2 to 10 percent of the total depth of the cohesionless soil. During some of these blasting events, the porewater pressure response was monitored (Kummeneje and Eide, 1961; Obermeyer, 1980; Klohn et al., 1981). See Table 2.5 for the summary of published results of explosion compaction tests.

3. Pits Away From Blast (Air Blast Loading)

Perry (1972) and Rischbieter et al. (1977) attempted to liquefy sand samples by placing them at various distances from an HE explosive event. The sand was surface loaded in compression by the air blast. For testing buoyancy, Perry (1972) placed objects of various density buried at different depths. Table 2.6 shows the summary of these tests.

4. Line Explosives

Sanders (1982) evaluated the liquefaction potential as a result of a planned detonation by relating blast induced liquefaction to earthquake induced liquefaction. A summary of the prediction is given in Table 2.7.

5. Small Explosives Tests

For charge weights of less than 1000 kilograms (most being less than 10 kilograms), experiments have been conducted to examine the influence of various parameters on liquefaction potential. The effects of the charge weight, its location relative to the surface, its pattern, and its sequence of detonation (delayed versus simultaneous when several charges are involved) have been investigated by many researchers (Ivanov, 1967; Kok, 1977; Lyakhov, 1961; Puchkov, 1962; Rischbieter, 1978; Dill, 1966; Trense, 1977; Damitio, 1978). Field measurements include the peak and residual porewater pressure, the duration of the excess porewater pressure, the settlement and occasionally the ground acceleration at some distance (Carnes, 1981; Yamamura and Koga, 1974; Studer and Kok, 1980; Florin and Ivanov, 1961; Prakash and Gupta, 1970; Arya et al., 1978; Drake, 1978; Schaepermeier, 1978; Carnes, 1981). See Table 2.8 for the summary of published small explosive tests.

F. Empirical Relationships

1. Pore Pressure Ratio Based on Charge Weight and Distance

The porewater pressure ratio, PPR, also termed the liquefaction coefficient, L, is utilized for analyzing the liquefaction potential of a soil. The porewater pressure ratio is the change of the porewater pressure due to loading related to the initial effective stress. Studer

and Kok (1980) developed the following relationship for estimating the porewater pressure ratio (liquefaction coefficient) from a buried explosion.

$$PPR = u_r/\sigma_o' = 1.65 + 0.64 \ln (W^{1/3} / R) \quad \text{Eq. 2.1}$$

where PPR is the porewater pressure ratio, u_r is the residual excess porewater pressure, σ_o' is the initial effective stress, W is the charge weight in kg, and R is the distance from the explosive in meters. The porewater pressure ratio (liquefaction coefficient) ranges from zero to one with zero being no increase in residual porewater pressure and one being full liquefaction. Equation 2.1 is plotted in Figure 2.4 as a function of charge weight and distance. Figure 2.5 gives measured PPR from centrifuge explosive tests.

2. Liquefaction Based on Charge Weight

Lyakhov (1961) estimated that the optimum depth of an explosive, h (in meters), for maximum radius liquefaction is:

$$h = 2.5\ W^{1/3} \quad \text{Eq. 2.2}$$

where W is the charge mass in kilograms. For an explosive charge buried at the optimum depth, the maximum radius of liquefaction can be estimated from:

$$R = k_1\ W^{1/3} \quad \text{Eq. 2.3}$$

where R is the radial distance from the blast (in meters) and k is an empirical constant given in Table 2.9. Kok (1977, 1978) reported that k_1 has a value of 6.67 (Figure 2.6).

Ivanov (1967) estimated that to ensure a contained explosion, the charge weight per delay must be less than:

$$W = 0.055\ h^3 \qquad \text{Eq. 2.4}$$

where h is the buried charge depth in meters from Equation 2.2. For a fully contained explosion, the depth of liquefaction, d, (in meters) below the charge is:

$$d = 1.5\ h \qquad \text{Eq. 2.5}$$

where h is the buried charge depth in meters from Equation 2.2.

3. Pore Pressure Ratio Based on Peak Particle Velocity, Strain and Stress

For saturated soils, Puchkov (1962) examined the limits of the peak particle velocity for liquefaction. He concluded that a soil will not liquefy when the peak particle velocity is less than 7 cm per second. Obermeyer (1980) reported that no significant increase in residual porewater pressure were generated for peak particle velocities as large as 2 cm per second. A safe maximum particle velocity of 5 to 10 cm per second is recommended for structural stability of earth filled dams (Charlie et al., 1985).

For single charges located in water saturated soil, the peak particle velocity (in meters per second) as a function of the distance (in meters) and the charge weight (in kilograms) is (Drake and Ingram, 1981):

$$V_{pk} = (7.2)\ (R/W^{1/3})^{-1.15} \qquad \text{Eq. 2.6}$$

Table 2.10 presents several empirical equations developed to estimate peak stress in water and water saturated soil. For a stress wave traveling through an elastic media, a linear relationship exists on the

wave front between the peak compressive stress, σ_{pk}, and the peak particle velocity, V_p. This relationship, given by Kolsky (1963) and Timoshenko and Goodier (1970) is:

$$\sigma_{pk} = (\rho V_c) V_p \qquad \text{Eq. 2.7}$$

where ρ is the total mass density of the medium and V_c is the compressive stress wave propagation velocity through the medium. The quantity, "ρV_c" is commonly referred to as the acoustic impedance or specific acoustic resistance of the medium.

The peak compressive strain, ϵ_{pk}, developed in a medium subjected to a one-dimensional compressive stress wave can be determined from the following equation (Kolsky, 1963; Timoshenko and Goodier, 1970):

$$\epsilon_{pk} = \frac{V_p}{V_c} \qquad \text{Eq. 2.8}$$

In experiments conducted by Veyera (1985) on quartz sand, no significant porewater pressure increase was recorded for strains less than 0.005 percent. Measured PPR are shown in Figure 2.7 as a function of peak strain. The scatter in the data points can be explained by variations in initial density and initial effective stress of the soil. Liquefaction occurred under single compressive strains greater than 0.01 percent for low effective stresses and low relative densities and 1 percent for high effective stresses and high relative densities. Utilizing Equations 2.7 and 2.8, for a saturated soil at a void ratio of 0.7, Table 2.11 lists relationships between peak compressive strain, peak particle velocity and a peak stress. A peak compressive strain of 0.01 percent corresponds to a peak particle velocity of 0.15 m/sec and a peak stress of 500 kPa. Veyera

(1985) developed the following relationship for estimating the porewater pressure ratio as a function of peak strain, ε_{pk}, initial effective stress, σ_o', and initial relative density, D_r. The statistical best fit of several models examined is:

$$PPR = (16.30)\ (\Sigma\varepsilon_{pk})^{.331}\ (\sigma_o')^{-.308}(D_r)^{-.179} \qquad \text{Eq. 2.9}$$

where D_r and ε_{pk} are both in percent, and σ_o' is in kPa. Equation 2.9 is plotted in Figure 2.7 for D_r equal to 10 percent, σ_o' equal to 86 kPa, D_r equal to 80 percent and σ_o' equal to 690 kPa.

G. Analytical and Theoretical Methods

The passage of stress waves associated with the detonation of an explosive in a saturated soil results in a transient increase in porewater pressure and a possible increase in residual excess porewater pressure. For saturated soils, the volume reduction is prevented by the increase in porewater pressure which, if large enough, can produce liquefaction. For a period of time, the liquefied soil particles are actually suspended with no intergranular stress, and the soil loses its shear strength. Following liquefaction, the soil consolidates as the particles settle, creating a migration upward of excess porewater. The duration of the liquefied state depends upon the drainage path, permeability and compressibility of the soil. As consolidation takes place, the soil regains its strength (Terzaghi, 1956; Charlie et al., 1981; Blouin and Shinn, 1983). Kim and Blouin (1984) used a dynamic finite element analysis to model the porewater pressure during and following the passage of a compressive stress wave. Their analysis utilized Biot's (1962) theory of wave

propagation through a porous media. Veyera (1985) and Charlie et al. (1987) used a finite difference analysis also utilizing Biot's theory to analyze porewater pressure increase in laboratory shock testing. These analyses predicted that liquefaction can be induced by a compressive stress wave and are in good agreement with our experimental results.

H. Summary

Clear evidence of blast-induced liquefaction of water saturated soils exist in the literature. Fountains of water and sand boils have occurred and excess porewater pressure have been measured. Flow of soils toward and into craters and significant ground settlement surrounding craters have been observed. Empirical relationships to evaluate blast-induced liquefaction have been developed from limited field explosive tests. Proper engineering judgement should be employed when using such relationships for specific conditions. Only limited success has been made in theoretically understanding or analytically modeling blast induced porewater pressure increases and liquefaction. A major problem in gaining a better theoretical understanding of blast induced liquefaction is the complex stress-strain behavior of granular material containing pore fluid. Soil is inherently a multiphase system and both static and dynamic loads applied to a soil mass are carried in part by the mineral skeleton and in part by the pore fluid. Any theoretical or analytical model must incorporate the response of the mineral skeleton, the pore fluid and their interaction.

Figure 2.1 Liquefaction is evident from the geysering of water and sand (about 1 m high) through an instrument borehole in an explosion-produced crater (Dial Pack).

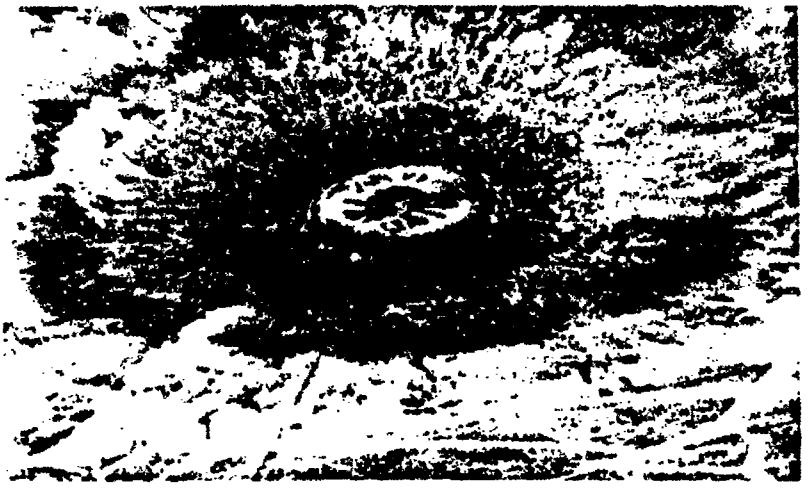

Figure 2.2 Example of explosion-induced liquefaction. A large, 300 m diameter crater was produced with explosives (Dial Pack).

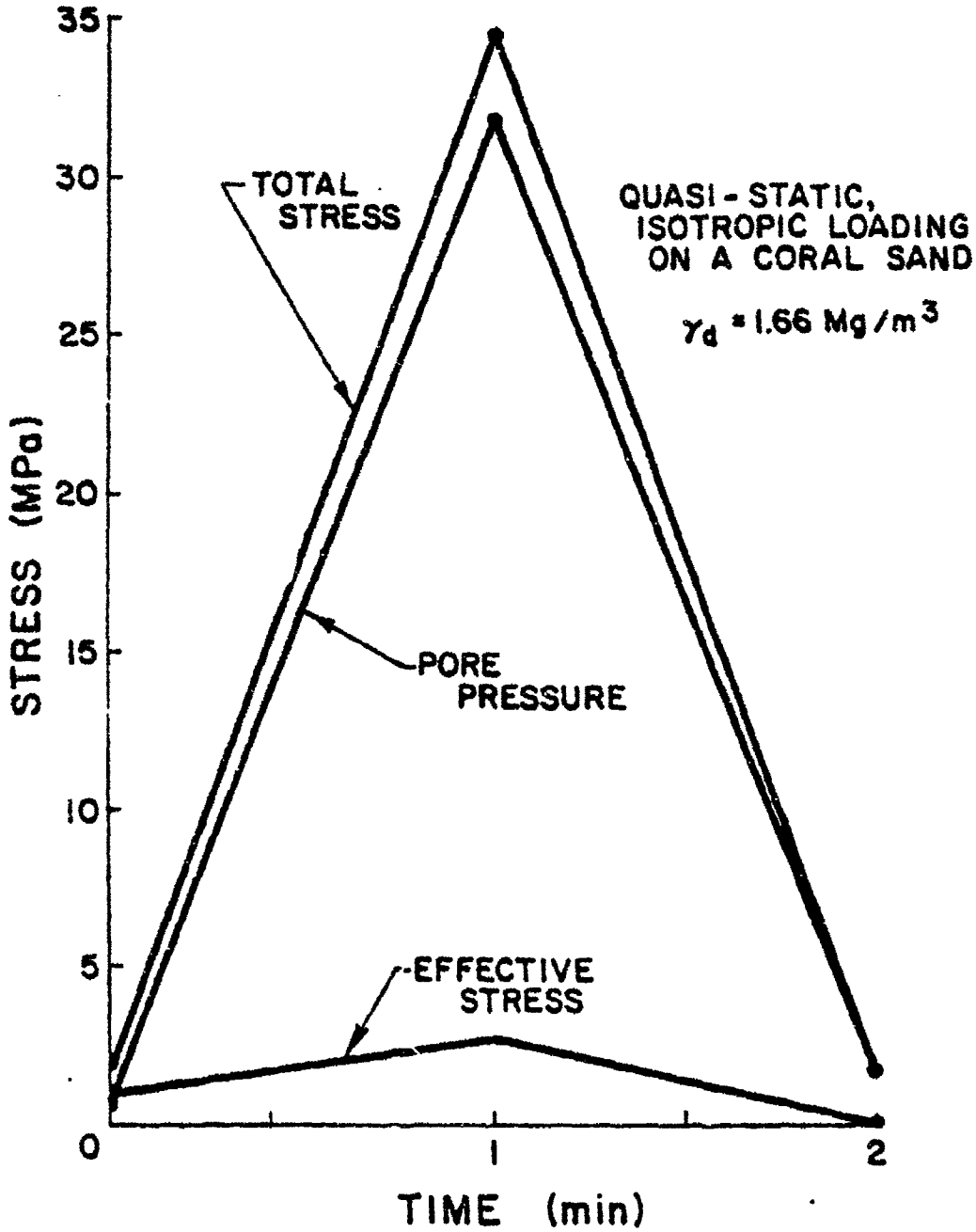

Figure 2.3 Liquefaction during the unloading phase from a cycle of isotropic compressive loading. Source: Fragaszy et al., (1983).

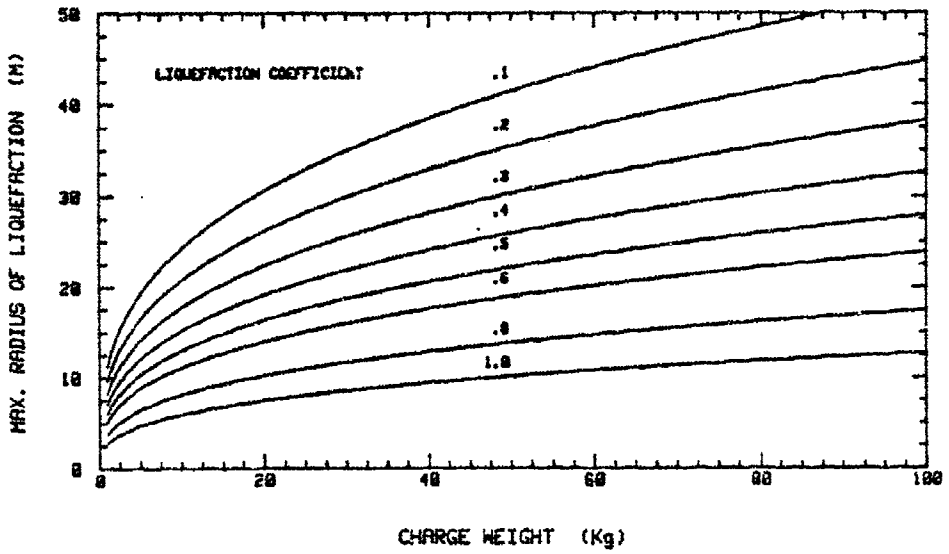

Figure 2.4 Liquefaction coefficient as a function of charge weight and distance (Studer and Kok, 1980).

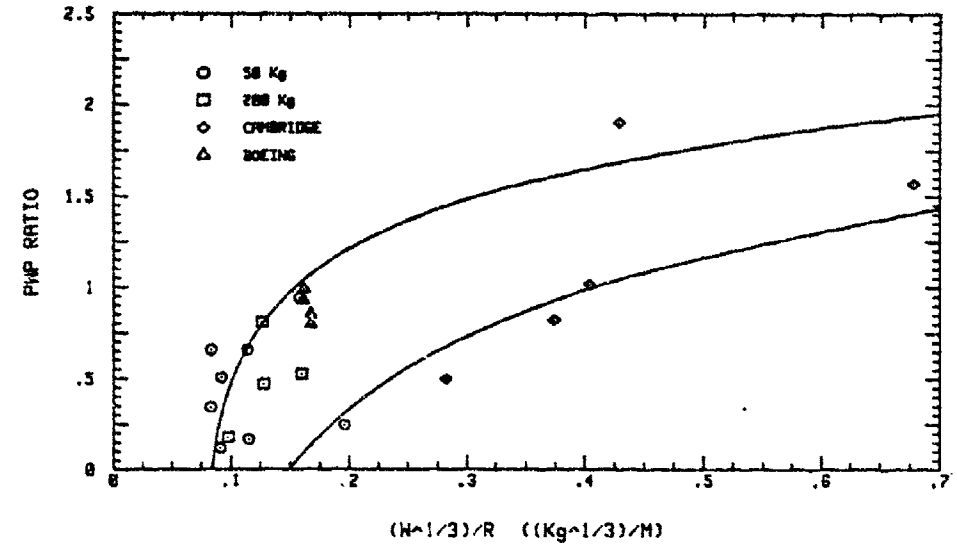

Figure 2.5 Porewater pressure ratio as a function of charge weight and distance from explosive centrifuge modeling experiments (Fragaszy et al., 1983).

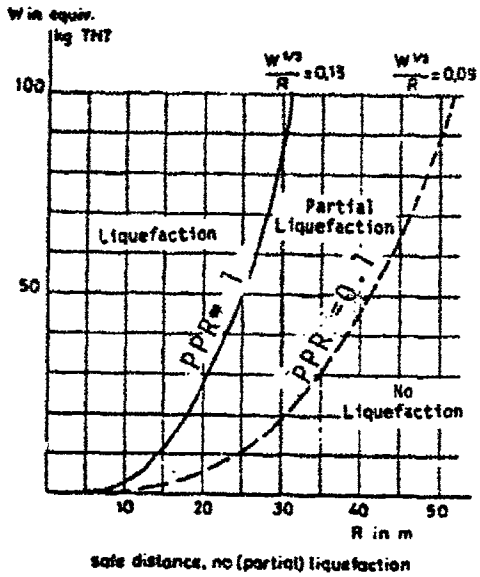

Figure 2.6 Liquefaction coefficent to be expected as a function of charge and distance (Kok, 1977).

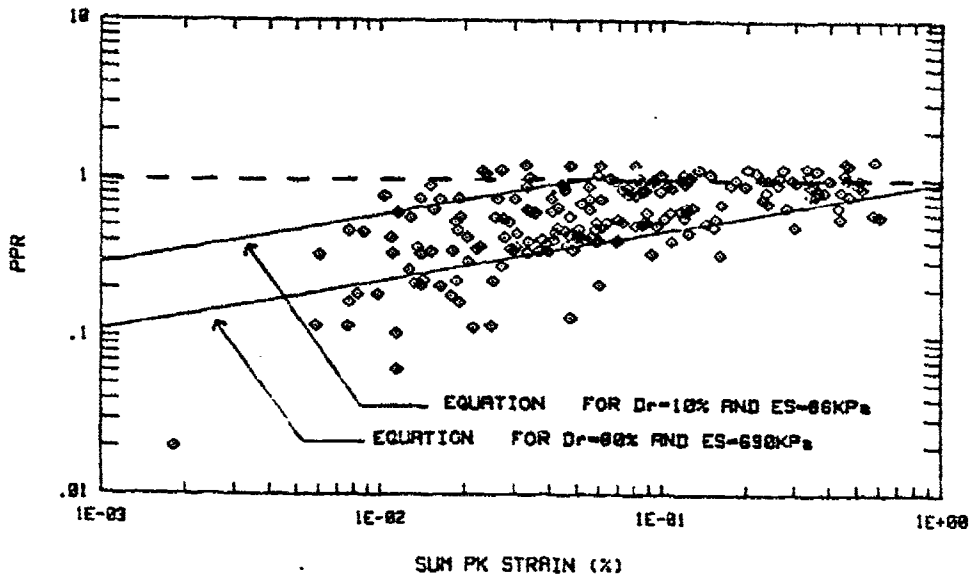

Figure 2.7 Porewater pressure ratio for Monterey No. 0/30 sand equation as function of density and effective stress (Veyera, 1985).

Table 2.1 Reference summary of published research on liquefaction of saturated cohesionless soil by impact loading.

LABORATORY TESTS: IMPACT LOADING

CASE No.	AUTHOR OF ARTICLE	TYPE OF LOADING	SOIL TYPE AND DENSITY	DEGREE OF WATER SATURATION (%)	RESIDUAL POREWATER PRESSURE (kPa)	PEAK POREWATER PRESSURE (kPa)	PEAK PARTICLE VELOCITY (m/sec)	COMMENTS
I-1	Kok (1977)	Hammer on cylinder	Loose sand	100	---	---	---	Compaction decreases with increase in number of impacts
I-2	Ruygrok & Van Der Kogel (1980)	Falling weight (100 kPa)	Sand Dr = 8-93%	85-97%	.5	2	---	Transient negative pwp some liquefaction observed
I-3	Vesic et al. (1967)	Impact weight (4.5kg)	Dense sand Dr = 80%	100	---	1175	---	Positive pwp only if soil densifies
I-4	Florin & Ivanov (1961)	Surface impact	Loose Sand γ = 2Mg/m^3	100	---	---	---	Liquefaction observed
I-5	Tanimoto (1967)	Pendulum	Loose fine sand	100	4	9	---	Settlement is the result of the impact and the dissipation of pwp

Table 2.2 Reference summary of published research on liquefaction of saturated cohesionless soil by shock loading.

LABORATORY TESTS: SHOCK LOADING

CASE No.	AUTHOR OF ARTICLE	TYPE OF LOADING	SOIL TYPE AND DENSITY	DEGREE OF WATER SATURATION (%)	RESIDUAL POREWATER PRESSURE (kPa)	PEAK POREWATER PRESSURE (kPa)	PEAK PARTICLE VELOCITY (m/sec)	COMMENTS
II-1	Charlie & Veyera (1985)	Shock tube projectile (69kPa)	Loose sand Monterey No. 0/30	100	1034	5380	1.5	Some sample liquefied pwp increases at V_p = .02 to .05 m/s
II-2	Studer & Hunziker (1977)	Shock tube and Compressed air (25MPa)	Loose sand (γ_d = 1.3-1.6 Mg/m³)	99.5	---	20 to 150	---	Some liquefaction
II-3	Van Der Kogel et al. (1981)	Shock tube	Porous stone	Dry Semi-saturated ≈ 100	---	50	---	---
II-4	Perry (1972)	Shock tube (635-1550 kPa)	Reid - Bedford sand (γ_d = 1.4-1.67 Mg/m³)	99	---	---	---	Liquefaction as a function of density and loading
II-5	Mason & Walter (1968)	Air blast (1400 kPa)	Beach sand Well graded	100	---	8.3	---	---
II-6	True (1969)	Air Blast (970 kPa)	Different sands (Dr = 75%)	<100 and 100	---	710	---	---
II-7	Studer (1978)	tunnel test (33 MPa - 110MPa) (Test 1977-Balmholz)	Quartz sand (1.5 Mg/m³)	100	1.5	5	---	Liquefaction at the surface of the samples
II-8	Veyera (1985)	Shock tube projectile (70kPa)	Monterey No. 0/30 (Dr = 0-80%)	100	690	5000	---	Liquefaction
II-9	Hubert (1986)	Shock tube projectile (60kPa)	Eniwetok coral sand (Dr = 0-100%)	≈ 100	520	5000	---	Liquefaction

Table 2.3 Reference summary of published research on liquefaction of saturated cohesionless soil by centrifuge and triaxial.

LABORATORY TESTS: CENTRIFUGE & TRIAXIAL

CASE No.	AUTHOR OF ARTICLE	TYPE OF LOADING	SOIL TYPE AND DENSITY	DEGREE OF WATER SATURATION (%)	RESIDUAL POREWATER PRESSURE (kPa)	PEAK POREWATER PRESSURE (kPa)	PEAK PARTICLE VELOCITY (m/sec)	COMMENTS
III-1	Schmidt & Fragaszy & Holsapple (1981)	1 to 13g explosive in 400G	Ottawa sand Silicon sand Alluvium	≈100	---	---	---	tests performed for craters evaluation
III-2	Fragaszy et al (1983)	Compression wave (34.5 MPa) in 62G	Ottawa and Eniwetok sand γ_d = 1.5 Mg/m³)	100	940 and 520	4130 and 4330	---	some tests liquefied
III-3	Fragaszy & Voss (1986)	Quasistatic in triaxial cell (1.72 to 34.5 MPa)	Eniwetok and Monterey $\gamma_{d_{min}}$ = 1.5 Mg/m³	100	(E) 1030 (M) 710	(E) 31730 (M) 31250	---	Liquefaction easier to produce on Eniwetok than Monterey sand

Table 2.4 Reference summary of published research on liquefaction of saturated cohesionless soil by large scale explosives.

FIELD TESTS: LARGE EXPLOSIVES

CASE No.	AUTHOR OF ARTICLE	TYPE OF LOADING	SOIL TYPE AND DENSITY	DEPTH TO GROUND WATER TABLE (m)	RESIDUAL POREWATER PRESSURE (kPa)	PEAK POREWATER PRESSURE (kPa)	PEAK PARTICLE VELOCITY (m/sec)	COMMENTS
IV-1a)	Charlie (1978) Dial Pack	500 tons (surface)	layered sand, silt and clay (Dr = 50 to 85%)	≈ 6.7	≈ 7m of head for 1 hour	---	---	shear strength measured water flowed for 1000 hours
IV-1b)	Langley et al. (1972) Dial Pack	500 tons (surface)	sand, clay and silt layers (Dr = 50 to 80%) (of cohesionless materials)	≈ 6.7	≈ 7m	---	---	Geysers, springs and sand boils
IV-2a)	Banister & Ellett (1974) Rio Blanco	3 x 30 ktons (buried: 2000m)	clayey silt (Dr = 60%)	≈ 0	14 2.1 km away 6.4m depth	117	1.5	no liquefaction observed one sand boil acc. = 18g, 2.1km away
IV-2b)	Banister, et al. (1976)	3 x 30 ktons (buried: 2000m)	loose sand and silt	≈ 5	$.17\bar{\sigma}v$	$1.3\bar{\sigma}$ 2km away	---	nuclear simulation
IV-3	Blouin (1978) Pacific Proving Ground	13-15 Mtons (surface)	Coral Sand	≈ 0	---	---	---	liquefaction craters
IV-4	Jaramillo & Pozega (1974) Middle Gust	20 and 100 tons (surface)	---	0	140 33m away	550	---	craters
IV-5	Melzer (1978) Predice Throw II	2 x 100 tons (surface)	silty clay over sand (15 to 75%)	2	---	---	.3	broad craters
IV-6	Nordyke (1976)	.2 to 125 ktons (buried)	interbedded rock and alluvium	2 to 20	---	---	---	various Russian tests water filled craters
IV-7	Roddy (1976) Prairie Flat	500 tons (surface)	interbedded sand, silt and clay	7	---	---	---	water filled crater
IV-8	Jones (1976) Snowball	500 tons (surface)	sand, silt and clay interbedded	7	---	---	---	water filled crater

Table 2.5 Reference summary of published research on liquefaction of saturated cohesionless soil for compaction purposes.

FIELD TEST: COMPACTION PURPOSE

CASE No.	AUTHOR OF ARTICLE	TYPE OF LOADING	SOIL TYPE AND DENSITY	DEPTH TO GROUND WATER TABLE (m)	RESIDUAL POREWATER PRESSURE (kPa)	PEAK POREWATER PRESSURE (kPa)	PEAK PARTICLE VELOCITY (m/sec)	COMMENTS
V-1	Kummeneje & Eide (1961)	.7 to 2.4 kg buried: 7m	fine & coarse sand (n = 45-50%)	≈ 0	≈ 21.5	---	---	
V-2	Kok (1978a)	13kg buried: 12m per borehole	loose fine sand (n = 45%)	2	300	2000	---	Grid pattern, 500 charges
V-3	Queiroz, Oliveira & Nazario (1967)	4kg per borehole	Loose sand	≈ 0	---	---	---	Grid pattern: water surgence at surface
V-4	Obermeyer (1980)	16 to 30 kg/delay	uranium tailing	≈ 0	---	300	---	Delayed multiple charges No pwp increase
V-5	Klohn, Garga & Shukin (1981)	5kg per borehole buried: 5m	silty sand tailing (γ_d = 1.3 to 1.6 Mg/m³)	≈ 0	5.5m	---	---	Grid pattern Complete dissipation of of pwp averaged 24 hours

NOTE: Several other articles have been written on the use of explosives to compact soil However, porewater pressures were not measured or reported and therefore are not included in Table V.

Table 2.6 Reference summary of published research on liquefaction of saturated cohesionless soil pits away from blast.

FIELD TESTS: Sand Pit Away From Blast

CASE No.	AUTHOR OF ARTICLE	TYPE OF LOADING	SOIL TYPE AND DENSITY	DEGREE OF WATER SATURATION (%)	RESIDUAL PORE WATER PRESSURE (kPa)	PEAK PORE WATER PRESSURE (kPa)	PEAK PARTICLE VELOCITY (m/sec)	COMMENTS
VI-1	Perry (1972)	100 tons - 97.5 m away	uniform sand (Dr: 6 to 64%)	--- < 100	---	---	---	no liquefaction observed
VI-2	Rischbieter, Corvin, Metz & Schaepermeier (1977)	1.25kg/borehole 4m away	fine sand	≠ 100	20	50	---	negative and positive liquefaction for successive blasts

Table 2.7 Reference summary of published research on liquefaction of saturated cohesionless soil for line explosives.

FIELD TEST: LINE EXPLOSIVES

CASE No.	AUTHOR OF ARTICLE	TYPE OF LOADING	SOIL TYPE AND DENSITY	DEPTH TO GROUND WATER TABLE (m)	RESIDUAL PORE WATER PRESSURE (kPa)	PEAK PORE WATER PRESSURE (kPa)	PEAK PARTICLE VELOCITY (m/sec)	COMMENTS
VII-1a	Sanders (1982)	10.3 kg per linear foot of crevasse in boreholes	silty sand	6	---	---	0.10	no liquefaction hazards predicted

Table 2.8 Reference summary of published research on liquefaction of saturated cohesionless soil for small explosives.

FIELD STUDY: SMALL EXPLOSIVES

CASE No.	AUTHOR OF ARTICLE	TYPE OF LOADING	SOIL TYPE AND DENSITY	DEPTH TO GROUNDWATER TABLE (m)	RESIDUAL POREWATER PRESSURE (kPa)	PEAK POREWATER PRESSURE (kPa)	PEAK PARTICLE VELOCITY (m/sec)	COMMENTS
VIII-1	Damitio (1978)	5kg (delayed) buried	loose sand	≈ 0	---	---	---	---
VIII-2	Long, Ries, & Michalopoulos (1981)	3 delayed charges .25 - 9kg in hole	silty sand over sandstone layer	≈ 2	5m rise in piezometer	---	---	---
VIII-3	Carnes (1981)	.5-150kg (buried: 0-1m)	fine & uniform dense sand	0-1.5	none	35	---	Liquefied craters
VIII-4	Trense (1977)	3kg (buried: 11.2m)	med. sand some clay & some shell pieces	1.2	---	---	---	---
VIII-5	Yamamura & Koga (1974)	.2 - 1kg-single (buried: 4-8m)	fine to coarse sand multi-layered (Dr = 50 to 80%)	0-2.3	50	265	---	acc. = 8g 4m away and 6m deep
VIII-6	Studer & Kok (1980)	2.5kg-single (buried: 11m)	loose sand (e ≥ 40%)	≈ 0	40	4	---	---
VIII-7	Klohn, Garga & Shukin (1981)	5kg - 3 charges simultaneous	loose silty sand tailing (γ_d = 1.4-1.6 Mg/m³)	≈ 0	48 at 5m	---		Sand boils
VIII-8	Florin & Ivanov (1961)	5kg (buried: 4.5m)	well graded (n=37-46%)	≈ 0-1	---	---	---	Standard liquefaction test
VIII-9A	Prakash & Gupta (1970)	1kg (buried: 6m)	loose sand	≈ 0	80% of initial $\bar{\sigma}$ at 3m away and 6m deep	---	---	vertical acc. = 1.88g at 10m Liquefaction was not observed
VIII-9B	Prakash (1981)	1-3kg (buried)	sands	≈ 0	48% of initial $\bar{\sigma}$ at 2.5m away	---	---	Liquefaction was not observed

(next page)

Table 2.8 continued

FIELD STUDY: SMALL EXPLOSIVES

CASE No.	AUTHOR OF ARTICLE	TYPE OF LOADING	SOIL TYPE AND DENSITY	DEPTH TO GROUNDWATER TABLE (m)	RESIDUAL POREWATER PRESSURE (kPa)	PEAK POREWATER PRESSURE (kPa)	PEAK PARTICLE VELOCITY (m/sec)	COMMENTS
VIII-10	Ivanov (1967)	5kg single (buried: 4.5m)	loose sand (2.66 Mg/m³)	Near surface ≈ 0	---	3.8m rise in piezometer	---	Liquefaction
VIII-11	Kok (1977)	divided charges in pvc pipe back-filled with sand	loose sand	≈ 0	---	---	---	Liquefaction coefficient $L = \Delta pwp/\bar{\sigma}_i$
VIII-12	Solymar et al. (1984)	multiple simultaneous 40-426 kg (buried: 5 to 20m)	loose alluvium γ_{sat}=123-134 pcf	≈ 0	---	---	.1 to .2	Settlement, residual pwp for 60 minutes
VIII-13	Arya et al. (1978)	10kg single (buried 16m)	Poorly graded sand (Dr: 30%)	10	---	≈ 20% of $\bar{\sigma}_v$	acc. = .6g at 8m away	
VIII-14	Drake (1978)	1.8-7.25kg (single buried)	dense sand (1.59-1.75Mg/m³)	.7	---	+38.5 to +21.4 at 3m	---	Loosened sand, little liquefaction
VIII-15	Dill (1967)	6.3 & 907 kg (surface)	sand with organics and coral sand	below sea level	---	---	---	detonation in water, sand shear strength doubled
VIII-16	Schaepermeier (1978b and c)	50 & 200kg (buried: ≈ 10m)	loose sand	4	60-80	9-18	1.2	Meppen test (under the structure) Acc: peak 100g No liquefaction. Neg. porewater pressure around the structure
VIII-17	Studer, Kok & Trense (1978)	50 & 200kg (buried: ≈ 10m)	loose sand	4	---	up to 50	---	Meppen test (in the free field) No liquefaction Neg. porewater pressure.
VIII-18	Carnes (1981)	.1 to 7.25kg single (buried: 1m)	masonry sand	≈ 0-0.5	1186	---	---	Test in basin 15 x 15 x 1.6m No liquefaction observed
VIII-19	Dowding & Hryciw (1986)	blasting caps (buried: .5m) 1-2 shots in bin	uniform sand Dr = 50%	≈ 0	---	≈15	---	Liquefaction for densification purposes

Table 2.9 Table of constant for estimated radius of liquefaction (Ivanov, 1967).

Soils	Relative Density (%)	K_1
Fine Sand	0 - 20	25 - 15
Fine Sand	30 - 40	9 - 8
Fine Sand	$\geq$ 40	$\leq$ 7
Medium Sand	30 - 40	8 - 7
Medium Sand	$\geq$ 40	$\leq$ 6

Note : K_1 is for single charges

Table 2.10 Empirical Equations Developed to Estimate Peak Stress in Water and Water Saturated Soil

Reference	Equation
Cole (1948)*	$\sigma_{pk} = 54{,}900 \left(\frac{R}{W^{1/3}}\right)^{-1.13}$
Lyakhov (1961)	$\sigma_{pk} = 58{,}900 \left(\frac{R}{W^{1/3}}\right)^{-1.05}$
Drake and Little (1983)	$\sigma_{pk} = 20{,}000 \left(\frac{R}{W^{1/3}}\right)^{-2.35}$
Crawford et al. (1974)	$\sigma_{pk} = 10{,}000 \left(\frac{R}{W^{1/3}}\right)^{-3.00}$

Note: *peak stress in water
σ_{pk} = peak water or porewater pressure in kPa
R = radius in meters
W = charge mass in kg

Table 2.11 Relationship Between Peak Compressive Strain, Velocity, and Peak Stress Generated by a Compressive Shock Wave in a Linear Elastic Media.

ε_{pk} (%)	V_{pk} (m/sec)	σ_{pk} (kPa)	Notes on Residual Porewater Pressure
0.01	0.15	500	no significant increase
0.05	0.75	2,500	liquefaction of loose sand under low effective stress
0.01	1.50	5,000	
1.00	15.00	50,000	liquefaction of dense sand under high effective stress

Notes:
saturated soil at void ratio = 0.7
low effective stress = 86 kPa
high effective stress = 690 kPa
loose sand at 10 percent relative density
dense sand at 80 percent relative density
ε_{pk} = peak compressive strain in percent
V_{pk} = peak particle velocity in m/sec
σ_{pk} = peak stress in kPa

III. LABORATORY SHOCK TESTS ON SAND

The results of laboratory shock tests which we conducted on five saturated cohesionless soils are presented in this chapter. An overview of our equipment, instrumentation, test procedures is also presented.

A. Introduction

The one-dimensional, shock loading system, designed by Charlie and Veyera (1985), was used to investigate the porewater pressure response of five saturated sands subjected to shock loading. The shock apparatus, funded by the United States Air Force Office of Scientific Research (Grant AFOSR-80-0260), is located in the Geotechnical Engineering Research Laboratory of the Civil Engineering Department of Colorado State University. For greater details on the equipment, instrumentation and procedures, see Veyera (1985) and Charlie et al. (1985).

B. Test Equipment and Instrumentation

To simulate an explosive loading condition, high amplitude compressive stress waves with submillisecond rise time to peak are needed. To meet this requirement, the shock loading system is designed to apply a compressive shock wave loading of up to 35,000 KPa to a saturated sand sample. Cross sectional views of the sample container, confining pressure tube, piston, momentum trap and the location of the porewater pressure transducers and pressure ports and valves are shown in Figure 3.1.

Transient and static porewater pressure was measured with porewater pressure transducers. The piezoresistive, silicon diaphragm, strain gauge pressure transducers are air blast transducers modified by

the manufacturer by mounting a small perforated plate over the transducer's casing (Endevco Model 8511a-5KM1). This modification allowed the static and transient porewater pressure to be measured in the sample.

A dual time base digital waveform recorder was used for recording the porewater pressure at two sampling rates: rapid at the beginning as the stress wave passes to record the transient porewater pressure response and then slower to record the residual pore pressure. The computer system to store, manipulate and analyze the data consisted of a desktop computer, a floppy disk device for mass storage, a dot-matrix line printer, and a graphic plotter (Figure 3.2).

Figure 3.3 shows the shock facility prepared for loading. The photograph shows the monentum trap in the foreground, followed by the sample container, the confining pressure tube and the air cannon the background.

C. Physical Properties of the Soils

Several index tests were performed on each sample to investigate various physical properties. All tests were conducted according to the standard laboratory procedures where applicable and include the following:

- grain size analysis (ASTM D422),
- soil classification (ASTM D2487),
- specific gravity (ASTM D854),
- relative density determination (ASTM D2049),
- photomicrograph (Bureau of Reclamation),

- spectrographic analysis (Bureau of Reclamation), and
- skeleton stress-strain curves (Hendron, 1963)

Test results are given in later sections of this report.

The water saturated sand samples used in this experimental investigation represent a two-phase medium. The presence of the solid particles in the water affects the density and the compressibility of the soil-water mixture. These changes in density and compressibility need to be considered in evaluating compressive stress wave propagation velocity, peak stress and peak strain. A procedure presented by Richart et al. (1970) was followed and will be outlined here.

The total mass density, ρ_t, of a fully saturated soil-water mixture can be determined from:

$$\rho_t = \rho_w \frac{G_s + e}{1 + e} \qquad \text{Eq. 3.1}$$

where G_s is the specific gravity of the solid particles, ρ_w is the mass density of water and e is the void ratio defined as the volume of voids divided by the volume of solids.

The compressibility of a fully saturated soil-water mixture, considering the solid particles to be suspended in the water, consists of two contributing factors: the compressibility of the solid particles and the compressibility of the fluid. The mixture compressibility can be determined from:

$$\frac{1}{B_{mix}} = \frac{1}{B_w}\left(\frac{e}{1 + e}\right) + \frac{1}{B_s}\left(\frac{1}{1 + e}\right) \qquad \text{Eq. 3.2}$$

where B_w is the bulk modulus of the water and B_s is the bulk modulus of the soil particles. For quartz particles, B_s is about 30,680 MPa and for distilled, de-aired fresh water at 20 degrees Celsius, B_w is about 2,140 MPa (Richart et al, 1970). It should be noted that the theory of mixtures assumes that the solid particles are suspended in the water. The total stress will be somewhat larger since the solid particles are actually in contact with one another. For small strain conditions, this difference is small and can neglected.

Using the bulk modulus and the total mass density for the mixture, the compressive stress wave propagation velocity through the mixture, V_{mix}, can be found from:

$$V_{mix} = \left[\frac{B_{mix}}{\rho_t} \right]^{0.5} \qquad \text{Eq. 3.3}$$

The value of V_{mix} includes the effects of density and compressibility. Calculated values of V_{mix} for quartz sand (G_s = 2.65) and coral sand (G_s = 2.80) are given in Table 3.1. The values for V_{mix} for the granitic sand and gravels are very similar to those for quartz sand. By substituting V_{mix} for V_c and ρ_t for ρ, Equations 2.7 and 2.8 can also be used to relate peak particle velocity, peak strain and peak stress in a soil-water mixture.

D. Variation of Parameters

The following six parameters were varied in a systematic and controlled manner for this study:

- the initial relative density of the samples,
- the initial effective stress on the samples,
- the shape of the soils grains (subrounded and angular)
- the size of the soil grains (silt, sand and gravel)
- the hardness of the soil grains (quartz, granite and coral)
- the number and intensity of applied shock loads.

The initial relative density of the samples used in the experimental investigations ranged from 0 to 100 percent. To obtain a sample near zero relative density, the sand was placed using a metal funnel. The funnel was slowly lifted upward and simultaneously rotated inside the sample container while keeping the spout about 1.27 cm above the placed material. The preparation of samples at relative densities greater than zero percent and less than one hundred percent was accomplished using a method presented by Ladd (1978) called the undercompaction method. Ten layers of equal weight were placed using the funnel approach described previously. The layers were individually compacted to successively higher percentages of the final sample density, varying linearly by layer. The first layer was five percent undercompacted. The preparation of samples at relative densities of one hundred percent was accomplished by funnel placement followed by vibration of the sample container. Soils were subjected to initial effective stresses ranging from 86 kPa to 690 kPa. The sample's back pressure was maintained at 345 kPa with the confining pressure adjusted according to the required effective stress. The samples were loaded by compressive stress wave loadings between 0.10 MPa and 4.2 MPa per impact.

To evaluate the influence of each factor, a statistical analysis of the data was performed to develop a model for predicting the porewater pressure ratio, PPR (also termed the liquefaction coefficient, L). The porewater pressure ratio is a nondimensionalized factor defined as:

$$PPR = \frac{u_r}{\sigma_o'} \qquad \text{Eq. 3.4}$$

where

σ_o' = the initial effective stress,

u_r = the residual change in porewater pressure after passage of the stress wave.

In nondimensionalized form, the changes in porewater pressure following loading of soils having differing initial effective stress can be compared. The results from laboratory and field investigations can also be compared.

E. Sample Saturation

To ensure full saturation of the sample, carbon dioxide gas was introduced at the sample's bottom and then distilled, de-aired water was slowly introduced. After about three pore volumes of water had passed through the sample, a backpressure Of 345 kPa was applied and the sample's porewater pressure response was "quasistatically" checked to determine the degree of saturation. It was observed that the porewater pressure response decreased with increasing sample density and effective stress. Calculations of the porewater pressure ratio for saturated sands utilizing

methods suggested by Skempton (1954) using skeleton stress-strain relationships, showed similar trends. The C-parameter is defined as

$$C = \Delta u/\Delta\sigma \qquad \text{Eq. 3.5}$$

where Δu is the change in porewater pressure and $\Delta\sigma$ is the change in confining pressure. Lambe and Whitman (1969) present the following relationship to calculate C, where D is the constrained modulus of the soil skeleton and B_{mix} is the bulk modulus of the soil particle and water mixture, and is given by Equation 3.2.

$$C = 1/(1 + D/B_{mix}) \qquad \text{Eq. 3.6}$$

Utilizing Equations 3.2 and 3.6 and laboratory tests to obtain the constrained modulus, the theoretical C-parameter for 100 percent saturation may be found. Increases in the contrained modulus of the soil skeleton will affect the C-parameter by lowering its value below 1.0 (Lee et al., 1969). When the C-parameter was close to its theoretical value, the soil was considered saturated. Measured compressive stress wave propagation velocities through the samples also showed they were saturated at C values close to that given by Equation 3.6.

F. Quartz Beach Sand (Monterey 0/30, California)

Shock testing was conducted by Veyera (1985) to evaluate residual porewater pressure increases and liquefaction potential of Monterey No. 0/30 sand as a function of peak shock induced compressive strain, soil density, and effective stress. Details of the grain size analysis, classification and relative density tests are given by Muzzy (1983) and Charlie et al. (1985). The soil was tested at four relative densities of 0, 20, 40 and 80 percent under four effective stresses of 86, 172, 345 and 690 kPa. The sand's characteristics are summarized below and in Appendix A.1.

1. Grain Size Distribution and Grain Shape

Monterey No. 0/30 is a fine, uniform, poorly graded sand (SP) with less than one percent of the material being finer than 0.150 mm. The D_{50} particle size is 0.45 mm. The coefficients of uniformity and curvature are 1.65 and 1.00, respectively. The grain shape is subrounded to subangular.

2. Shock Induced Porewater Pressure Ratio

To evaluate the influence of initial effective stress, initial sample density and applied compressive strain, a statistical multivariate regression analysis of the data was performed to develop a model for predicting the porewater pressure ratio, PPR, defined in Equation 3.4. A summary of numerical results of all samples tested is given in Tables A.2 through A.12.

The statistical best fit of all the models examined is:

$$PPR = (16.30)\ (\Sigma\varepsilon_{pk})^{.331}\ (\sigma_o')^{-.308}(D_r)^{-.179} \qquad \text{Eq. 3.7}$$

where D_r and ε_{pk} are both in percent, and σ_o' is in kPa. The $\Sigma\varepsilon_{pk}$ quantity is the cumulative compressive strain of the sample. For single (first) impacts, it represents the peak strain. For multiple strains under undrained conditions, the $\Sigma\varepsilon_{pk}$ term represents the peak strain applied at a given loading plus the peak strain induced during previous impacts. The coefficient of determination (R^2) and the standard error of estimate (S) for Equation 3.7 are 65.9 percent and 0.187, respectively.

The statistical model considering only the data from the first impact loadings from each data set has the following form:

$$PPR = (16.00)\ (\varepsilon_{pk})^{0.331}\ (\sigma_o')^{-0.308}\ (D_R)^{-0.179} \qquad \text{Eq. 3.8}$$

Equation 3.7 is plotted with the experimental PPR vs peak strain in Figure 3.4.

G. Quartz Beach Sand (Tyndall AFB, Florida)

The Tyndall beach sand was obtained at a location 500 m east of the NATO blast facility at Tyndall AFB, Panama City, Florida. The Tyndall beach sand, a fine, subrounded, quartz sand, was shock tested by Hubert (1986) at relative densities of 55, 63 and at 73 percent under an effective stress of 345 kPa. The sand's characteristics are given below and summarized in Table A.14 in Appendix A.2.

1. Grain Size Distribution and Grain Shape

The soil is a uniform, poorly graded material (SP) with a D_{50} size of 0.22 mm. The minimum particle size is greater than 0.075 mm (#200 sieve). The grain shape is subrounded. The coefficients of uniformity and curvature are 1.47 and 1.04, respectively.

2. Shock Induced Porewater Pressure Ratio

A multivariate, regression analysis was not performed due to a limited amount of sand (only 3 tests could be performed). Figure 3.5 shows Veyera's (1985) equation for Monterey No. 0/30 sand relative to the data for the 55, 63 and 75 percent relative density tests under an effective stress of 345 kPa. Veyera's (1985) equation for medium quartz beach sand fits the actual data for the Florida sand quite well. Table A.15 presents the results of the shock tests.

H. Granitic River Sand (Poudre River, Colorado)

The Poudre Valley Sand, an angular granitic sand, was shock tested by Hubert (1986). Nine samples of the Poudre Valley sand were impacted until liquefaction occurred (porewater pressure ratio reached 1.0). The soil was tested at four relative densities of 20, 40, 60 and 80 percent under three effective stresses of 86, 172, and 517 kPa. The sand characteristics are summarized below and given in Table A.16 in Appendix A.3.

1. Grain Size Distribution and Grain Size

The sand is poorly graded (SP) with a D_{50} size of 0.52 mm. The grain shape is angular. The coefficients of uniformity and curvature are 3.85 and 0.95, respectively.

2. Shock Induced Porewater Pressure Ratio

The results were evaluated by using linear regression analysis. The best fitted equation for the data is:

$$PPR = 10.59\ (\Sigma\varepsilon_{pk})^{.429}\ (\bar{\sigma})_o^{-.171}\ (D_r)^{-.181} \qquad \text{Eq. 3.9}$$

The coefficient of determination (R^2) and the standard error of estimate (S) are 61.0% and 0.2114 respectively.

In Table A.17, the results of the nine tests may be found. In Figure 3.6, Equation 3.9 is plotted with the combined data.

Most tests were found to liquefy upon the first impact when peak compressive strains exceeded 0.2 percent. Liquefaction could not be induced even under multiple impacts if the strains were less than 0.01 percent. Between 0.01 and 0.2 percent strain, the number of impacts

required to induce liquefaction was found to be a factor of strain amplitude, initial effective stress and initial relative density.

I. Granitic River Fine Sand and Gravel (Poudre Valley, Colorado)

Shock testing was conducted by Chouicha (1987) to evaluate the effects of grain size (fine sand vs gravel) on the liquefaction potential. Tests were conducted on samples of Poudre Valley sand and gravel sieved and recombined to give the desired grain size distribution. Each soil was tested at relative densities of 30 and 70 percent under effective stresses of 207 and 345 kPa. The fine sand and gravel characteristics are summarized below and given in Table A.18 in Appendix A.4.

1. Grain Size Distribution, Fine Sand

The sand is uniform, poorly graded (SP) with a minimum particle size greater than 0.075 mm (#200 sieve). The grain shape is angular, the D_{50} particle size for this material is 0.20 mm. The coefficients of uniformity and curvature are 1.50 and 1.11, respectively.

2. Grain Size Distribution, Gravel

The gravel is uniform, poorly graded soil (GP) with less than 4 percent of the material being finer than 4.75 mm (#4) and the D_{50} particle size is 8.9 mm. The grain shape is angular. The coefficients of uniformity and curvature are 1.50 and 1.07, respectively.

3. Shock Induced Porewater Pressure Ratio

Figures 3.7 and 3.8 show the effect of mean grain size on the porewater pressure ratio and the liquefaction potential for the fine sand, the gravel and for data from both combined. The general trend is for gravel to be more resistant to liquefaction. In other words, the pore pressure ratio increases with decreasing mean grain size at a given sample sum of the peak strains. The test results are given in Tables A.19 to A.22.

The best fit statistical models have the following forms:

Fine Sand Data

$$PPR = 114.82\ (\Sigma\varepsilon_{pk})^{0.518}\ (\sigma_o')^{-0.329}\ (D_r)^{-0.380} \qquad \text{Eq. 3.10}$$

(R^2 = 94.3 percent and S = 0.0353)

Gravel Data

$$PPR = 15.85\ (\Sigma\varepsilon_{pk})^{0.400}\ (\sigma_o')^{-0.236}\ (D_r)^{-0.119} \qquad \text{Eq. 3.11}$$

(R^2 = 92.9 percent and S = 0.0329)

All Data (fine sand and gravel)

$$PPR = 34.67\ (\Sigma\varepsilon_{pk})^{0.44}\ (\sigma_o')^{-0.264}\ (D_r)^{-0.236} \qquad \text{Eq. 3.12}$$

(R^2 = 91.2 percent and S = 0.0387)

Equations 3.10, 3.11 and 3.12 are plotted on Figures 3.7, 3.8 and 3.9, respectively.

J. Coral Beach Sand (Eniwetok, South Pacific)

Shock testing was conducted by Hubert (1986) to evaluate the residual porewater pressure increases and liquefaction potential of coral sand. The soil was tested under relative densities of 0, 20, 40, 60, 80 and 100 percent under effective stresses of 172, 345, and 517 kPa. The Eniwetok coral sand was furnished by the Air Force Weapons Laboratory in Albuquerque, New Mexico and by the U.S. Army Waterways Experiment Station in Vicksburg, Mississippi. The coral sand characteristics are summarized below and given in Table A.23 in Appendix A.5.

1. Grain Size Distribution and Grain Shape

The physical properties of the sand were included with the sand shipment and were used for this experiment. The grain size analysis indicates a uniformly graded sand (SP), D_{50} equal to 0.48 mm and no particles smaller than the number 200 sieve (0.075 mm). The grain shape is subrounded to subangular. The coefficients of uniformity and curvature are 1.66 and 1.09 respectively.

2. Induced Porewater Pressure Ratio

A summary of the tests results are given in Tables A.24 to A.29 and plotted in Figure 3.10. The best fit data for the PPR is:

$$PPR = 5.81\ (\Sigma\varepsilon_{pk})^{0.429}\ (\sigma'_o)^{-0.176}\ (D_R)^{-0.022} \qquad \text{Eq. 3.13}$$

with R^2 equal to 61.6 percent and S equal to 0.272.

K. Summary

Four saturated cohesionless sands and one gravel were subjected to compressive shock wave loading. The best fit multivariate regression model to predict the PPR as a function of peak strain, effective stress and relative density for each soil tested are:

Monterey No. 0/30 (Subrounded Quartz Sand, D_{50} = 0.45 mm)

$$PPR = (16.30)\ (\Sigma\varepsilon_{pk})^{.331}\ (\sigma_o')^{-.308}\ (D_R)^{-.179} \qquad \text{Eq. 3.7}$$

Tyndall AFB Sand (Subrounded Quartz Sand, D_{50} = 0.22 mm)

(multivariate regression not conducted - Eq. 3.7 fits data)

Poudre Valley Sand (Angular Granitic Sand, D_{50} = 0.52 mm)

$$PPR = (10.59)\ (\Sigma\varepsilon_{pk})^{.429}\ (\sigma_o')^{-.171}\ (D_R)^{-.181} \qquad \text{Eq. 3.9}$$

Poudre Valley Fine Sand (Angular Granitic Sand, D_{50} = 0.20 mm)

$$PPR = (114.82)\ (\Sigma\varepsilon_{pk})^{.518}\ (\sigma_o')^{-.329}\ (D_R)^{-.380} \qquad \text{Eq. 3.10}$$

Poudre Valley Gravel (Subangular Granitic Sand, D_{50} = 0.90 mm)

$$PPR = (15.85)\ (\Sigma\varepsilon_{pk})^{.400}\ (\sigma_o')^{-.236}\ (D_R)^{-.119} \qquad \text{Eq. 3.11}$$

Coral Sand (Subrounded Coral Sand, D_{50} = 0.48 mm)

$$PPR = (5.81)\ (\Sigma\varepsilon_{pk})^{.429}\ (\sigma_o')^{-.176}\ (D_R)^{-.022} \qquad \text{Eq. 3.13}$$

where ε_{pk} and D_r are in percent and σ_o' is in kPa.

To compare these multivariate regression models, the PPR predicted by each of these equations are plotted on Figure 3.11 as a function of peak strain for D_R = 50% and σ_o' = 100 kPa. All equations predict liquefaction (PPR = 1) when the peak strain, ε_{pk}, exceeds 0.1 percent.

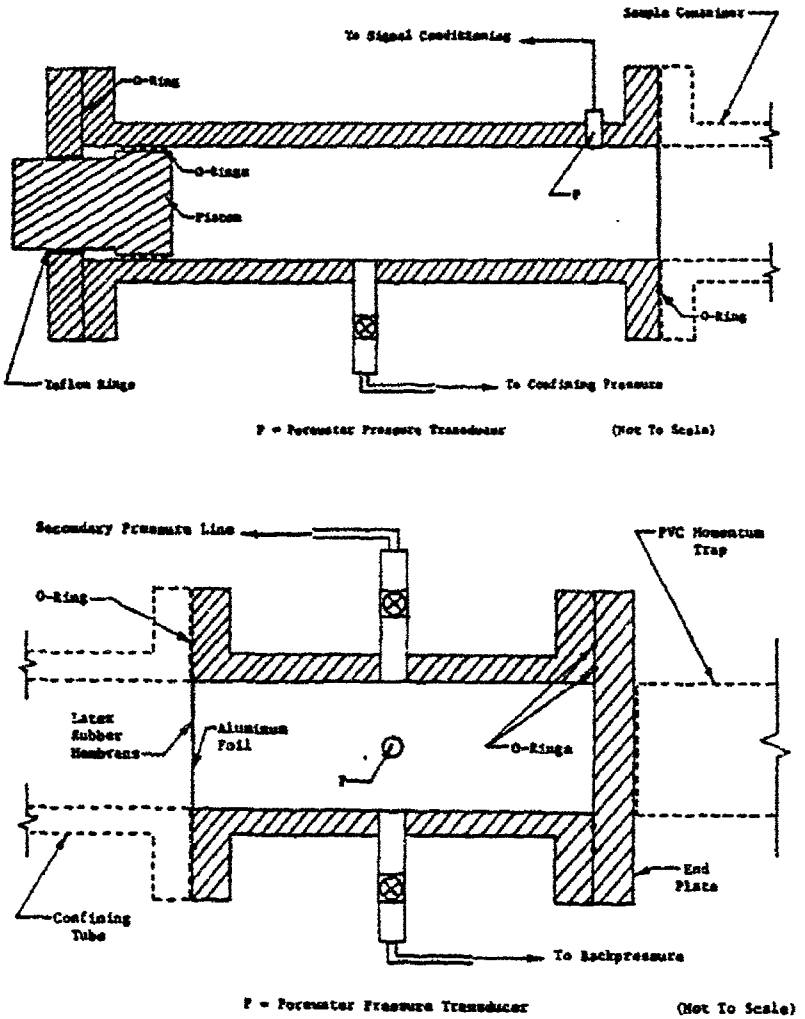

Figures 3.1(a and b) Cross-section of the confining pressure tube and the sample container (Veyera, 1985).

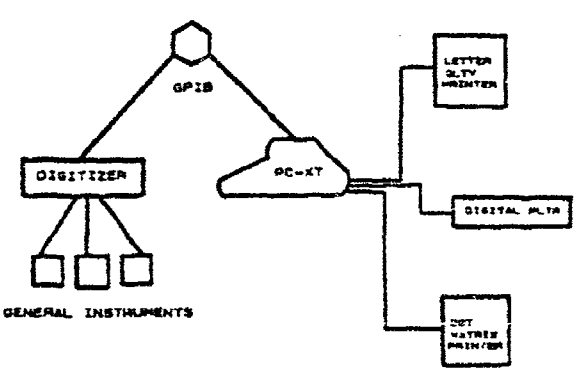

Figure 3.2 Hardware arrangement.

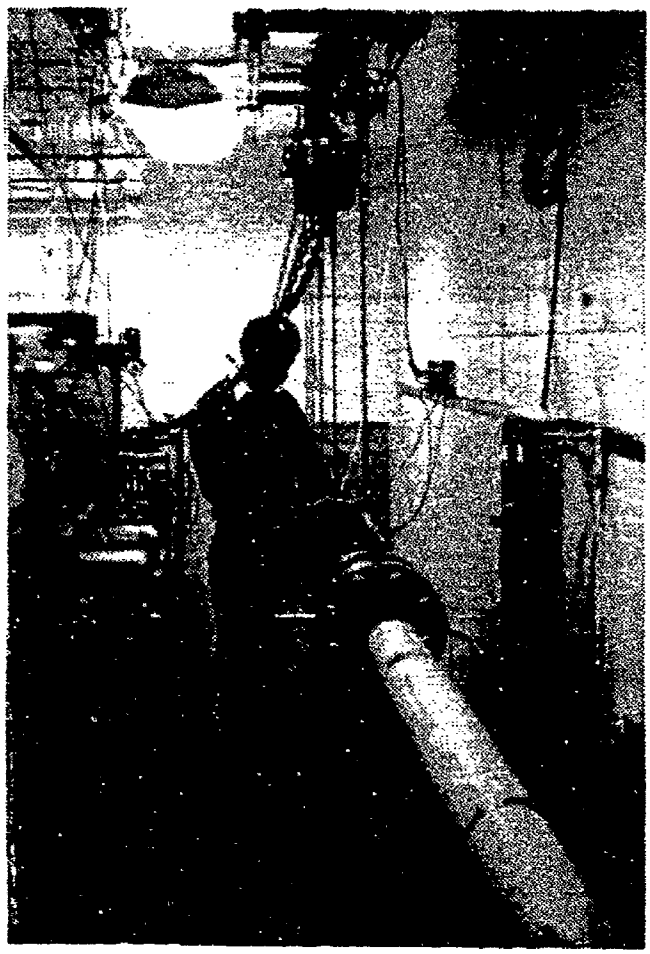

Figure 3.3 Experimental shock facility prepared for loading (view from momentum trap).

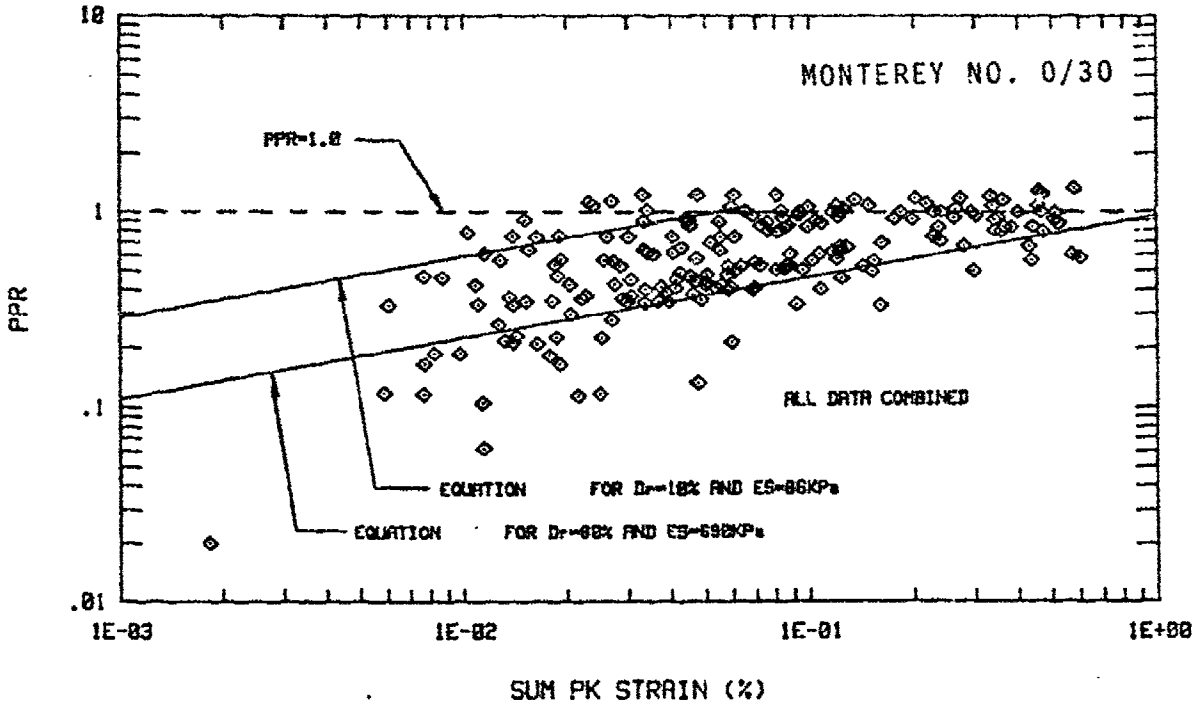

Figure 3.4 Porewater pressure ratio for Monterey No. 0/30 sand as a function of density and effective stress.

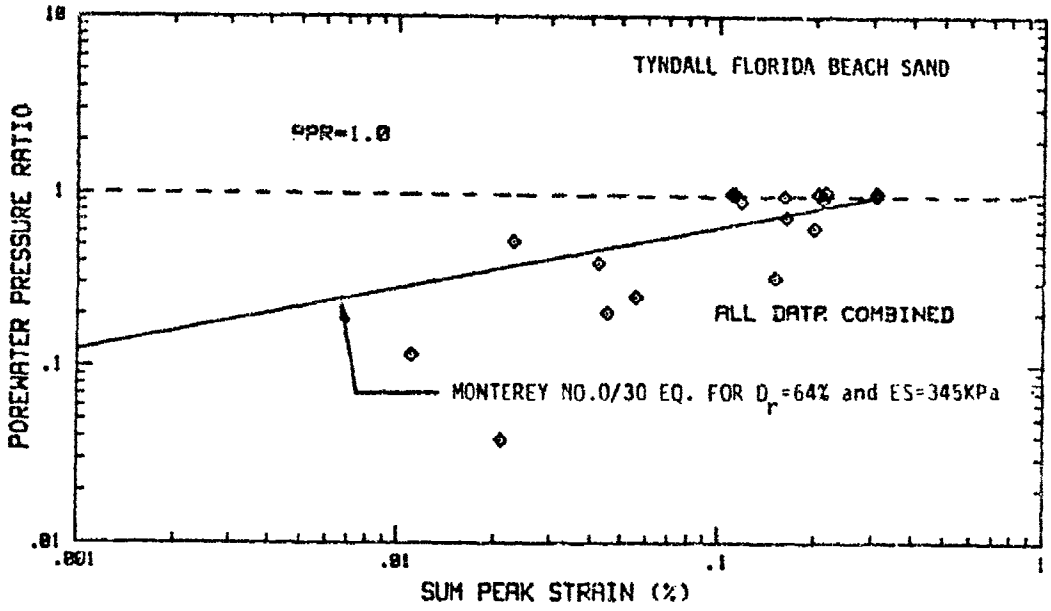

Figure 3.5 Porewater pressure ratio for Tyndall beach sand as a function of the strain.

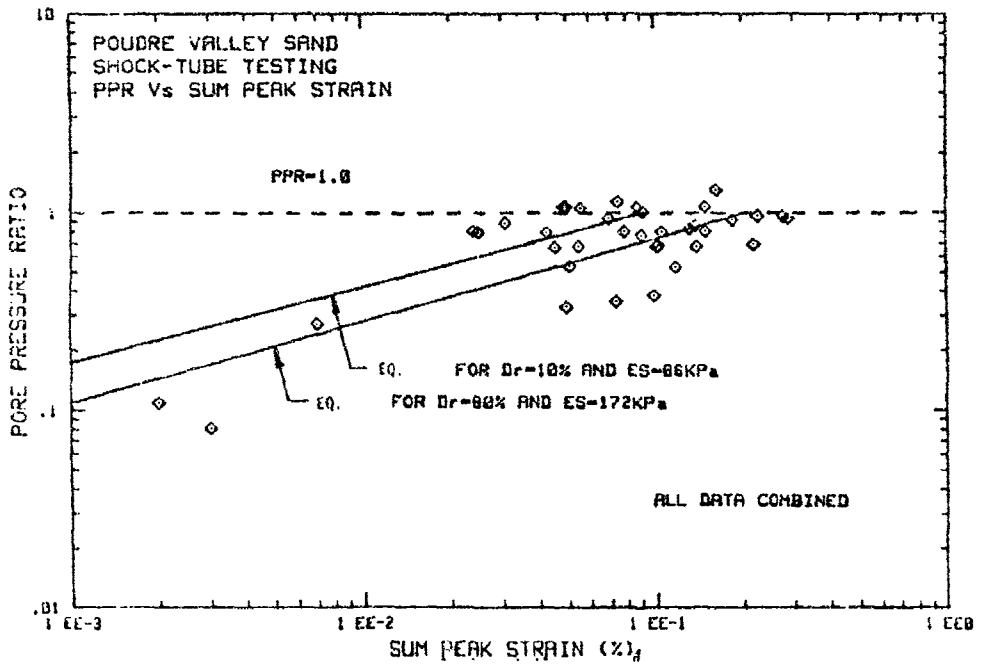

Figure 3.6 Porewater pressure ratio for Poudre Valley Sand as a function of the strain.

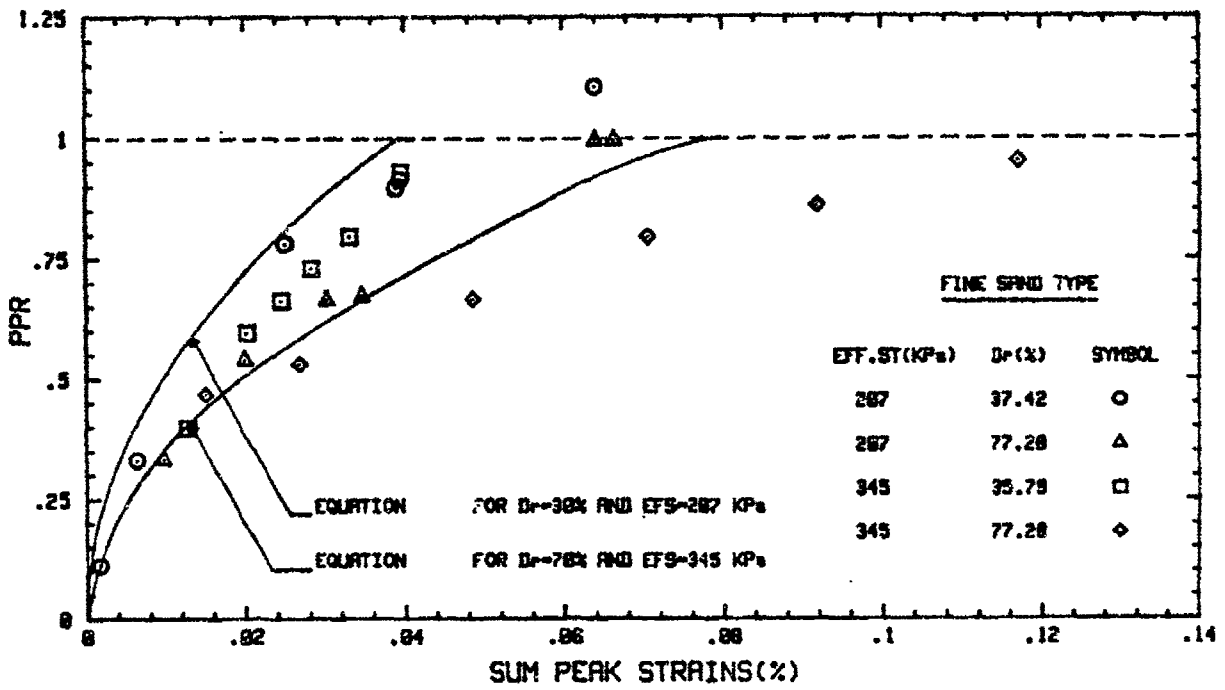

Figure 3.7 Porewater pressure ratio as a function of the sum of the peak strains for all data of fine sand.

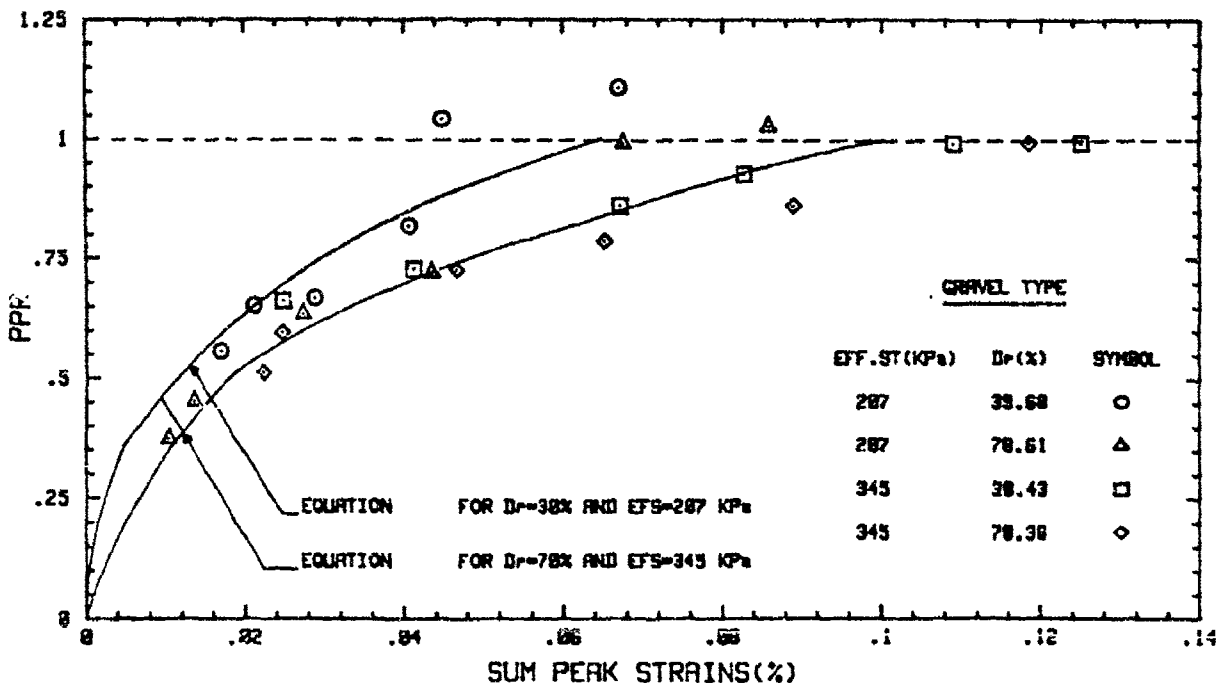

Figure 3.8 Porewater pressure ratio as a function of the sum of the peak strains for all data of gravel.

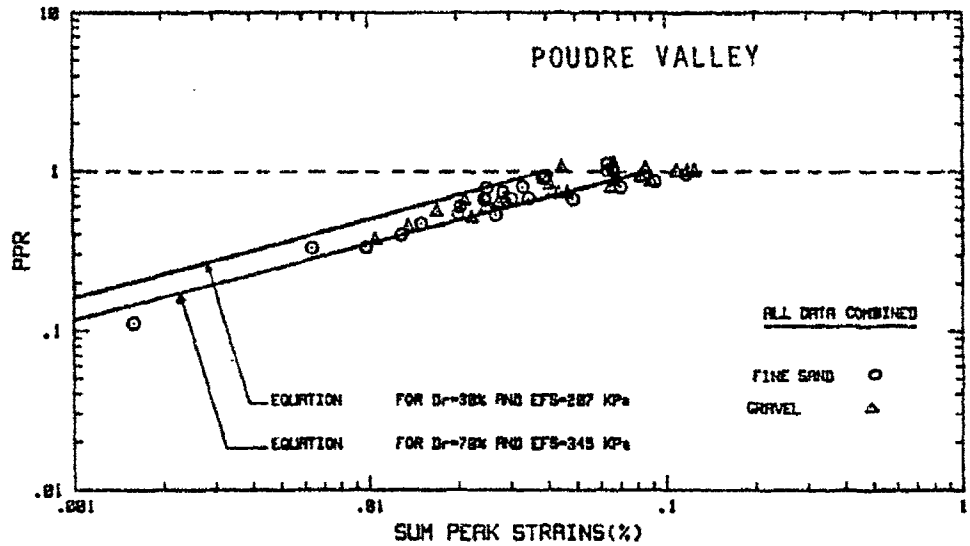

Figure 3.9 Porewater pressure ratio as a function of the sum of the peak strains, Poudre Valley fine sand and gravel.

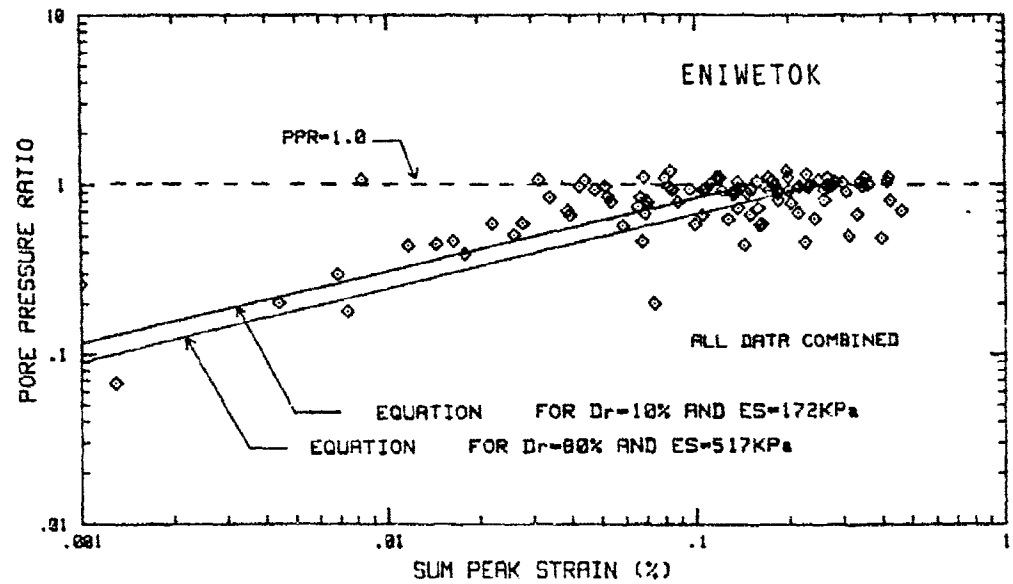

Figure 3.10 Porewater pressure ratio for Eniwetok coral sand as a function of the strain, relative density and effective stress.

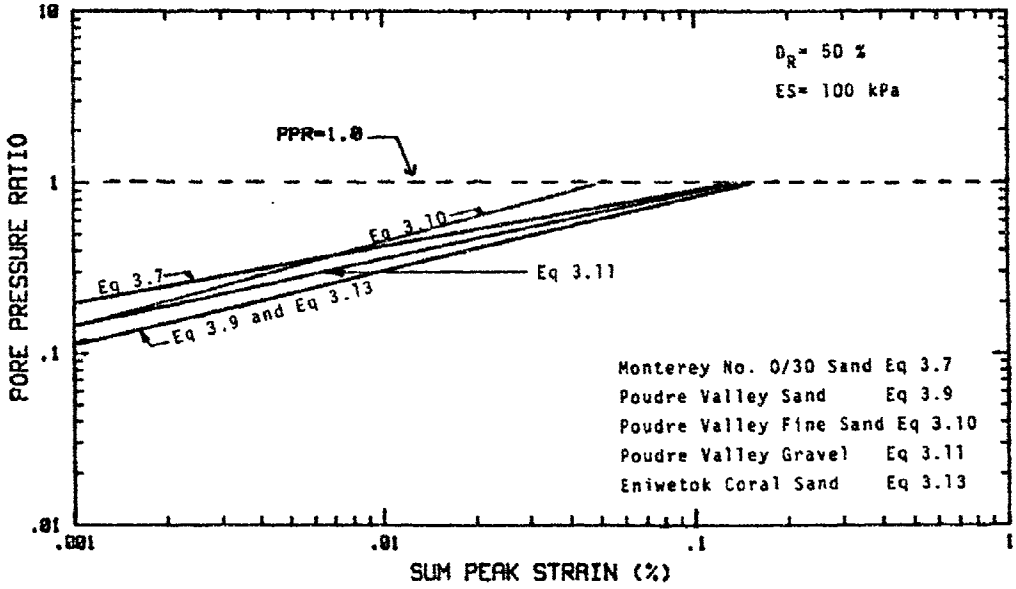

Figure 3.11 Porewater pressure ratio as a function of the strain for the five soils tested (D_R = 50% and σ'_o = 100 kPa).

Table 3.1 (a) Stress Wave Propagation Parameters for Quartz Sand (G_s = 2.65)

e	ρ_t (Kg/M^3)	B_{mix} (KPa)	V_{mix} (M/sec)	V_{mix}/V_w	$\rho_t V_c$ ($Kg/(M^2-sec)$)
.803	1915	4421407	1519	1.013	2908885
.779	1926	4485912	1526	1.017	2940602
.755	1940	4554171	1532	1.021	2972080
.731	1953	4626521	1539	1.026	3005667
.707	1967	4703343	1546	1.031	3040982
.683	1980	4785064	1555	1.037	3078900
.659	1995	4872167	1563	1.042	3118185
.635	2009	4965202	1572	1.048	3158148
.611	2024	5064797	1582	1.055	3201968
.587	2040	5171672	1592	1.061	3247680
.563	2056	5286654	1604	1.069	3297824

Table 3.1 (b) Stress Wave Propagation Parameters for Coral Sand (G_s = 2.80)

e	ρ_t (Mg/m³)	B_{mix} (MPa)	V_{mix} (m/s)	V_{mix}/V_w
.818	1.541	4579	1724	1.149
.797	1.560	4640	1725	1.150
.777	1.579	4702	1726	1.151
.755	1.598	4774	1728	1.152
.735	1.617	4843	1730	1.153
.713	1.637	4922	1734	1.156
.693	1.657	4999	1737	1.158
.673	1.676	5080	1741	1.161
.652	1.698	5170	1745	1.163
.631	1.720	5267	1750	1.167
.609	1.743	5374	1756	1.171

IV. LABORATORY SHOCK AND QUASI-STATIC TESTS ON SILT

This chapter summarizes our results of uniaxial quasi-static and shock loading laboratory tests conducted by Bolton (1988) on saturated quartz beach sand, on saturated clayey silt and on saturated sand clayey silt mixtures. These tests were run at the request of DNA.

A. Introduction

Very little information is available about the porewater pressure response of water saturated silts subjected to explosive induced shock waves. To gain needed data, a series of uniaxial laboratory quasi-static and shock loading tests were conducted on a sand, on a clayey silt, and on a sand-clayey silt mixture. Tests were conducted at various initial void ratios and initial effective stresses. The quasi-static tests subjected the samples to slowly increasing confining stress (no inertia effects) and the resultant increase in the sample's porewater pressure was recorded. Following loading the confining stress was slowly reduced to the original value and the decrease in porewater pressure was recorded. The excess porewater pressure after unloading is termed the quasi-static residual porewater pressure. The shock loading tests subjected the sample to a transient compressive shock wave having submillisecond rise time to peak and the resultant increase in the sample's porewater pressure was recorded. The excess porewater pressure after the stress wave has passed is termed the shock induced residual porewater pressure.

B. Test Equipment and Procedure

The one-dimensional, confined loading system, designed by Charlie, Veyera and Muzzy (1982) and used by Charlie, et al. (1985), was utilized by Bolton (1988) for this research. Details of the experimental equipment and instrumentation, as well as the experimental set-up and testing procedures, are discussed briefly in Chapter III of this report. Full details can be found in Charlie et al. (1985).

C. Test Instrumentation

To measure the porewater pressure time history, special porewater pressure transducers and high speed recording systems were utilized. These components are discussed briefly in the following sections.

1. The Porewater Pressure Transducers

Piezoresistive porewater pressure transducers were used to measure quasi-static transient and static porewater pressure. The piezoresistive, silicon diaphragm, strain gauge pressure transducers are air blast transducers modified by the manufacturer by mounting a stainless steel perforated plate over the transducer's pressure sensor (ENDEVCO Model 8511a-5KM1) . This modification allowed the sample's porewater pressure to be measured.

2. Data Recording System

For the quasi-static tests, a strip-chart recorder was utilized to record both the applied pressure and the sample's porewater pressure response. For the shock tests, a dual time base digital waveform recorder was used for recording the applied pressure the the sample's porewater

pressure at two sampling rates, rapid at the beginning as the stress wave passes to record the transient porewater pressure response and then slow to record the residual pore pressure were used. The computer system to store, manipulate and analyze the data consisted of a desktop computer, a floppy disk device for mass storage, a dot-matrix line printer, and a graphics plotter.

D. Physical and Index Properties of the Soils

Basic physical and index properties for Monterey No. 0/30 sand, Bonny silt and the sand-silt mixture are given in Table 4.1. The sand-silt mixture consisted of equal weights of Monterey No. 0/30 sand and Bonny silt. Monterey No. 0/30 sand is a poorly graded, sub-rounded, quartz beach sand (SP) obtained from Monterey, California and Bonny silt is a wind blown deposit of clayey silt (MC) and is typical of loess deposits found in Colorado, Kansas, Nebraska and Wyoming. The Bonny silt was obtained by the Bureau of Reclamation from the borrow area at Bonny Reservoir in eastern Colorado.

E. Quasi-Static Tests

Samples of sand and sand-clayey silt mixtures were placed at void ratios of 0.66 and 0.80 and samples of clayey silt were placed at a void ratio of 0.95. Figure 4.1 presents the gradation for these three soils. These samples were then consolidated to an initial effective confining stress of 172 kPa. The air dried soil was placed and compacted in ten layers. To ensure uniform soil density, the under compaction method was utilized with the first layer being 5 percent undercompacted and the last layer compacted to the required void ratio. To ensure full saturation,

the soil was first flushed with carbon dioxide gas, a vacuum was applied, then three pore volumes of deaired water was introduced into the bottom of the sample, and a backpressure of 345 kPa was applied to the porewater. Table 4.2 lists the symbols used for the tests listed in the following sections.

1. Sand

The residual porewater pressure results from the quasi-static tests on the saturated sand at void ratios of 0.66 and 0.80 are given in Tables 4.3 and 4.4 Figures 4.3 and 4.4. Figures 4.5, 4.6 and 4.7 present the residual porewater pressure increase and PPR as a function of peak strain. The best fit multivariate regression models are:

$$PPR = 60\ (\Sigma\varepsilon_{pk})^{0.41}\ (\sigma_o')^{-.51}\ (D_R)^{-.14} \qquad \text{Eq. 4.1}$$

$$PPR = 43\ (\Sigma\varepsilon_{pk})^{0.41}\ (\sigma_o')^{-.51} \qquad \text{Eq. 4.2}$$

where ε_{pk} is percent strain, σ_o' is the effective stress in kPa, e is the void ratio and D_r is the relative density in percent.

2. Sand-Clayey Silt Mixture

The results of the quasi-static tests on the saturated Monterey No. 0/30 sand and Bonny silt mixture at void ratios of 0.66 are given in Table 4.5 and Figures 4.8 and 4.9. The best fit multi-regression model is given in Equation 4.3. The sand-clayey silt mixture and the clayey silt were analyzed together since there were no dramatic difference in behavior.

3. Clayey Silt

The results of the quasi-static tests on Bonny silt at a void ratio of 0.95 are given in Table 4.6 and Figures 4.8 and 4.9. The best fit multivariate-regression model is:

$$PPR = 10\ (\Sigma\varepsilon_{pk})^{0.728}\ (\sigma'_o)^{-0.039} \qquad \text{Eq. 4.3}$$

F. Shock Tests

1. Sand

The results of the shock tests on the saturated sand are given in Chapter III in Figures 3.4 and in Appendix A. The best fit regression model is given by Equation 3.7 in terms of peak strain, effective stress and relative density. The best fit multivariate regression model in terms of void ratio effective stress and peak strain is:

$$PPR = 16\ (\Sigma\varepsilon_{pk})^{0.33}\ (\sigma'_o)^{-0.31}\ (D_r)^{-0.18} \qquad \text{Eq. 4.4}$$

$$PPR = 18\ (\Sigma\varepsilon_{pk})^{0.55}\ (\sigma'_o)^{-0.35}\ (D_r)^{-0.18} \qquad \text{Eq. 4.4}$$

2. Sand-Clayey Silt Mixture

The results of the shock tests on the saturated sand-clayey silt mixture are given in Tables 4.7 and Figures 4.10 and 4.11. The best fit multivariate-regression model is the same as for clayey silt, shown in Equation 4.5. These two soils were analyzed together since there were no dramatic differences in behavior.

3. Clayey Silt

The results of the shock tests on the saturated clayey silt at a void ratio of 0.95 are given in Table 4.7 and Figures 4.10 and 4.11. The best fit multivariate regression model for both the sand-clayey silt mixture and the clayey silt is:

$$PPR = 10.2\ (\Sigma\varepsilon_{pk})^{0.728}\ (\sigma_o')^{-0.039} \qquad \text{Eq. 4.3}$$

G. Summary

The tests results indicate that the residual porewater pressure increase for Monterey No. 0/30 sand is approximately the same for both quasi-static and shock loading. The residual porewater pressure increase for both the sand-silt mixture and the clayey silt is greater for quasi-static than for shock loading.

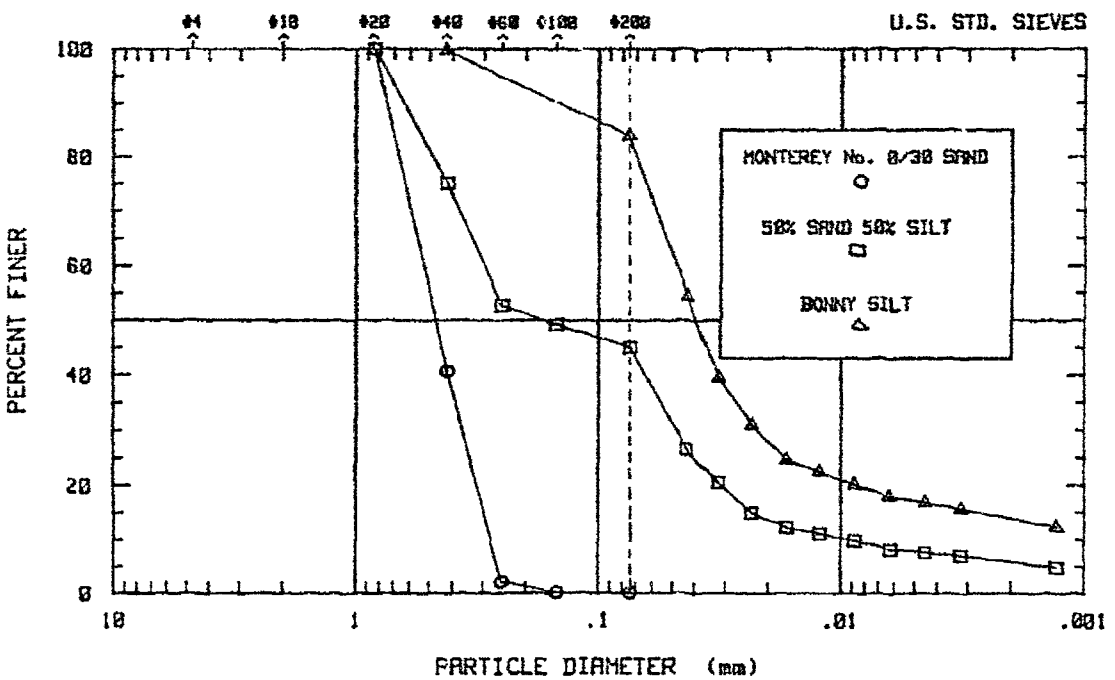

Figure 4.1 Grain size distributions for soils used in this study.

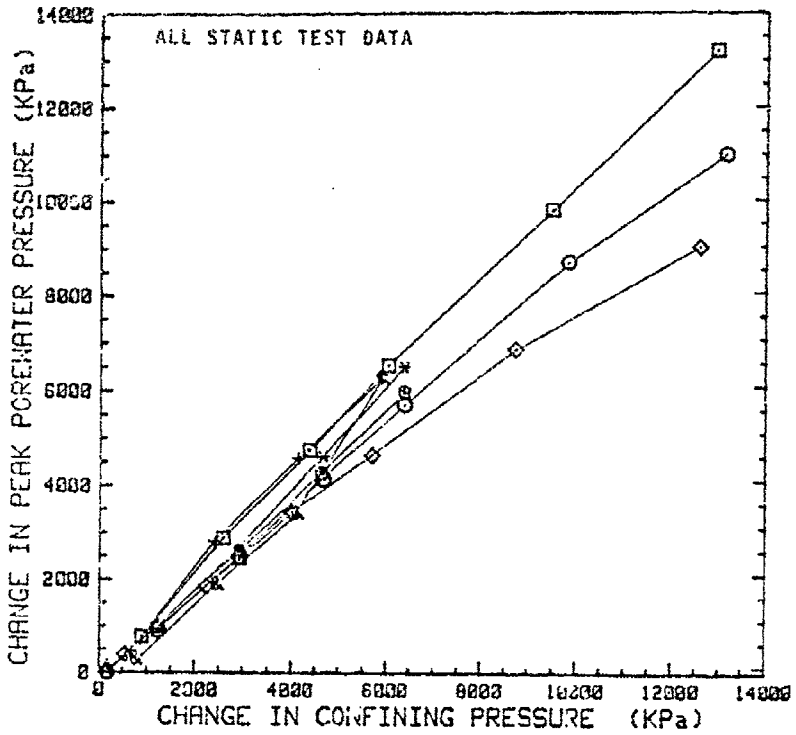

Figure 4.2 Change in peak porewater pressure as a function of the change in confining pressure in terms of soil type, void ratio, and initial effective stress for all static tests.

Table 4.2 List of Symbols for Figures 4.2 to 4.11

Static Tests

- ⊙ Monterey No. 0/30 sand, D_R = 8.61%, effective stress = 172 kPa
- ⊡ Monterey No. 0/30 sand, D_R = 9.11%, effective stress = 517 kPa
- △ Monterey No. 0/30 sand, D_R = 63.37%, effective stress = 172 kPa
- ◇ Monterey No. 0/30 sand, D_R = 63.80%, effective stress = 517 kPa
- * Silty sand, e = 0.669, effective stress = 172 kPa
- + Silty sand, e = 0.669, effective stress = 517 kPa
- @ Bonny silt, e = 0.932, effective stress = 172 kPa
- & Bonny silt, e = 0.939, effective stress = 517 kPa

Dynamic Tests

- ✚ Silty sand, e = 0.627, effective stress = 172 kPa
- $ Bonny silt, e = 0.935, effective stress = 172 kPa

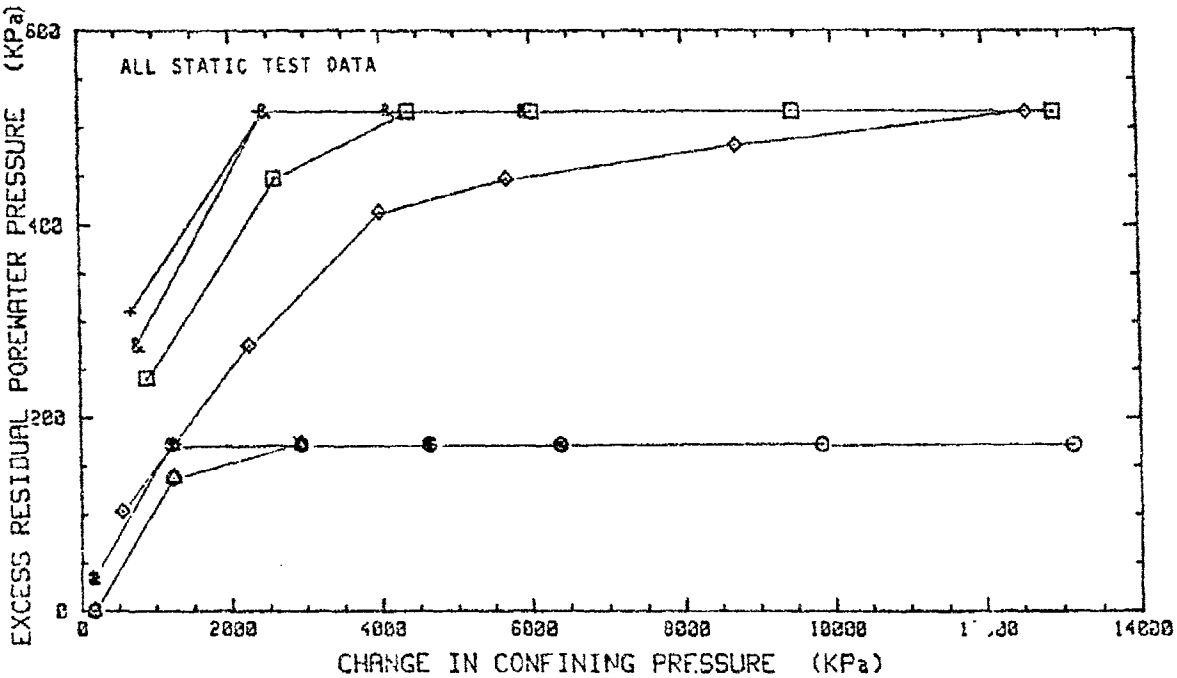

Figure 4.3 Excess residual porewater pressure as a function of the change in confining pressure in terms of soil type, void ratio, and initial effective stress for all static tests.

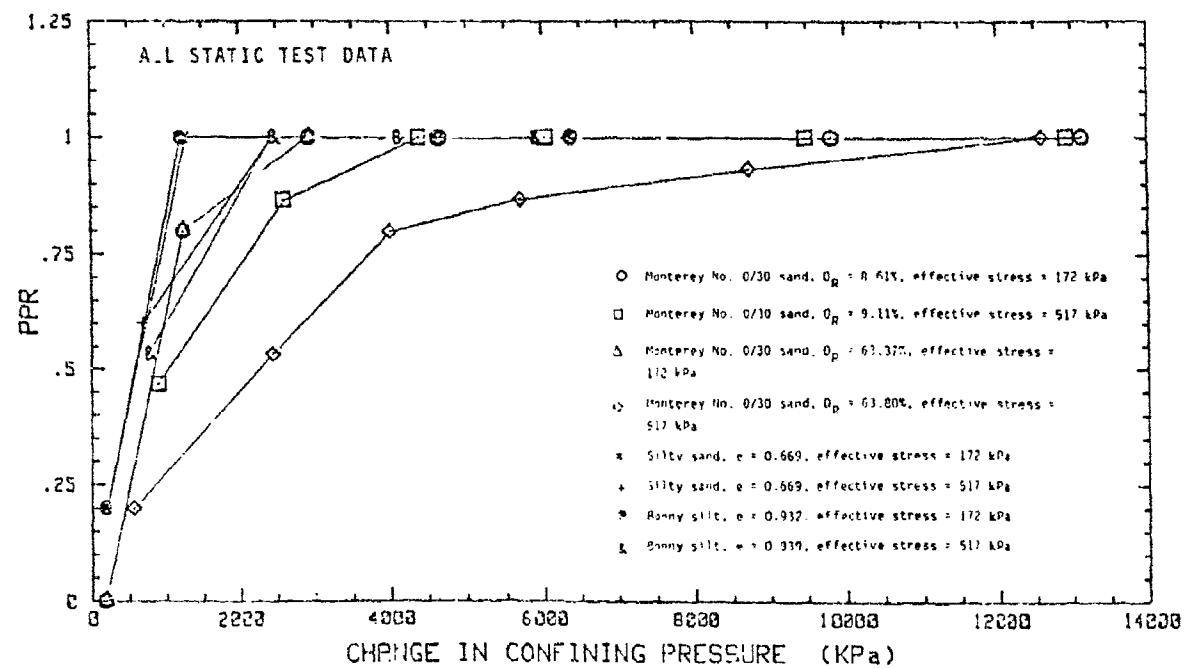

Figure 4.4 Porewater pressure ratio as a function of the change in confining pressure in terms of soil type, void ratio, and initial effective stress for all static tests.

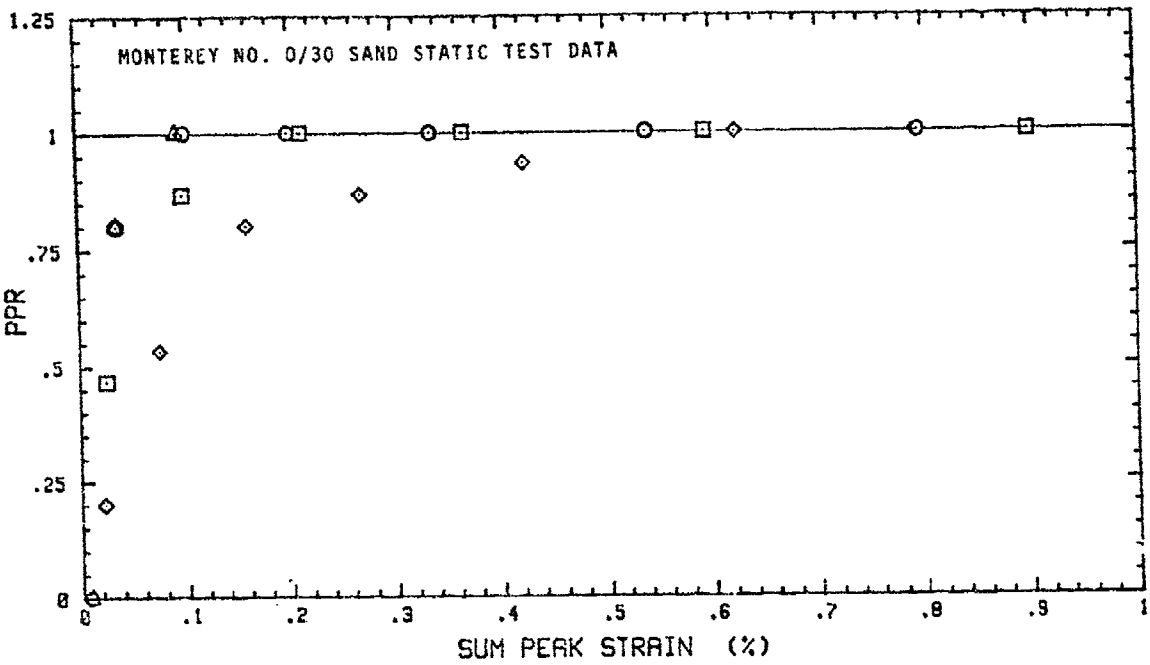

Figure 4.5 Porewater pressure ratio as a function of the sum of the peak sample strain in terms of void ratio and initial effective stress for all Monterey No. 0/30 sand static tests.

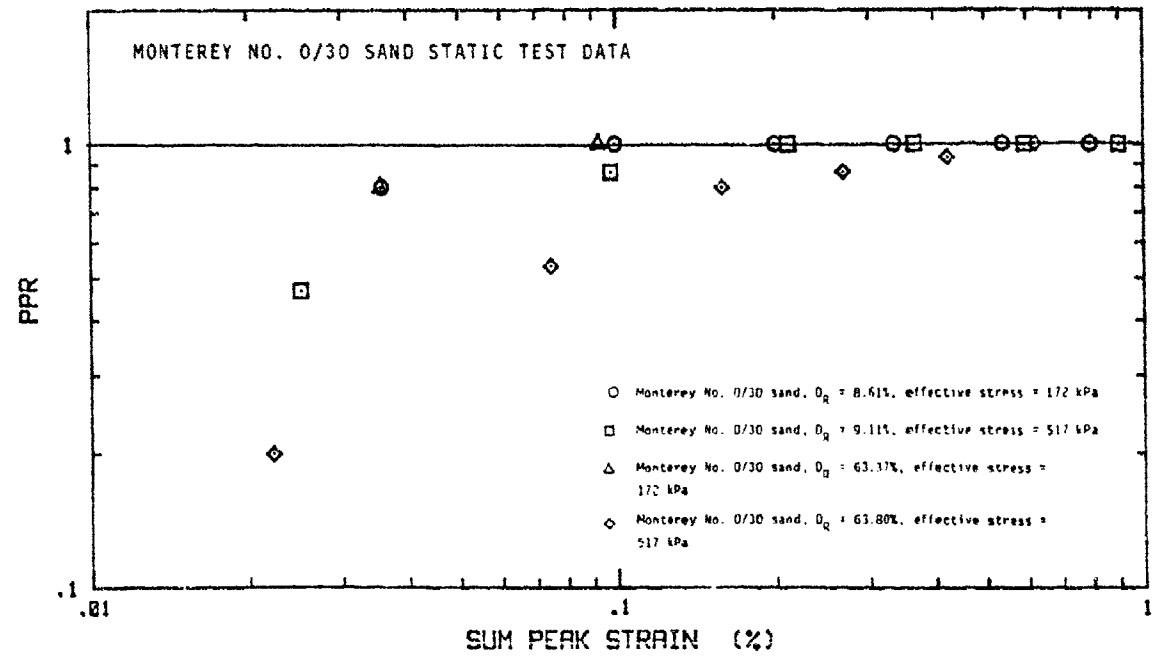

Figure 4.6 Porewater pressure ratio as a function of the sum of the peak sample strain in terms of void ratio and initial effective stress for all Monterey No. 0/30 sand static tests.

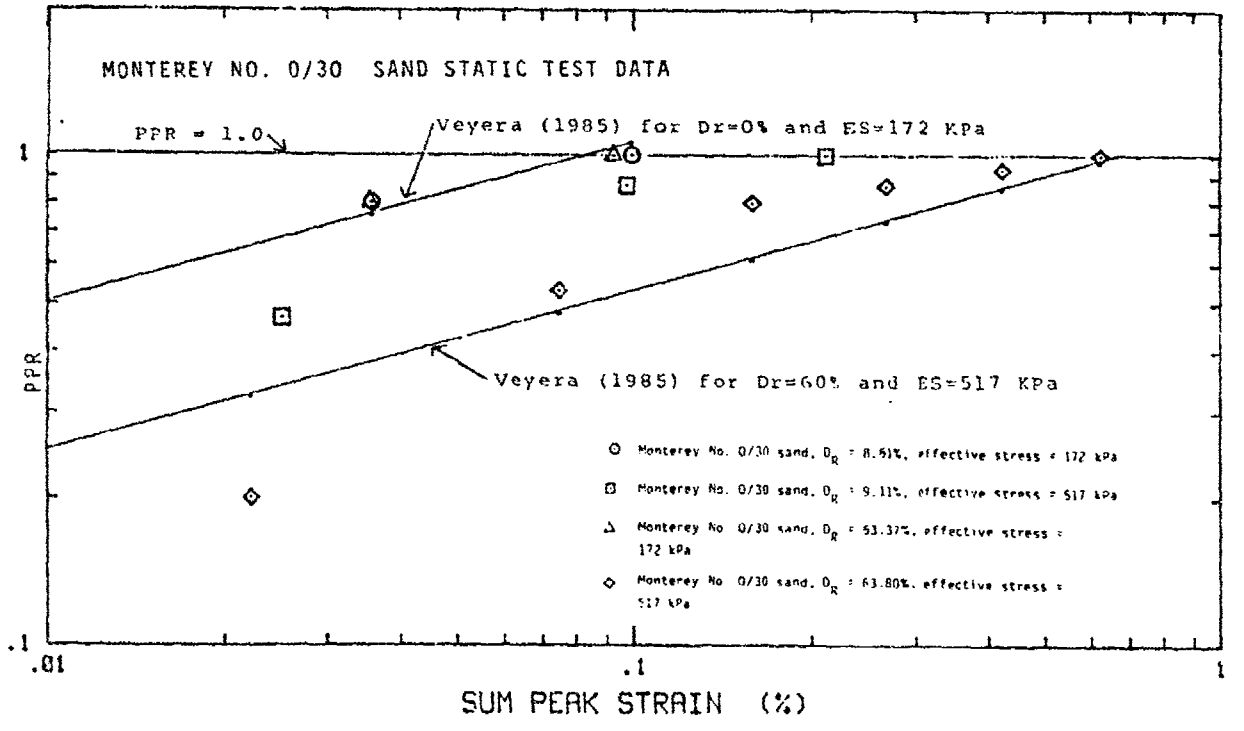

Figure 4.7 Comparison of porewater pressure ratio for static tests as predicted by experimental analysis and Veyera (1985) equation for dynamic tests (Monterey No. 0/30 sand) utilizing D_R.

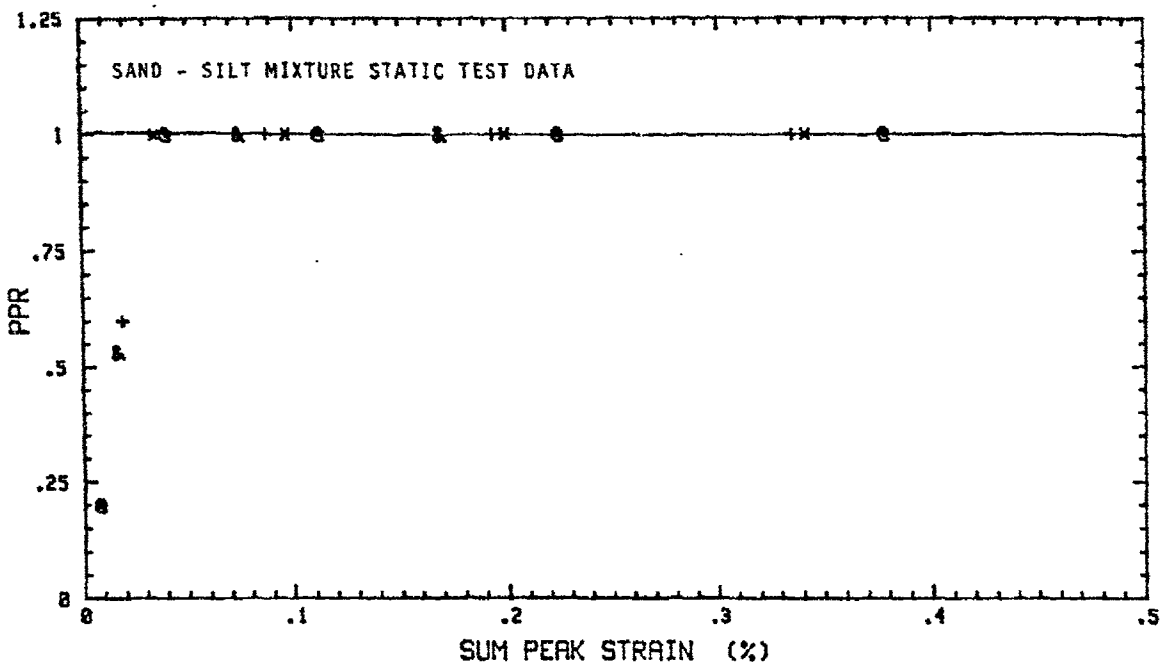

Figure 4.8 Porewater pressure ratio as a function of the sum of the peak sample strain in terms of soil type, void ratio, and initial effective stress for 50% sand, 50% silt and Bonny silt static

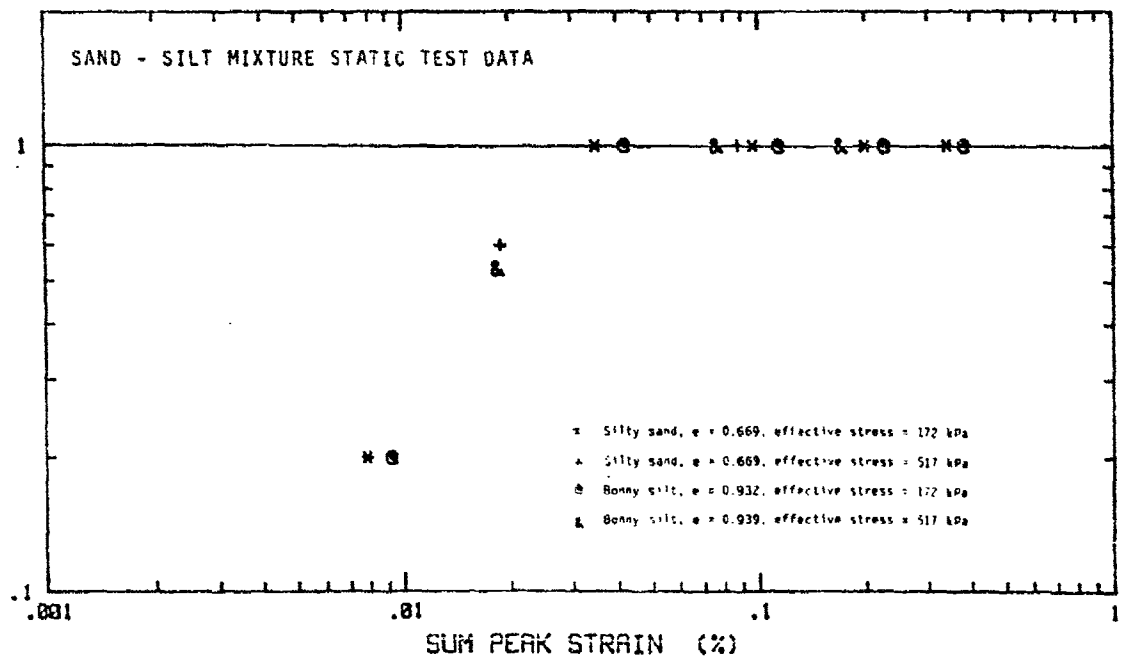

Figure 4.9 Porewater pressure ratio as a function of the sum of the peak sample strain in terms of soil type, void ratio, and initial effective stress for 50% sand, 50% silt and Bonny silt static tests.

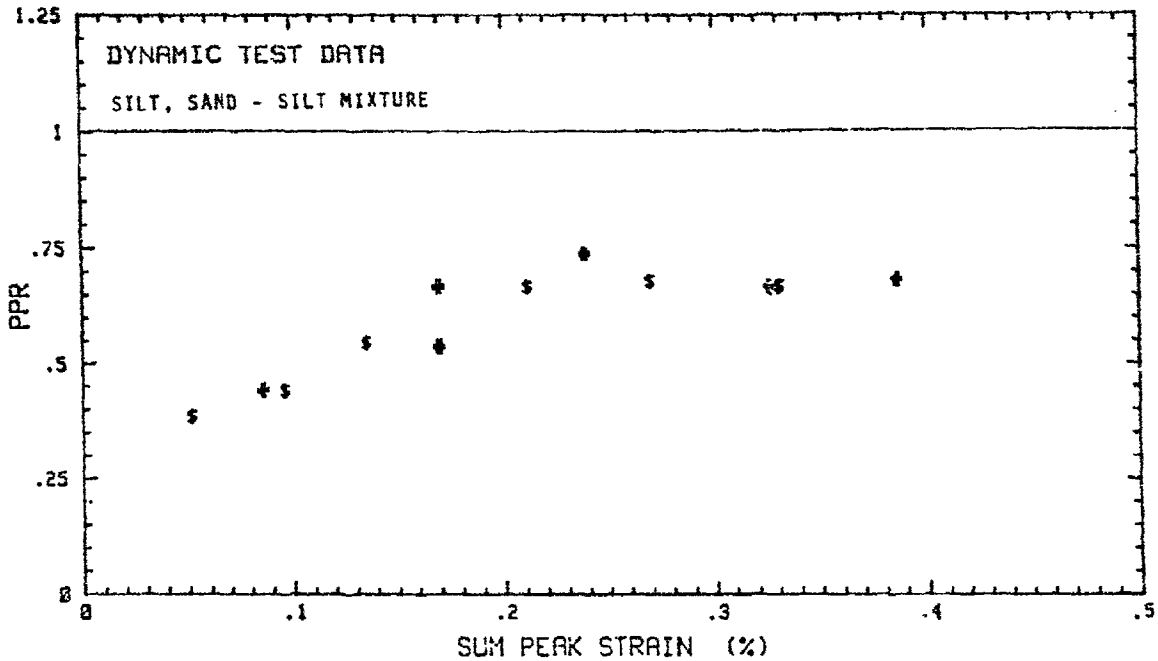

Figure 4.10 Porewater pressure ratio as a function of the sum of the peak sample strains in terms of soil type and void ratio for dynamic tests.

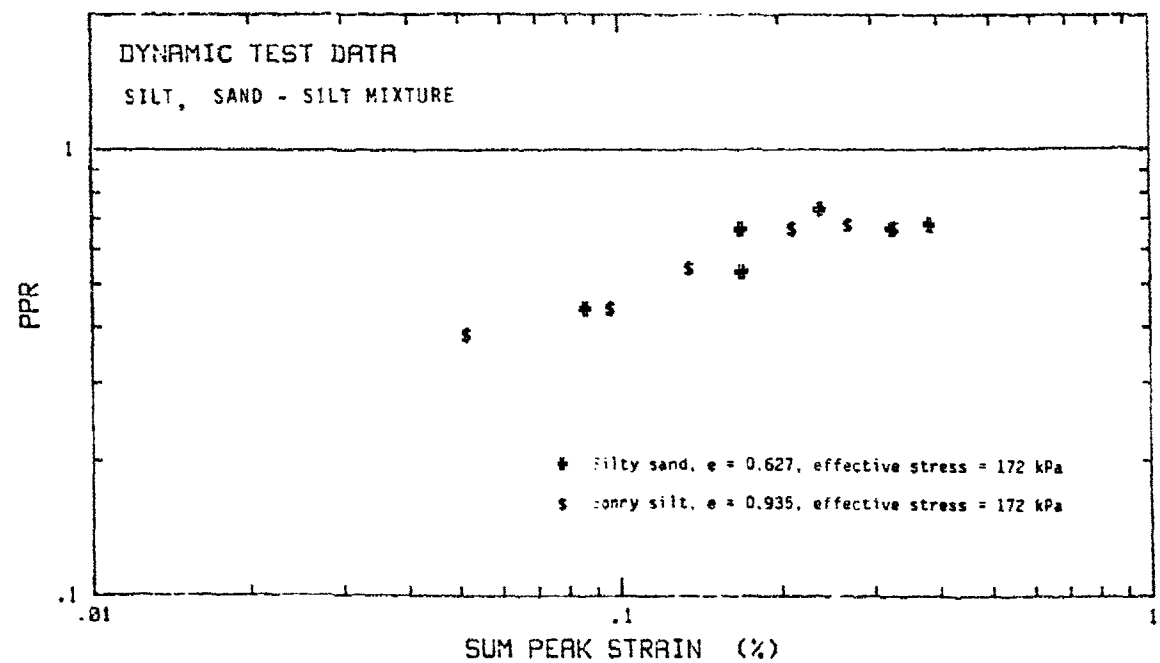

Figure 4.11 Porewater pressure ratio as a function of the sum of the peak sample strains in terms of soil type and void ratio for dynamic tests.

Table 4.1. Physical Properties of Monterey No. 0/30 Sand, Bonny Silt and a 50-50 Mixture of These Soils

	Monterey No. 0/30 Sand	Bonny Silt	50-50 Mixture Sand-Silt
USCS Classification	SP	ML	SM
Specific Gravity	2.65	2.63	2.64
Particle Size Data			
D_{10}	0.29 mm	< 0.001 mm	0.01 mm
D_{30}	0.38 mm	0.025 mm	0.05 mm
D_{50}	0.45 mm	0.04 mm	0.15 mm
C_u	1.65	-	34.1
C_c	1.00	-	0.55
% passing #200 sieve	0.06%	83.9%	45%
% clay size	0%	14	6%
% sand	99.94%	16.1%	5.5%
% silt	0.05%	69.9%	39%
LL	0.06%	25	-
PL	-	21	-
PI	-	4	-
Relative Density	1700 kg/m^3		
max density		-	-
minimum dry density	1470 kg/m^3	-	-
Proctor Test			
Dry Density	-	1730 kg/m^3 @ 14.8% water content	-

Table 4.3. Quasi-static test results - Monterey No. 0/30 sand, D_r = 0% series.

Test ID	INITIAL Confining Pressure (kPa)	INITIAL Water Press. (kPa)	PEAK Confining Pressure (kPa)	PEAK Water Press. (kPa)	END Confining Pressure (kPa)	END Water Press. (kPa)	Resid. PWP Increase	PPR
		NOTE: SAMPLE NOT SATURATED						
D_r = 8.61 %	517	345	689	345	517	345	0	0.00
$\underline{e}$ = 0.783	517	345	1758	1255	517	483	138	0.80
$\bar{\sigma}$ = 172 kPa	517	345	3447	2841	517	517	172	1.00
c = 0.89	517	345	5171	4482	517	517	172	1.00
	517	345	6895	6068	517	517	172	1.00
	517	345	10342	9101	517	517	172	1.00
	517	345	13652	11446	517	517	172	1.00
D_r = 9.11%	862	345	1758	1124	862	586	241	0.467
$\underline{e}$ = 0.782	862	345	3447	3241	862	793	448	0.867
$\bar{\sigma}$ = 517 kPa	862	345	5240	5102	862	862	517	1.000
c = 0.95	862	345	6895	6860	862	862	517	1.000
	862	345	10342	10218	862	862	517	1.000
	862	345	13790	13652	862	862	517	1.000

Table 4.4. Quasi-static test results - Monterey No. 0/30 sand, D_r = 60% series.

Test ID	INITIAL Confining Pressure (kPa)	INITIAL Water Press. (kPa)	PEAK Confining Pressure (kPa)	PEAK Water Press. (kPa)	END Confining Pressure (kPa)	END Water Press. (kPa)	Resid. PWP Increase	PPR
D_r = 63.37 %	517	345	689	427	517	345	0	0.00
$\underline{e}$ = 0.652	517	345	1758	1310	517	482	137	0.800
σ = 172 kPa	517	345	3447	2779	517	517	172	1.000
c = 0.81	517	345	5206	4330	517	599*	*	--
	517	345	6895	4723*	517	599*	*	--
D_r = 63.80%	1207	689	1758	1089	1207	793	104	0.200
$\underline{e}$ = 0.651	1207	689	3447	2565	1207	965	276	0.533
σ = 517 kPa	1207	689	5206	4137	1207	1103	414	0.800
c = 0.80	1207	689	6895	5344	1207	1138	449	0.867
	1207	689	9929	7584	1207	1172	483	0.933
	1207	689	13790	9805	1207	1207	517	1.000

*Water leaked from under foil, do not use.

Table 4.5. Quasi-static test results - 50% Sand - 50% Silt Mixture

Test ID	INITIAL		PEAK		END			
	Confining Pressure (kPa)	Water Press. (kPa)	Confining Pressure (kPa)	Water Press. (kPa)	Confining Pressure (kPa)	Water Press. (kPa)	Resid. PWP Increase	PPR
$\underline{e}$ = 0.669	517	345	689	379	517	379	34	0.200
σ = 172 kPa	517	345	1724	1310	517	517	172	1.000
c = 0.81	517	345	3447	2979	517	517	172	1.000
	517	345	5171	4964	517	517	172	1.000
	517	345	6895	6861	517	517	172	1.000
$\underline{e}$ = 0.669	1034	517	1724	910	1034	827	310	0.600
σ = 517 kPa	1034	517	3447	3344	1034	1034	517	1.000
c = 0.77	1034	517	5171	5102	1034	1034	517	1.000
	1034	517	6895	6861	1034	1034	517	1.000

Table 4.6. Quasi-static test results - Bonny Silt

Test ID	INITIAL		PEAK		END			
	Confining Pressure (kPa)	Water Press. (kPa)	Confining Pressure (kPa)	Water Press. (kPa)	Confining Pressure (kPa)	Water Press. (kPa)	Resid. PWP Increase	PPR
$\underline{e}$ = 0.932	517	345	689	379	517	379	34	0.200
σ = 172 kPa	517	345	1724	1345	517	517	172	1.000
c = 0.81	517	345	3447	2965	517	517	172	1.000
	517	345	5137	4620	517	517	172	1.000
	517	345	6895	6343	517	517	172	1.000
$\underline{e}$ = 0.939	963	448	1758	758	1103	724	276	0.533
σ = 517 kPa	963	448	3447	2379	963	963	517	1.000
c = 0.81	963	448	5102	3896	963	963	517	1.000
	963	448	6895	6757*	963	963*	517*	--

*foil ruptured, data not useable

Table 4.7 Dynamic Test Results - 50% Sand - 50% Silt Mixture and Bonny Silt

Test ID	Effective Stress	Void Ratio	Impact	u_{pk} (KPa)	ϵ_{pk} (%)	PPR
50% sand 50% silt	172kPa	.627	1	4298	.08599	.441
			2	4162	.08328	.666
			3	23*	.00046*	.536*
			4	3438	.06879	.737
			5	4342	.08689	.666
			6	2986	.05974	.682
Bonny Silt	172kPa	.935	1	2126	.05159	.385
			2	1832	.04445	.441
			3	1606	.03896	.544
			4	3121	.07573	.666
			5	2397	.05816	.678
			6	2533	.06146	.668

* All data not read by Biomation

page left blank

V. FIELD EXPLOSIVE TESTS ON PLACED SAND

This chapter summarizes our results of explosive induced planar and spherical stress wave tests on water saturated sand conducted by Bretz (1988), Hassen (1988), and Schure (1988).

A. Introduction

We conducted a series of field explosive tests (21 spherical and 6 planar detonations) on large samples of placed Poudre Valley sand. The tests were designed to systematically evaluate porewater pressure increases and liquefaction of water saturated cohesionless soil subjected to explosive induced compressive stress waves. The soil was tested at three relative densities of 1, 50, and 89 percent for the spherical explosive detonations and at a relative density of 89 percent for the planar explosive detonations. The transient porewater pressure, total stress and acceleration were measured with transducers and recorded with transient data recorders during the passage of the stress wave and the residual porewater pressure after the passage of the stress wave was measured with a piezometer. Predictions based on AFOSR laboratory liquefaction research conducted by Veyera (1985) and Hubert (1986) as described in Chapter III, as well as the empirical models given in Chapter II, are analyzed and compared with the field results.

B. Test Site

We performed the field explosive tests at the explosive test site located at the Colorado State University Engineering Research Center. The facility, developed with AFOSR funding has a State of Colorado blasting

permit and allows control of soil conditions. As shown in Figure 5.1, the large soil sample is located below the regional groundwater table. Locating the sample below the water table minimized potential stress wave reflections from the sample's boundaries.

C. Instrumentation

We instrumented the sand during the sand placement with porewater pressure transducers, accelerometers, and stress gages to record the transient response as a function of distance and charge weight. Piezometers were utilized to obtain the late time porewater pressure response. Digital transient data recorders were utilized to record the response of the embedded instruments and high speed video cameras recorded the tests and the late time porewater pressure response. Strain gages were used to determine the changes in soil density. The exact location of the instrumentation is given by Bretz (1988), Hassen (1988) and Schure (1988).

D. Soil Properties

The tests were conducted on Poudre Valley sand, which is commercially produced by crushing gravel obtained from the Poudre River. This sand has an angular grain shape, a D_{50} grain size of 0.52 mm, a specific gravity of 2.68 and is classified as an SP in the USCS classification system. The physical and index properties are given in Table 5.1 and the gradation is given in Figure 5.2. Details of this material are given in Chapter III, Section H. Quasi-static stress-strain

curves for the sand under uniaxial (k_o) loading conditions are shown in Figures 5.3 and 5.4.

E. Soil Placement and Saturation

The sample size was 4.4 m in diameter by 1.7 m high. The soil volume was 26 m^3 and the dry mass of the sample was approximately 45,000 kg. We placed the sand loose in 0.3 meter thick lifts. Each lift was compacted (if required) with a vibratory compactor to the required dry density. After the final layer was placed, carbon dioxide (CO_2) was introduced to displace the air in the soil voids and to aid in saturating the soil. After the air was displaced, we displaced the CO_2 with water by upward flushing the soil with warm deaired water. Flushing the soil was continued for about two weeks until seismic velocity indicated full saturation ($V_c \cong 1{,}500$ m/sec).

F. Test Procedure

Once the sand was placed and saturated, we added 1.8 m of water above the top of the sample. Explosives were detonated in the water 1.2 m above the sand and 0.6 m below the water surface. Seven spherical and six planar detonations were performed on the saturated sand at a relative density of approximately 89 percent, seven spherical detonations at a relative density of approximately 1 percent and seven spherical detonations at a relative density of approximately 50 percent. Piezoresistive porewater pressure transducers (ENDEVCO Model 8511a-5kM1), resistive total stress cells, and piezoresistive accelerometers were

utilized to measure the soil's porewater pressure, total stress and acceleration during the passage of the explosively induced stress wave. Piezometers were used to measure the residual porewater pressure response. After each explosive detonation, the settlement of the sample was measured and checked against measurements recorded by the strain gages. After the tests were completed, the water was pumped out and the final location of the gages and other objects recorded.

We obtained the explosives from Buckley Power Company of Englewood, Colorado. Detonating cord (Primacord^R manufactured by the Ensign-Bickford Company) was used for the planar detonations. A water gel (Tovex 800^R manufactured by Dupont), was used for the smaller spherical detonations. Tovex 800^R has an energy rating of 894 calories per gram.

G. Planar Stress Wave Test Results

Hassen (1988) conducted explosive field tests on saturated Poudre Valley sand which had been placed at a relative density of 90 percent. To produce a planar compressive stress wave, a 7 m diameter grid of detonating cord (Primacord^R) was placed in the water 1.2 m above the sand's surface. Because the burn speed of detonating cord is approximately 6,700 m/sec, the center of the grid was lifted to ensure a true plane stress wave. The grid was center detonated with an instantaneous electric blasting cap. The detonating cord had spacings of 0.3 m or 0.6 m depending on the detonating cord explosive rating and explosive density required to produc the required peak stress.

Total explosive mass for the six grids detonated ranged from 0.531 to 2.55 kg, giving a charge density ranging from 0.15 to 0.73 gm/m^2. Figure 5.5 shows a typical porewater pressure time history as the stress wave passes through the sample as measured by the piezoresistive porewater pressure transducers. Figure 5.6 shows a typical porewater pressure ratio versus time as measured by the piezometers. Table 5.2 and Figures 5.7 and 5.8 show the measured peak porewater pressure, u_{pk}, and the peak pore pressure ratio, PPR, respectively, as a function of scaled distance. The best fit equations for this test data are:

$$u_{pk} = 30073 \left(\frac{R}{wi}\right)^{-0.342} \qquad \text{Eq. 5.1}$$

$$PPR = 1.11 \left(\frac{R}{wi}\right)^{-0.0844} \qquad \text{Eq. 5.2}$$

where u_{pk} is the peak porewater pressure in kPa, R is distance from charge in meters, and wi is the charge intensity in gm/m^2. The best fit equation for the pore pressure ratio as a function of the peak compressive strain is:

$$PPR = 1.48 \left(\varepsilon_{pk}\right)^{0.29} \qquad \text{Eq. 5.3}$$

where ε_{pk} is the peak strain in percent calculated from Equations 2.7 and 2.8.

H. Spherical Stress Wave Test Results

Bretz (1988) conducted explosive field tests on saturated Poudre Valley sand which had been placed at a relative density of 89 percent. To produce a spherical compressive stress wave, point charges were placed in the water 1.2 m above the center of the soil sample and 0.6 m below the

water surface. Six charge masses ranging from 0.03 kg to 7.02 kg were detonated. Schure (1988) conducted similar tests on saturated Poudre Valley sand on loose sand (D_R = 1%) and medium-dense sand (D_R ≈ 50%). Tables 5.3 and 5.4 and Figures 5.9, 5.10 and 5.11 show the measured PPR as a function of scaled distance ($R/W^{1/3}$) and peak compressive strain, ϵ_{pk}. The best fit equation for the peak porewater pressure for all spherical tests is:

$$u_{pk} = 50{,}000 \left(\frac{R}{W^{1/3}}\right)^{-1.5} \text{ kPa} \qquad \text{Eq. 5.4}$$

The best fit equations obtained by Bretz (1988) for the soil at a relative density of 89 percent are:

$$PPR = 1.15 \left(\frac{R}{W^{1/3}}\right)^{-0.25} \qquad \text{Eq. 5.5}$$

$$PPR = 1.23 \left(\epsilon_{pk}\right)^{0.167} \qquad \text{Eq. 5.6}$$

The best fit equations for the soil at a relative density of about 50 percent are:

$$PPR = 57.2 \left(\frac{R}{W^{1/3}}\right)^{-1.87} \qquad \text{Eq. 5.7}$$

$$PPR = 57.1 \left(\epsilon_{pk}\right)^{1.25} \qquad \text{Eq. 5.8}$$

The best fit equations obtained by Schure (1988) for the soil at a relative density of about 1 percent are:

$$PPR = 177 \left(\frac{R}{W^{1/3}}\right)^{-2.3} \qquad \text{Eq. 5.9}$$

$$PPR = 174 \left(\epsilon_{pk}\right)^{1.53} \qquad \text{Eq. 5.10}$$

Figures 5.12, 5.13 and 5.14 present the field data for spherical detonations including Equations 5.6, 5.8 and 5.10 for the pore pressure ratio as a function of peak strain at relative densities of 89, 50 and 1 percent, respectively. As expected, the soils at higher densities require greater peak strains to liquefy.

J. Summary

For the tests at a relative density of 89 percent conducted by Hassen (1988) and Bretz (1988), the best fit equations and the field data for the residual pore pressure increase induced by explosive induced planar and spherical stress waves and for laboratory shock induced planar stress wave are shown in Figure 2. Also plotted on Figure 5.2 is Equation 3.7 presented by Veyera (1985) for laboratory plane compressive shock loading of Monterey No. 0/30 sand. The prediction, based on the laboratory derived Equation 3.7, over predicts the pore pressure ratio for both the planar (Eq. 5.3) and spherical (Eq. 5.6) explosive detonations. The spherical explosive detonations result in a higher pore pressure ratio that the planar detonations producing a given peak compressive strain.

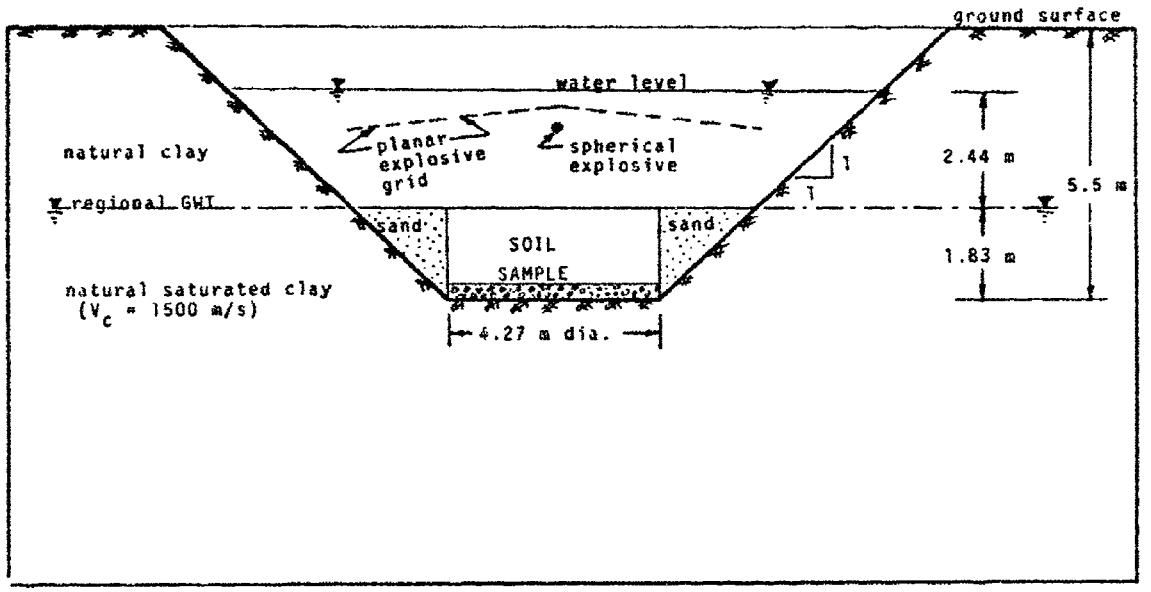

Figure 5.1 Cross-section of explosive test pit and soil sample.

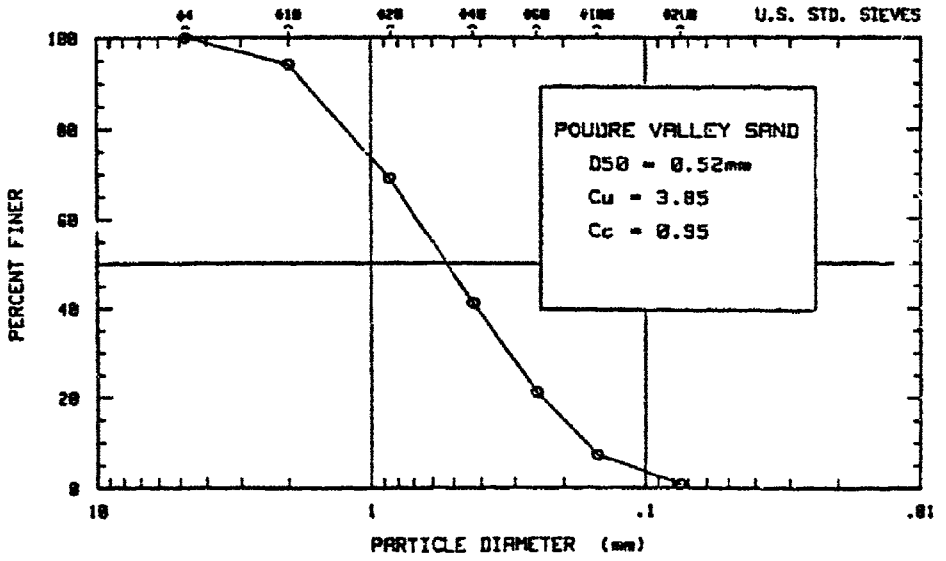

Figure 5.2 Poudre Valley sand gradation curve.

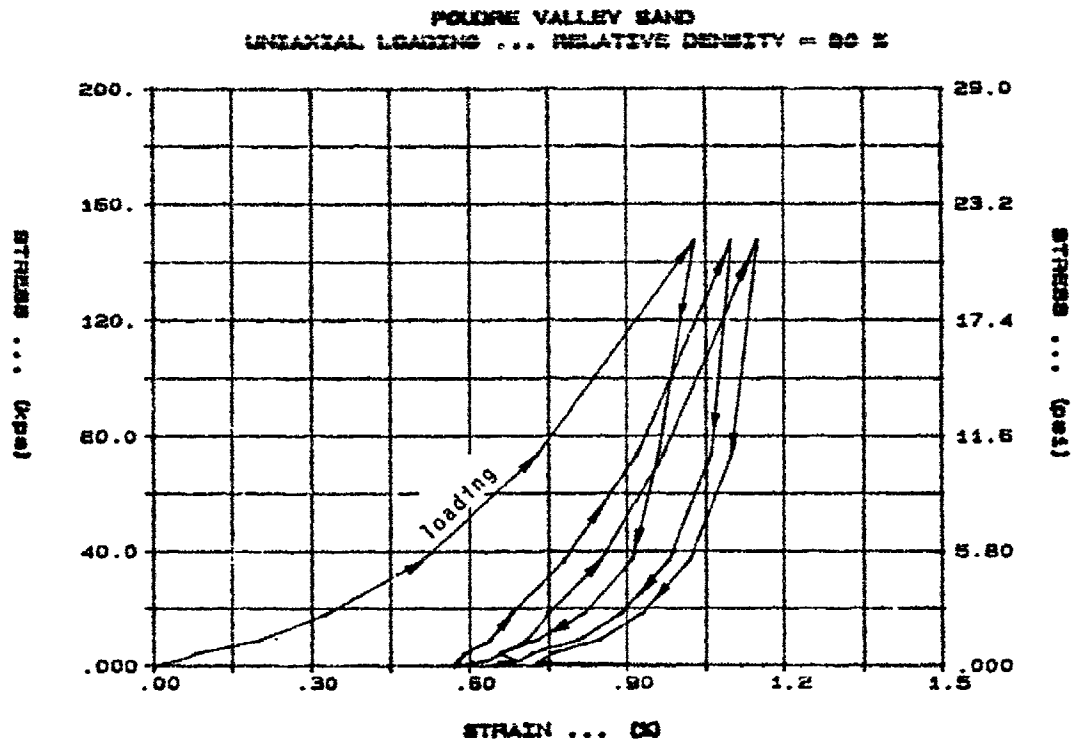

Figure 5.3 Stress-strain curves for uniaxial loading of Poudre Valley sand (arithmetic scale).

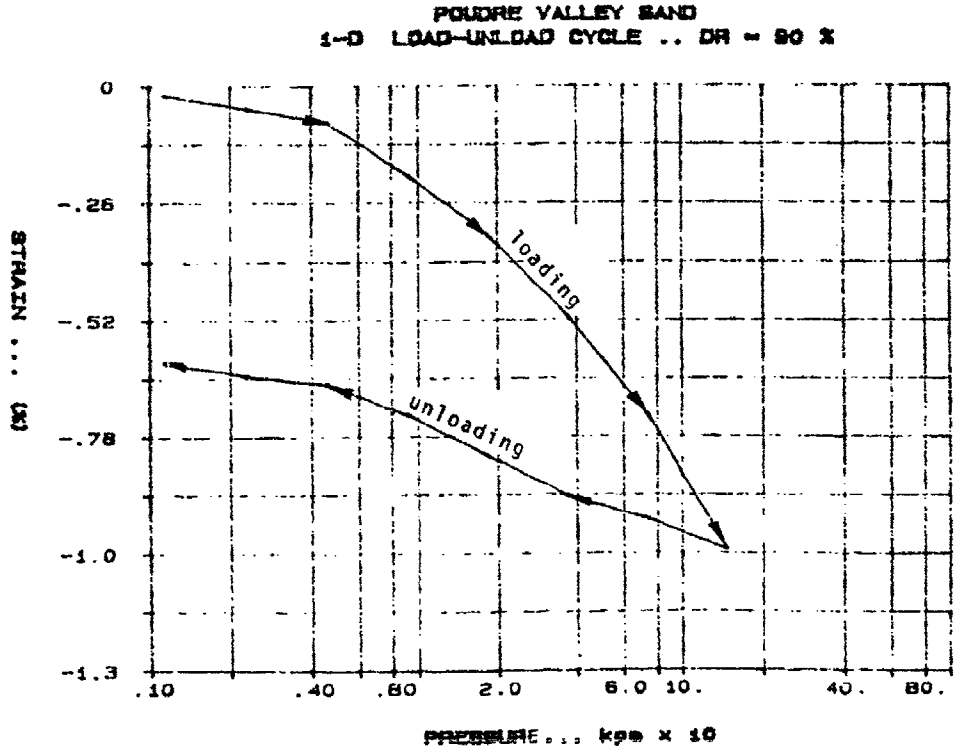

Figure 5.4 Stress-strain curves for uniaxial loading of Poudre Valley sand (logarithmic scale).

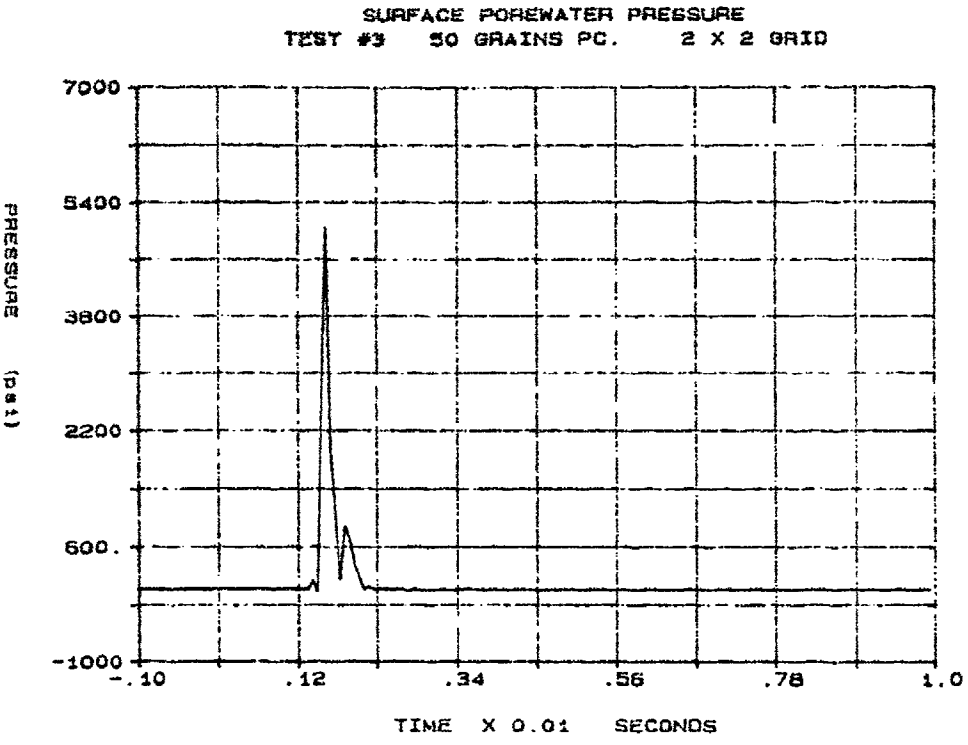

Figure 5.5. Typical pore pressure time history measured by the pressure transducers.

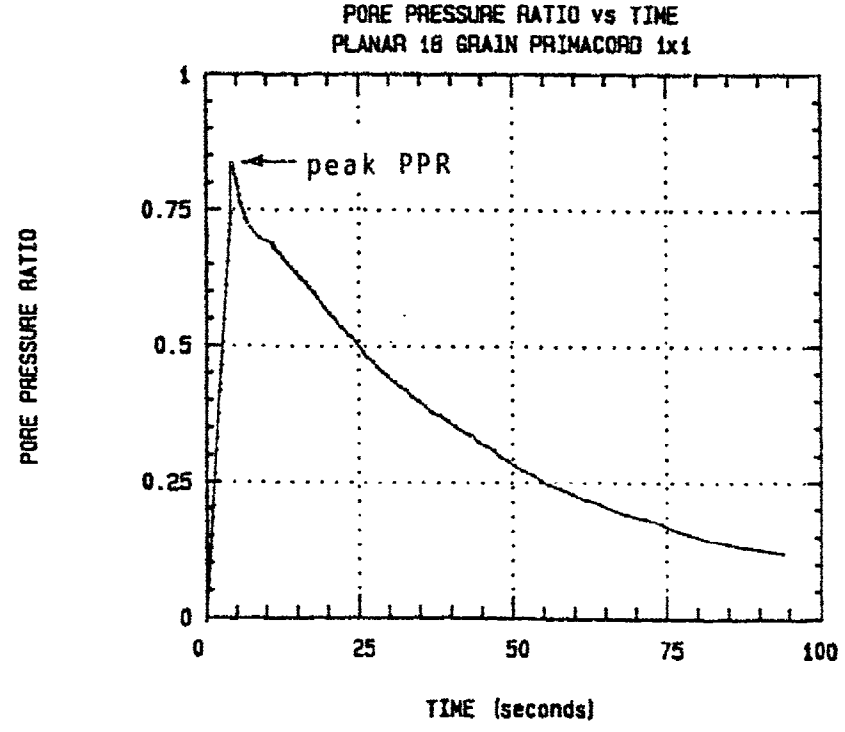

Figure 5.6 Typical pore pressure ratio versus time for the piezometer response.

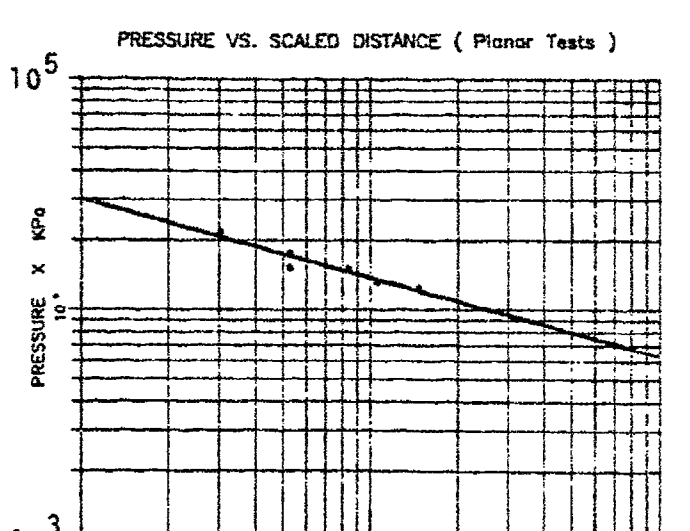

Figure 5.7 Measured peak porewater pressure for the planar detonations (D_r = 89%; Hassen, 1988)

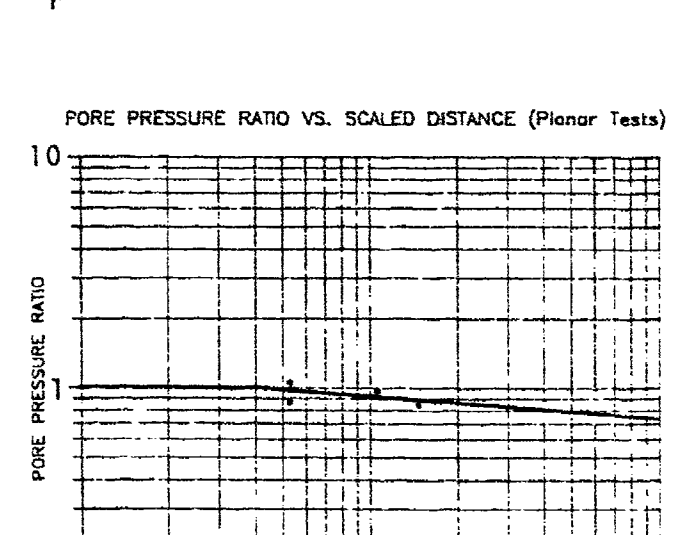

Figure 5.8 Measured pore pressure ratio for planar detonations (D_R = 89%; Hassen, 1988).

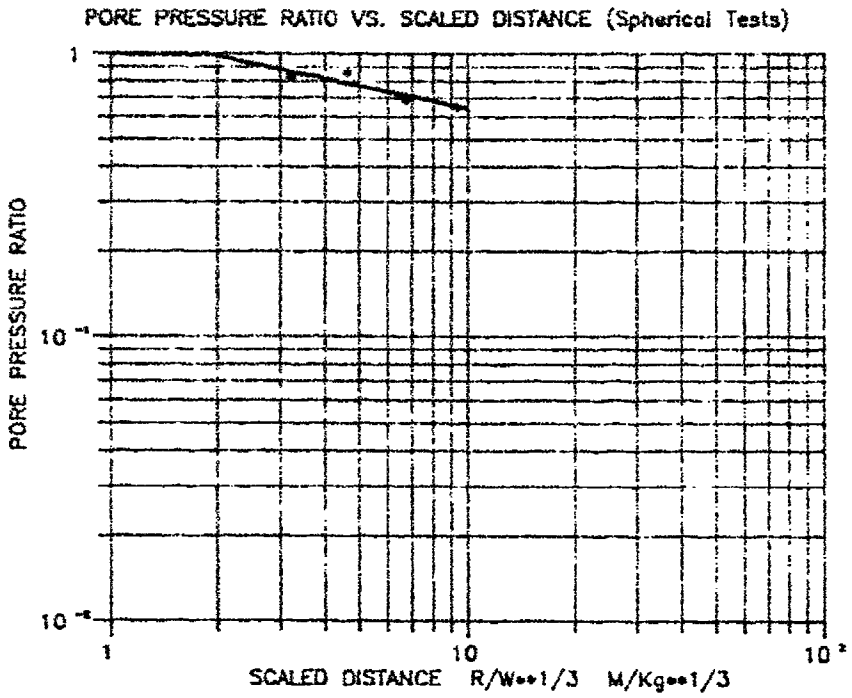

Figure 5.9 Pore pressure ratio for spherical shots as a function of scaled distance (D_R = 89%; Bretz, 1988).

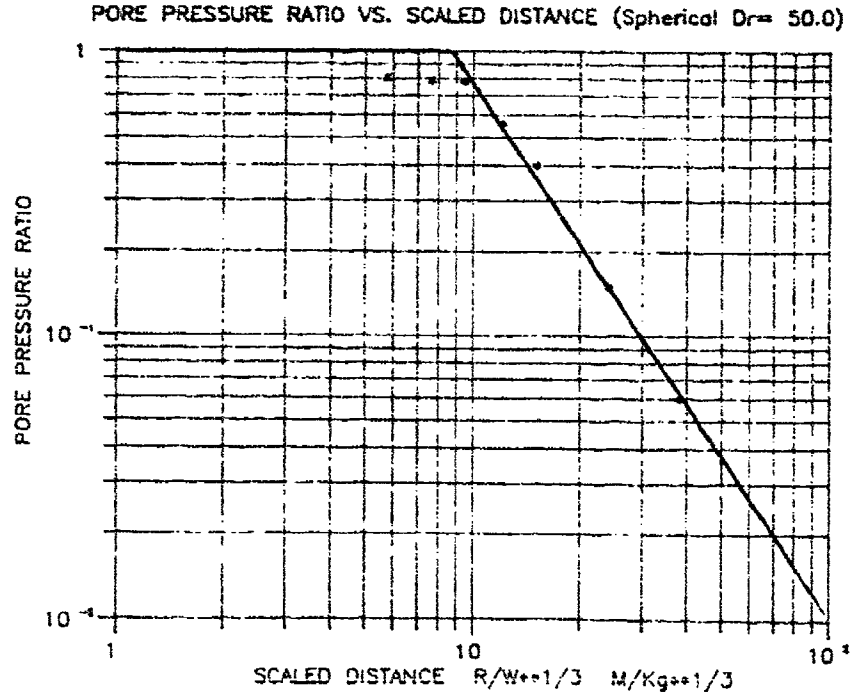

Figure 5.10 Pore pressure ratio for spherical shots as a function of scaled distance (D_R = 50%; Schure, 1988).

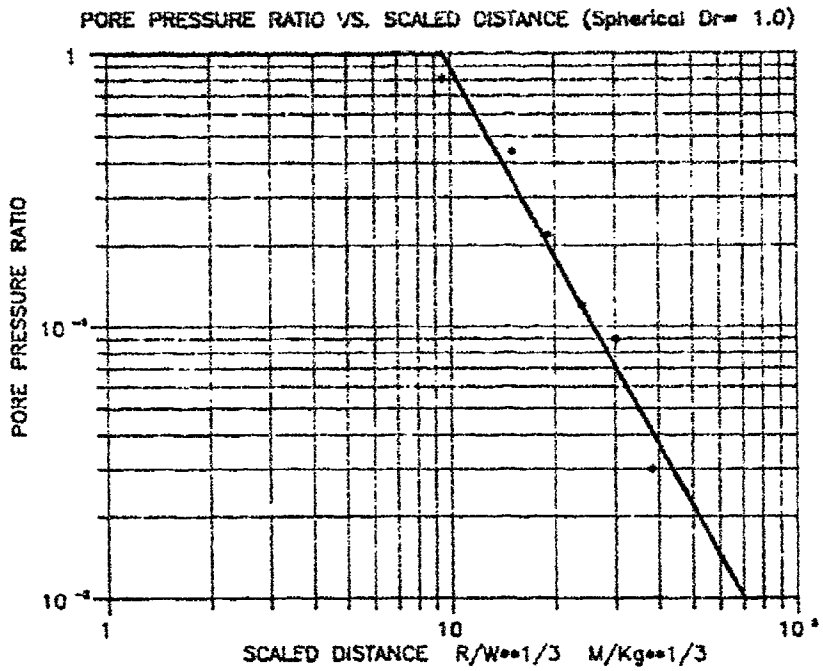

Figure 5.11 Pore pressure ratio for spherical shots as a function of scaled distance (D_R = 1%; Schure, 1988).

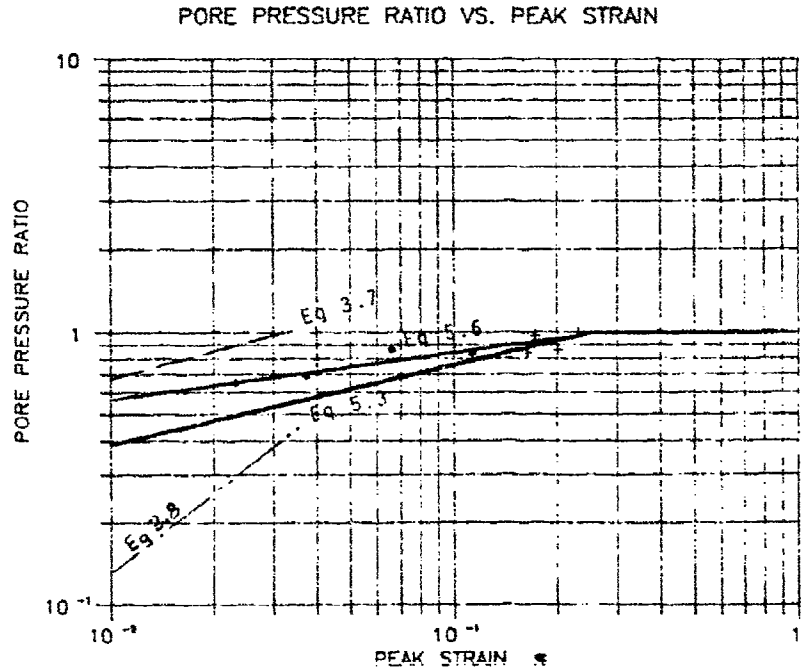

Figure 5.12 Comparison of pore pressure ratio for planar and spherical detonations (D_R = 89%; Bretz, 1988; Hassen, 1988)

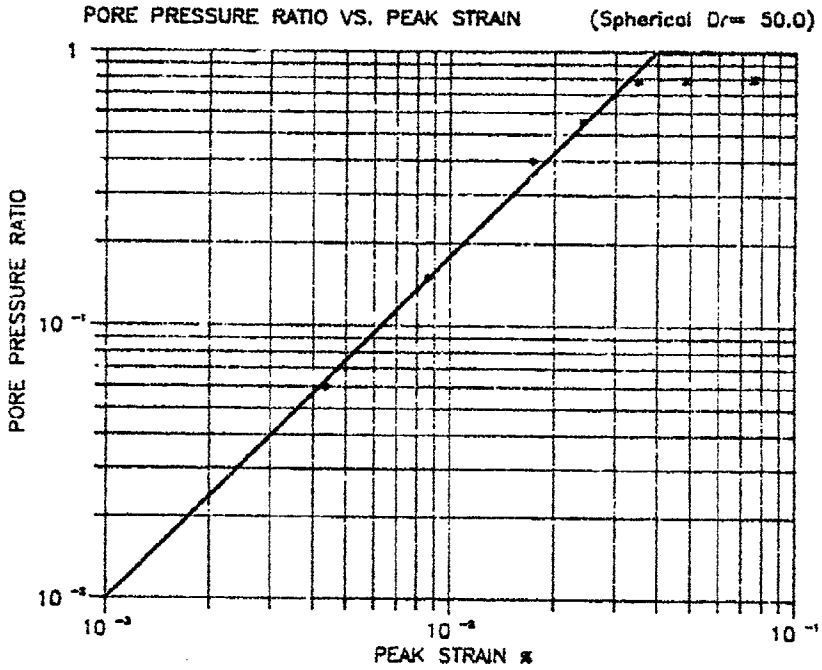

Figure 5.13 Pore pressure ratio for spherical shots as a function of peak strain (D_R = 50%; Schure, 1988)

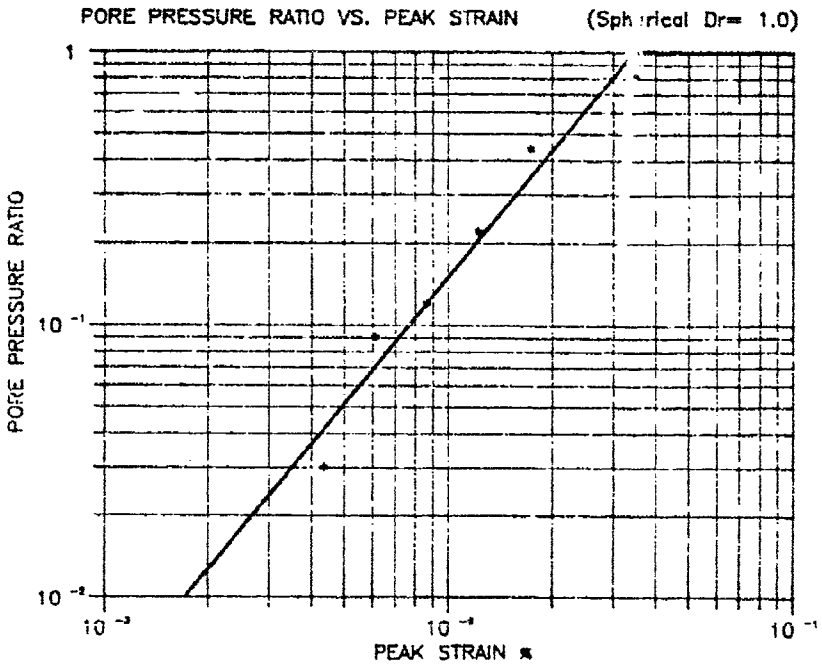

Figure 5.14 Pore pressure ratio for spherical shots as a function of peak strain (D_R = 1%; Schure, 1988)

Table 5.1 Index Properties of the Poudre Valley Sand

Unified Soil Classification System Group Symbol (angular grain shape)	SP
Mean Specific Gravity, G_s	2.68
Particle Size Distribution Data	
D_{10}, mm	0.18
D_{30}, mm	0.25
D_{50}, mm	0.52
C_u, (1)	3.85
C_c, (2)	0.95
Relative Density Test Data	
Dry Unit Weight, kg/m^3	
Maximum	1860
Minimum	1522
Void Ratio	
Maximum	0.76
Minimum	0.438
Quartz Mean Specific Gravity	2.65
Quartz Bulk Modulus, MPa	30680

(1) $C_u = (D_{30})^2/(D_{60} \times D_{10})$

(2) $C_c = D_{60}/D_{10}$

Table 5.2. Peak Residual Pore Pressure Increase for Poudre Valley Sand as a Function of Charge Weight, Distance and Soil Density for Planer Tests (Hassen, 1988)

Test No.	Total Charge Wt (kg)	Average Charge Weight per Area (kg/m^2)	Peak Rise of Water in Piezometer (m)	PPR	Explosive Used
Dense (relative density approximately 89 percent)					
P1	0.53	0.15	1.37	0.86	Primacord^R 3.8 g/m (61x61 cm grid)
P2	0.74	0.21	1.55	0.97	Primacord^R 5.3 g/m (61x61 cm grid)
P3	1.46	0.42	1.68	1.05	Primacord^R 10.7 g/m (61x61 cm grid)
P4	1.46	0.42	1.39	0.87	Primacord^R 10.7 g/m (61x61 cm grid)
P5	2.55	0.73	-	-	Primacord^R 10.7 g/m (30x30 cm grid)
P6	1.28	0.26	-	-	Primacord^R 5.3 g/m (30x30 cm grid)

Charge Location In water 1.22 m above tank and 0.61 m below water surface.

Piezometer is located at a depth of 1.67 m below soil surface and at a distance, R, from the charge grid of 2.89 m. The rise of water required for PPR = 1 is 1.6 m.

Table 5.3. Peak residual pore pressure increase for Poudre Valley sand as a function of charge weight, distance and soil density for spherical tests (Bretz, 1988).

Test No.	Charge Wt. W (kg)	Peak Rise of Water in Piezometer (m)	PPR	Scaled Distance, $R/W^{1/3}$ ($m/kg^{1/3}$)	Explosive Used
Dense (Relative Density Approximately 89 Percent)					
S1	0.03	1.22	0.65	9.3	Primacord®
S2	0.08	1.26	0.69	6.7	Primacord®
S3	0.25	1.56	0.86	4.6	Tovex 800®
S4	0.76	1.56	0.84	3.2	Tovex 800®
S5	2.25	1.30	0.70	2.2	Tovex 800®
S6	0.76	1.55	0.83	3.2	Tovex 800®
S7	7.02	1.10	0.65	1.5	Tovex 800®

Piezometer is located at a depth 1.67 m below soil surface and at a distance, R, from the charge of 2.89 m. The rise of water required for PPR = 1 is 1.6 m.

Charge Location in water 1.22 m above tank and 0.61 m below water surface (S7, 1.22 m above tank and 1 m below water)

Table 5.4 Peak residual pore pressure increase for Poudre Valley sand as a function of charge weight, distance and soil density for spherical tests (Schure, 1988).

Test No.	Charge Wt W(kg)	Peak Rise of Water in Piezometer (m) BGP	BP	MP	PPR BGP	BP	MP	Scaled Distance, $R/W^{1/3}$ ($m/kg^{1/3}$) BGP	BP	MP
Loose (relative density approximately 1 percent)										
L-1	0.0004	0.06	0.10	0.09	0.03	0.07	0.08	38	36	26
L-2	0.0008	0.14	0.17	0.16	0.09	0.12	0.22	30	28	21
L-3	0.0017	0.20	0.24	0.22	0.12	0.17	0.30	24	23	16
L-4	0.0035	0.34	0.37	0.32	0.22	0.26	0.44	19	18	13
L-5	0.0070	0.70	0.63	0.52	0.44	0.44	0.74	15	14	10
L-6	0.0141	-	0.88	0.62	-	0.62	0.88	12	11	8.2
L-7	0.0282	1.28	1.28	0.61	0.81	0.90	0.85	9.4	9.1	6.4
Med-dense (relative density approximately 50 percent)										
D-1	0.0004	0.09	0.12	0.09	0.06	0.09	0.13	38	37	28
D-2	0.0017	0.23	0.23	0.18	0.15	0.16	0.26	24	23	18
D-3	0.0070	0.62	0.53	0.50	0.40	0.38	0.71	15	15	11
D-4	0.0141	0.88	0.76	0.61	0.56	0.54	0.85	12	12	8.8
D-5	0.0282	1.22	1.22	0.64	0.78	0.86	0.89	9.4	9.1	7.0
D-6	0.0588	1.25	1.22	0.58	0.80	0.86	0.81	7.6	7.3	5.5
D-7	0.1171	1.28	1.16	0.55	0.81	0.81	0.76	5.9	5.8	4.3

piezometer	location	Distance from Charge loose (cm)	dense (cm)	Rise Required for PPR = 1 (m)
MP	0.76 m depth	1.98	2.13	0.71
BP	1.52 m depth	2.74	2.82	1.42
BGP	1.67 m depth	2.89	2.89	1.57

Charge location In water 1.22 m above tank and 0.61 m below water surface, explosive used: Primacord^{R}

VI. IN-SITU EXPLOSIVE TESTS ON ALLUVIAL SAND

This chapter summarizes our results of buried point source explosive detonations (spherical stress wave tests) on an alluvial sand deposit conducted by Jacobs (1988).

A. Introduction

We conducted a series of in-situ field explosive tests on an alluvial sand deposit to systematically evaluate explosive-induced porewater pressure increases and liquefaction of a water saturated natural sand deposit. The transient and long-term porewater pressure response was measured and compared to values predicted by various empirical models developed through previous laboratory and field research given in Chapter II.

B. Test Site and Soil Properties

The field test site is a natural braided river deposit located in the South Platte River approximately 4 km north of Kersey, Colorado. We conducted the tests on a sand island located in the river channel. Two borings and two cone penetrometer tests indicated that the first 3.5 m are composed of a dense poorly graded sand (SP) having an in-situ relative density of approximately 85 percent. Below 3.5 m is silt (ML) with a liquid limit of 40, plastic limit of 25 and a natural water content of 28 percent. Seismic tests indicate that the soil is saturated below a depth of 0.25 m (wave velocity of 1,582 to 1,595 m/sec). Shear wave velocities ranged from 162 m/sec at a depth of 1 meter to 277 m/sec at a depth of 3.5 meters. Shale bedrock is known to be located at a depth of approximately

33 m in this area. Based on the soil samples collected at 0.61 m intervals in the two borings on the sand island, the soil logs in Figure 6.3 were developed for each boring. Laboratory tests were performed on the recovered samples. Table 6.1 presents the results for the upper 3.65 m sand layer and Table 6.2 presents the results for the underlying silt layer. Figure 6.1 shows the profile at the island based on the two borings, two CPT tests and seismic data. For further details of the site, see Rwebyogo (1987) and Jacobs (1988).

C. Instrumentation

We instrumented the site at the locations shown in Figures 6.2 and 6.3 with porewater pressure and particle velocity transducers to record the transient response as a function of distance and charge weight. Piezometers were utilized to obtain late time porewater pressure response. Digital transient data recorders were utilized to record the transient response and high speed video cameras recorded the tests and the excess late time residual porewater pressure response. Surveying equipment was used to determine ground surface elevations.

D. Explosives and Test Procedures

The explosives we utilized were obtained from Buckley Power Company of Englewood, Colorado. Detonating cord (Primacord^R, manufactured by the Ensign-Bickford Company) was used for the smaller detonations and a water gel (Tovex 800^R manufactured by Dupont) was used for the larger detonations. The energy rating of Tovex 800^R is 894 calories per gram, which is about 10 percent less than TNT. Instantaneous electric blasting

caps were used to initiate all detonations. The blasting cap utilized had a maximum delay of 2.0 micro seconds after the electric energy was applied by the blasting machine.

Six detonations ranging from 0.0045 to 9.06 kg of explosives were detonated at a depth of 3.0 to 3.5 m. Detonations 1 to 5 occurred in borehole number one and the final detonations occurred in borehole number two.

E. Test Results

Table 6.3 lists the test sequence, explosive type, weight and depth of explosive detonated during the test program. The average compression wave velocity from the explosive to the water pressure and velocity gages was 1,680 m/sec.

i. Peak Transient Porewater Pressure

The transient porewater pressure was measured at a depth of 3.5 m at distances of 6.1 and 12.2 m for detonations 1 to 5 and at 15.5 and 19.2 m for detonation number 6. Figure 6.4 shows a typical porewater pressure time history for an explosive detonation recorded. Using the "cube root" scaling law, $R/W^{1/3}$, the peak porewater pressure values obtained for each detonation at each porewater pressure transducer are plotted on Figure 6.5. The equation representing the statistically best fit line using a linear least squares analysis for the alluvial site studied is

$$u_{pk} = 50{,}093 \left(\frac{R}{W^{1/3}}\right)^{-2.38} \qquad \text{Eq. 6.1}$$

where u_{pk} is the peak porewater pressure in kPa, R is the distance from the detonation in m, and W is the charge mass in kg. Figure 6.6 compares the recorded data and Equation 6.1 to other equations given in the literature given in Chapter II.

ii. Peak Particle Velocity

The particle velocity, monitored at the groundwater table, was measured in the transverse, longitudinal and vertical directions. The maximum vector sum of the three directions is presented as the peak particle velocity. The data is plotted in Figure 6.7. The statistically best fit line for the alluvial site is

$$V_{peak} = 8.745 \left(\frac{R}{W^{1/3}}\right)^{-2.06} \qquad \text{Eq. 6.2}$$

where V_{peak} is the peak particle velocity in m/sec. Figure 6.8 compares the recorded data and Equation 6.2 to other equations in the literature given in Chapter II.

iii. Settlement Survey

The survey results revealed that there was no significant settlement in the area surrounding the explosive detonations for detonations 1 to 5. Detonation number 6 (9.1 kg) produced a ground heave of 5 cm. These observations are consistant for a dense sand deposit.

iv. Residual Porewater Pressure and Porewater Pressure Ratio

Residual porewater pressure was measured by five piezometers. The elevation rise in each standpipe was recorded by using video recorders.

The results are presented as a dimensionless number known as the porewater pressure ratio, PPR, defined in Chapter 2. For the depth of the piezometer opening (3.5 m), the effective stress for the groundwater table elevation at the time of the tests was approximately 38 kPa. This means that a rise of 387 cm in any of the piezometer stand pipes would yield a pore pressure ratio of 1.0, defining a condition of liquefaction. The PPR time histories for each piezometer for the sixth detonation (9.10 kg) is given in Figure 6.9. The time histories for the other detonations are given in Jacobs (1988). The piezometers have a response time (natural frequency) of approximately one second.

The measured peak residual porewater pressure ratio, PPR, for all detonations is plotted in Figure 6.10. The statistically best fit equation for the measured data is

$$PPR = 2.60 \left(\frac{R}{W^{1/3}}\right)^{-1.366} \qquad \text{Eq. 6.3}$$

Because of the high permeability of the alluvial sand at the site, the residual porewater pressure dissipated very fast (less than five seconds). The piezometer system, with its response time of approximately one second, was unable to measure the peak residual porewater pressure immediately following the passage of the stress wave. Utilizing Terzaghi's consolidation theory, the actual peak residual porewater pressure is

$$PPR_{(peak)} = 4.8 \left(\frac{R}{W^{1/3}}\right)^{-1.48} \qquad \text{Eq. 6.4}$$

where $PPR_{(peak)}$ is the residual porewater pressure ratio just after the passage of the stress wave and before consolidation occurs. Equation 6.4 is plotted in Figure 6.11. This equation predicts liquefaction (PPR = 1) at a scaled distance, $R/W^{1/3}$, of 2.9 $m/kg^{1/3}$. Lyakhov (1961) equation in

Chapter II predicted liquefaction at a scaled distance between 2 and 8, depending on depth of the explosive soil type and soil density. Ivanov (1967) equation predicts liquefaction at a scaled distance of less than 6 $m/kg^{1/3}$. Studer and Kok's (1980) predicts liquefaction at a scaled distance of 2.8 $m/kg^{1/3}$. Equation 6.4 fits Studer and Kok's (1980) equation the best.

Utilizing a scaled distance of 2.9 $m/kg^{1/3}$ in Equation 6.4, the peak particle velocity required to cause liquefaction at the South Platte River Site is 0.98 m/sec. Dividing the peak particle velocity by the measured compressive wave velocity of 1,680 m/sec leads to a peak compressive strain of 0.058% required to cause liquefaction at the site. Solving Veyera's (1985) equation given in Chapter II at a relative density of 89% and an effective stress of 38 kPa leads to the following

$$PPR = 2.38\ (\varepsilon_{pk})^{0.331} \qquad \text{Eq. 6.5}$$

where ε_{pk} is the peak compressive strain in percent. As shown in Figure 6.12, at a strain of 0.06, a PPR of 0.93 is predicted by Veyera's equation which is very close to the peak strain causing liquefaction at the site.

F. Summary

The measured peak transient porewater pressure induced by an explosive detonation in the South Platte alluvial soil deposit was found to be similar magnitude to the predicted by Drake and Little (1983) and Drake and Ingram (1981) empirical equations. The empirical equations developed by Ivanov (1967), Lyakhov (1961) and Cole (1948) over-predict the peak transient porewater pressure in the South Platte River deposit.

The measured peak particle velocities induced by explosive detonations in the South Platte River deposit was found to be slightly greater in magnitude than predicted by empirical equations presented by Drake and Little (1983) and Drake and Ingram (1981).

The calculated PPR, utilizing the permeability and drainage conditions at the South Platte River deposit compared well to the empirical equations by Studer and Kok (1980) based on scaled distance and to Veyera's (1985) equation based on explosive induced strain.

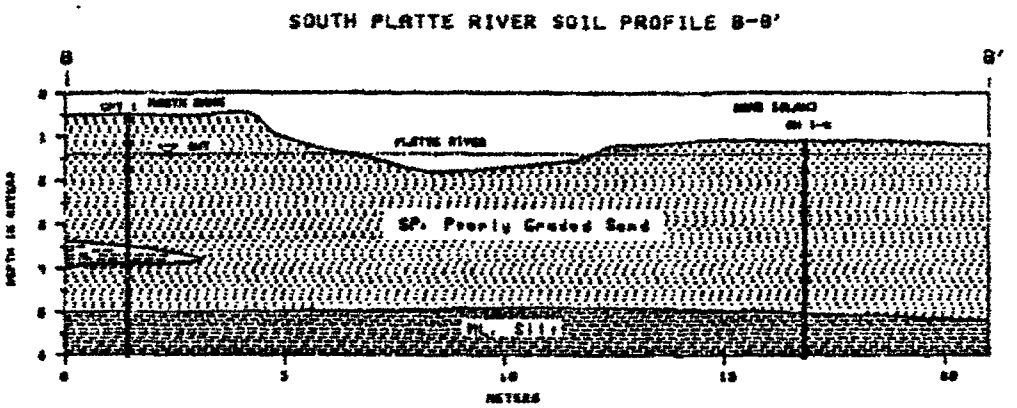

Figure 6.1(a) North-South cross-section through borehole one (BH-1).

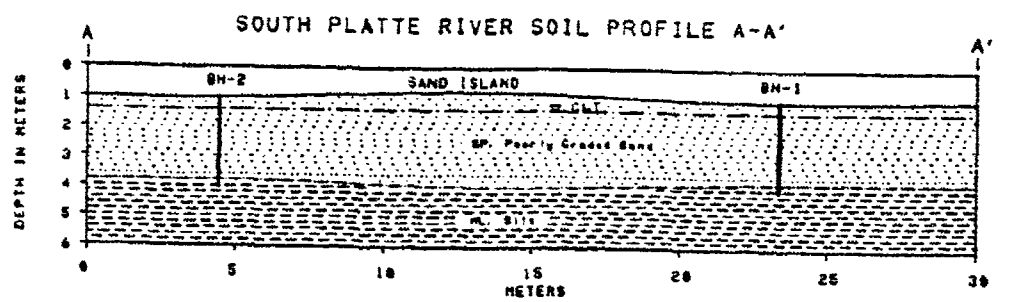

Figure 6.1(b) East-west cross-section through boreholes one and two (BH-1 and BH-2).

INSTRUMENTATION LAYOUT FOR DETONATIONS 1-5

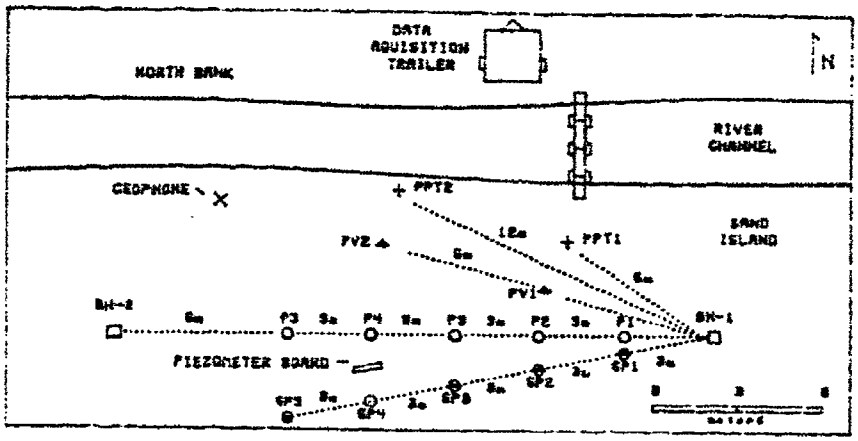

SP1 - SP5 = settlement plates one through five
P1 - P5 = piezometers one through five
PV1 - PV2 = particle velocity gauges one and two
PPT1 - PPT2 = porewater pressure transducers one and two

Figure 6.2 Instrumentation layout, plan view, for detonations one through five which utilizes borehole one as the explosive detonation point.

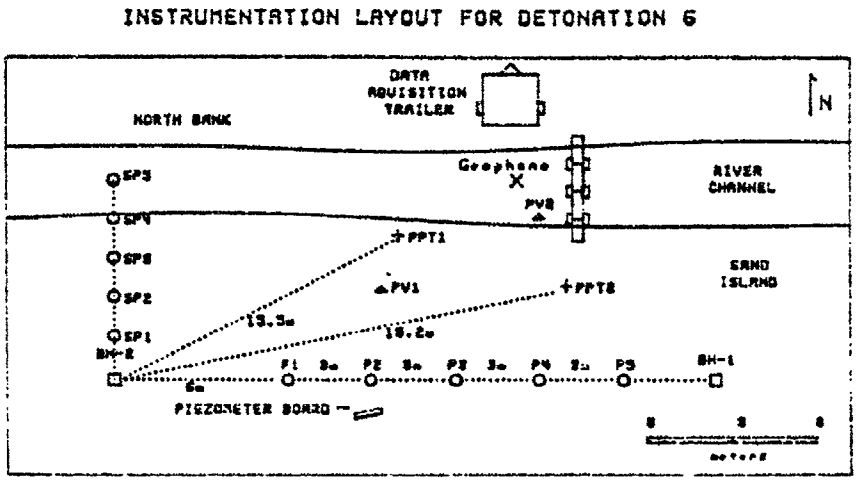

SP1 - SP5 = settlement plates one through five
P1 - P5 = piezometers one through five
PV1 - PV2 = particle velocity gauges one and two
PPT1 - PPT2 = porewater pressure transducers one and two

Figure 6.3 Instrumentation layout, plan view, for detonations six which utilizes borehole two as the explosive detonation point.

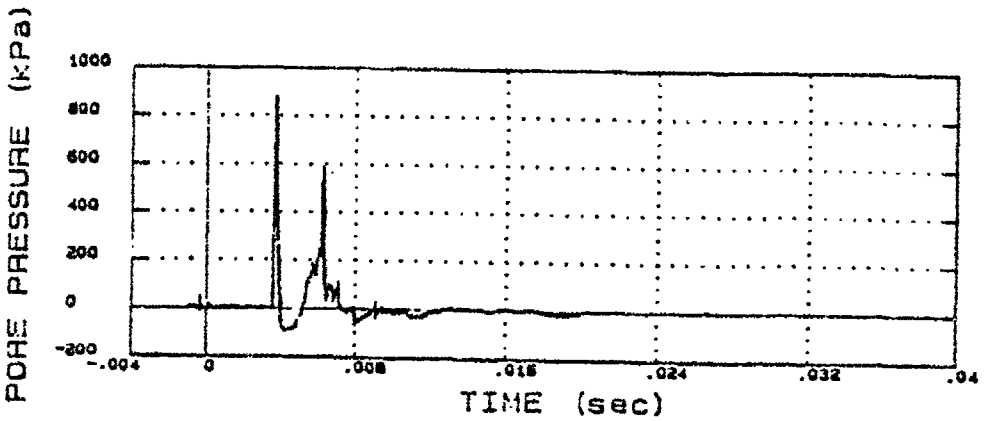

Figure 6.4 Typical stress-time history recorded using the Signal-Conditioner-TDR instrumentation system.

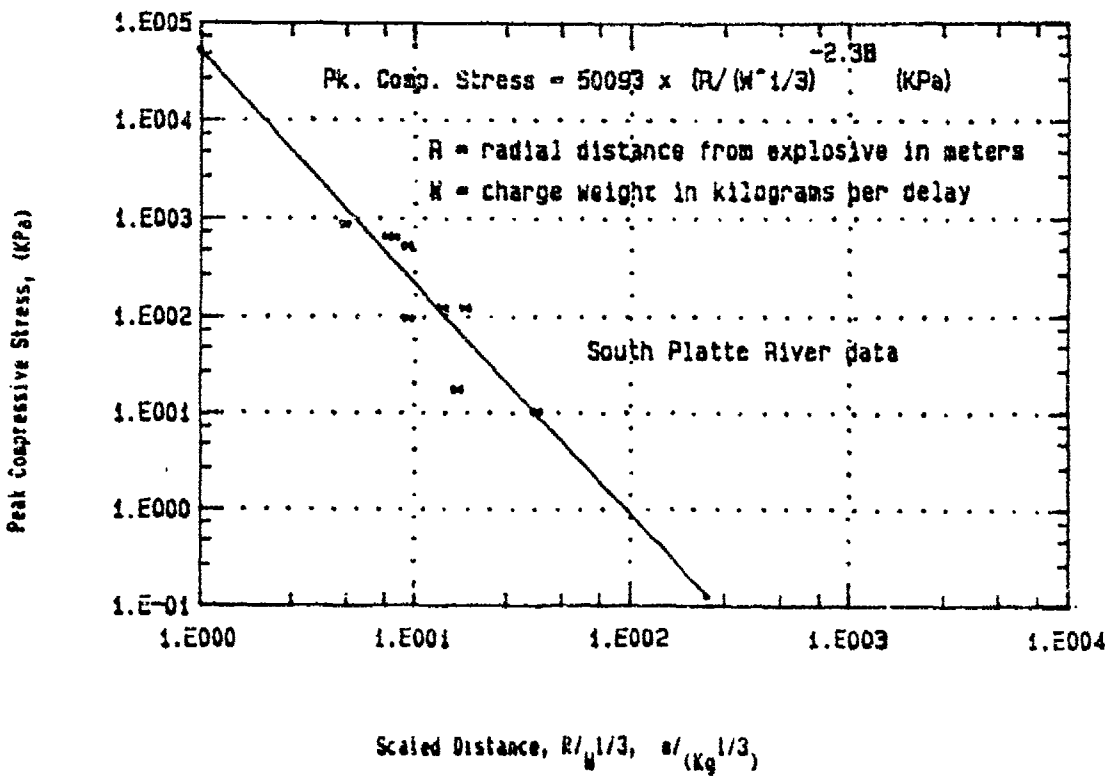

Figure 6.5 Peak compressive stress data for detonations one through six with the empirical equation representing the line of best through the data.

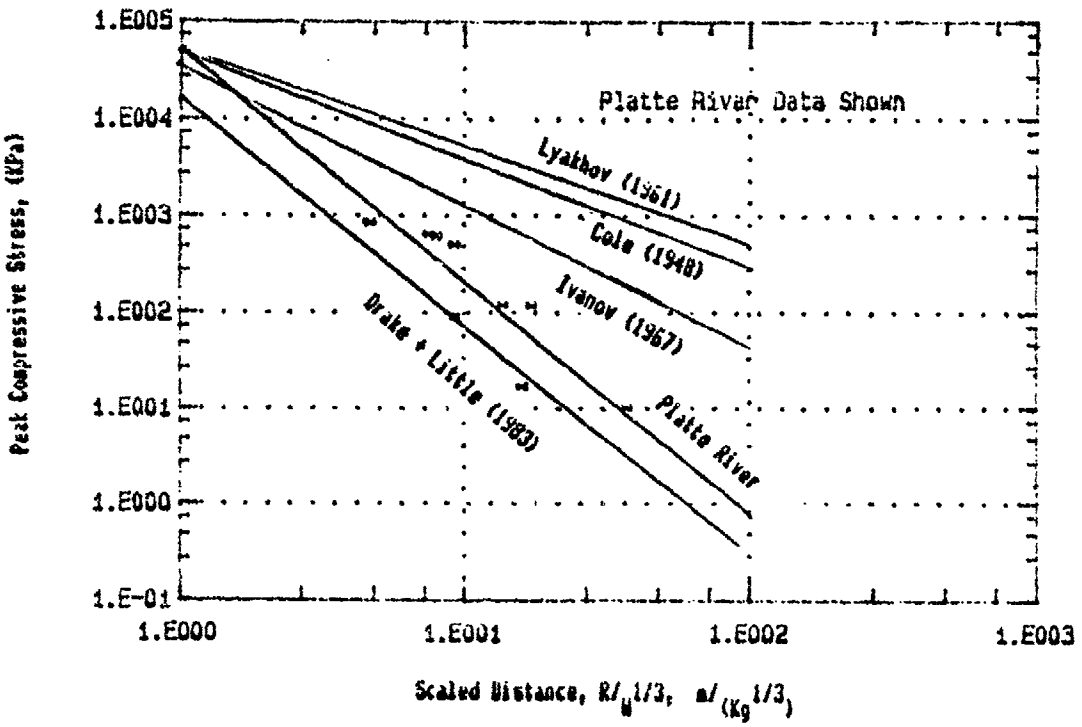

Figure 6.6 Peak compressive stress data for the South Platte River sand island, the statistically best fit line through the measured field data and other equations given in the literature.

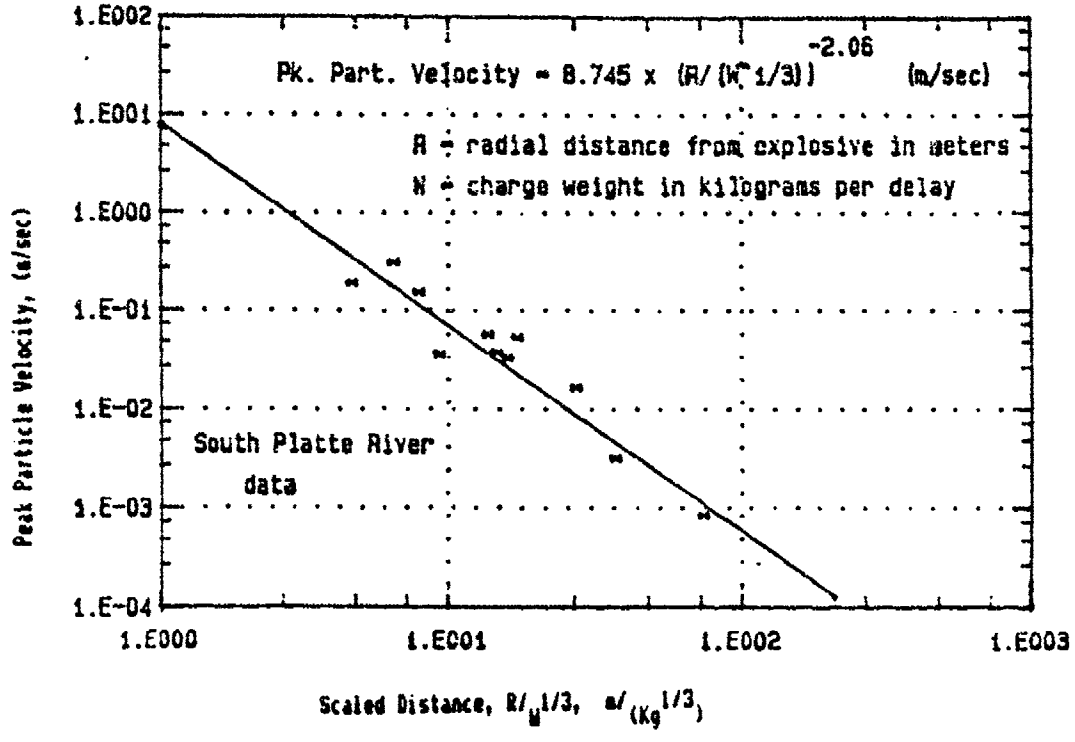

Figure 6.7 Peak particle velocity data and the empirical equation representing the line of best fit through the field data.

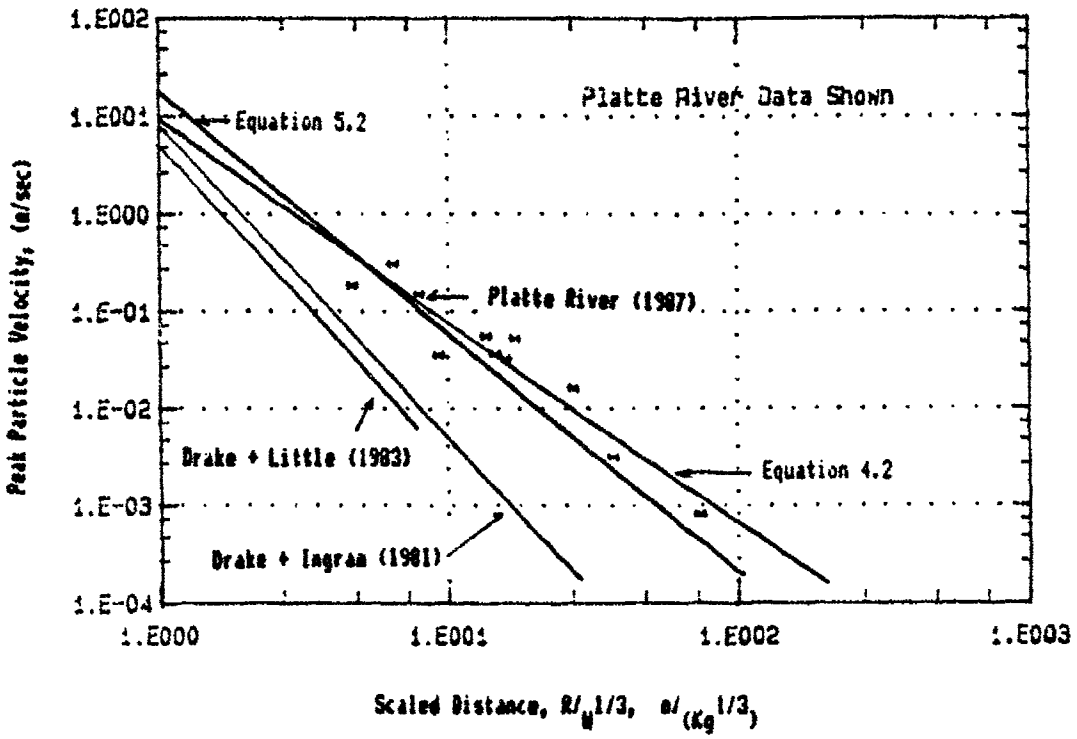

Figure 6.8 Peak particle velocity data for the South Platte River filed site. the best statistically best fit line through the data and other equations given in the literature.

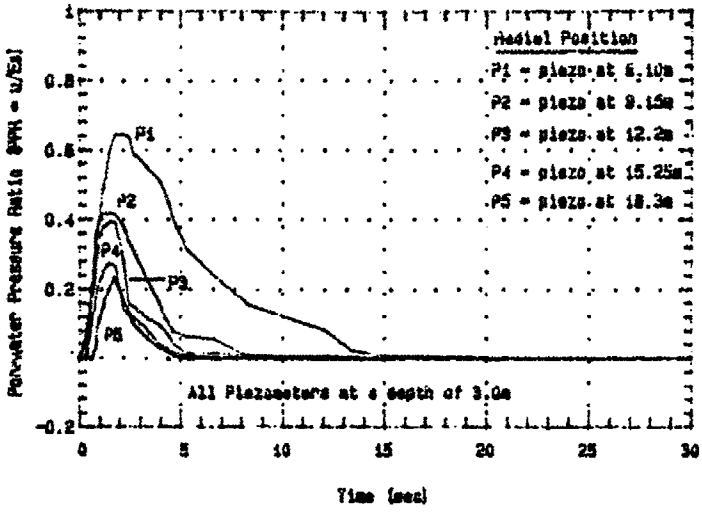

Figure 6.9 Residual porewater pressure expressed as the dimensionless porewater pressure ratio, (PPR = u/σ'), vs. time after detonation number six, (9.1030 kg).

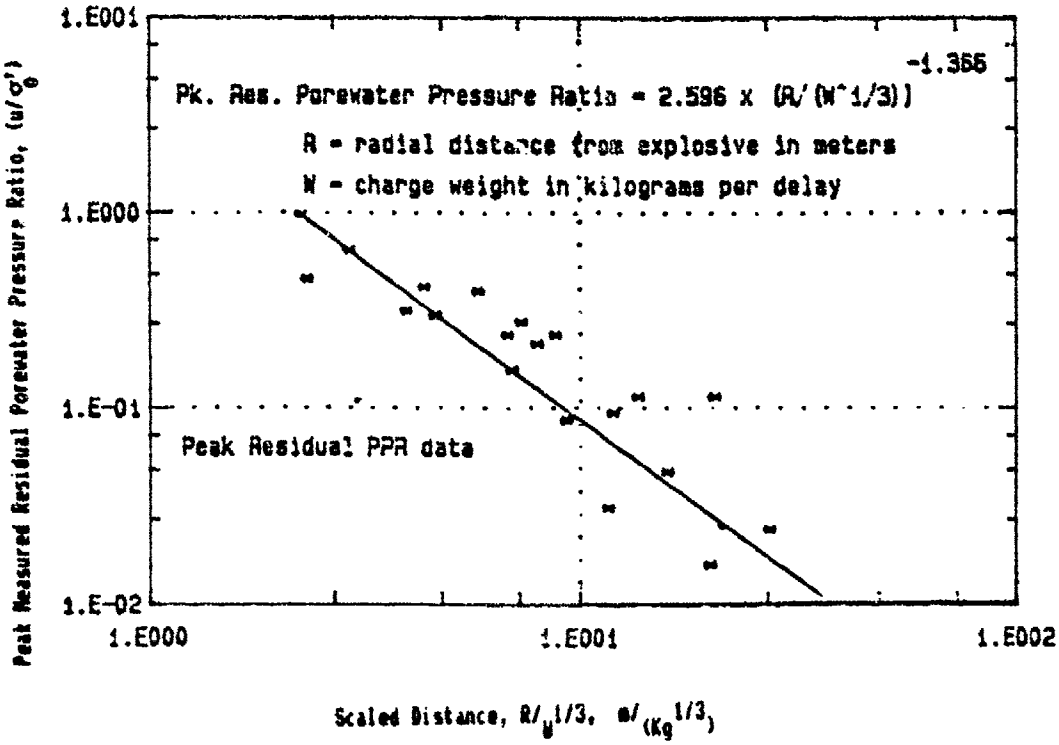

Figure 6.10 Peak residual porewater pressure ratio for all detonations and the empirical equation representing the line of best fit through the data.

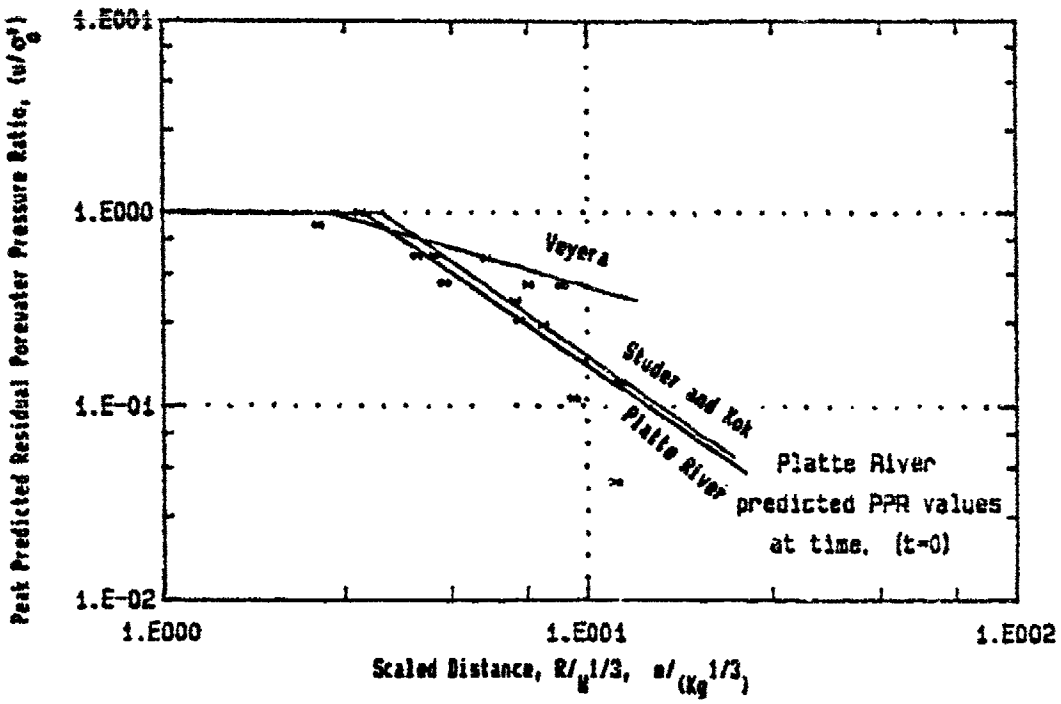

Figure 6.11 Calculated peak residual porewater pressure ratio at t = o+ for all detonations and Equation 6.4.

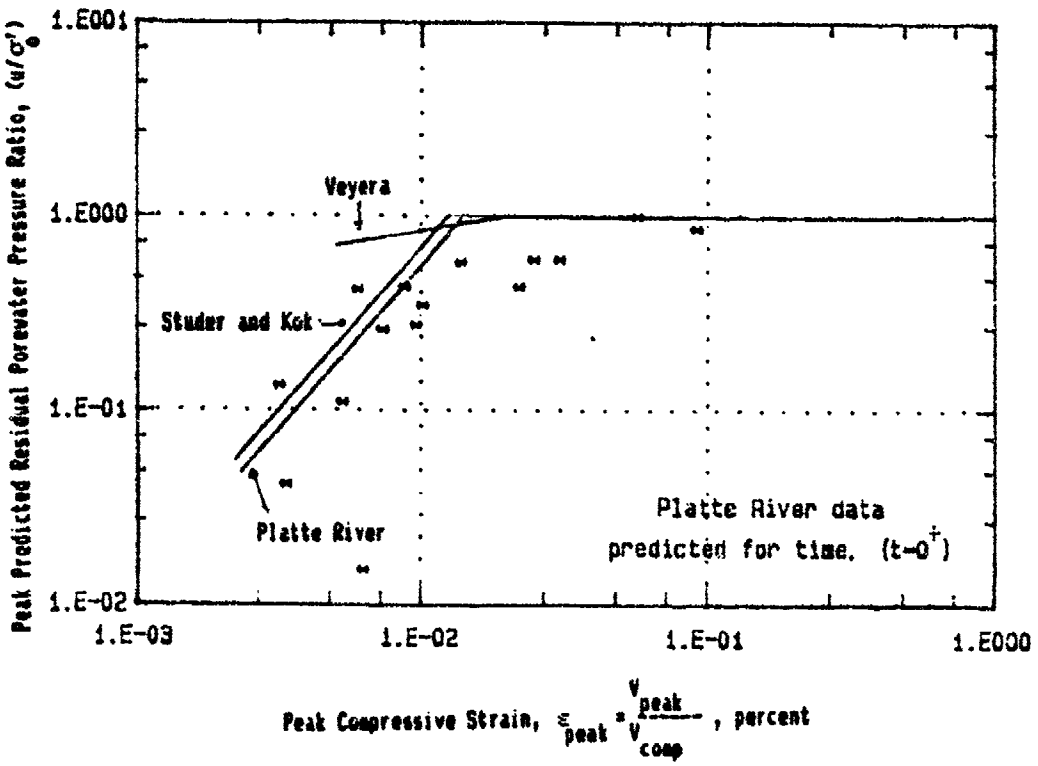

Figure 6.12 Statistically best fit equations for peak residual porewater pressure ratio predictions based on peak strain.

Table 6.1 Summarized laboratory test results for the upper 3.65 m sand layer

Soil Classification (USCS, ASTM D2487 and D442)

SP - rounded to sub-rounded coarse gravely poorly graded sand.
% passing #200 < 1%
D_{50} = 2 mm

Permeability

$k = 3.24 \times 10^{-2}$ cm/sec

Specific Gravity of Soil Solids (ASTM D854)

Gs = 2.63

Minimum and Maximum Density (ASTM D4254 and D4253)

$\gamma_{max} = 77$ KN/m^3 $\gamma_{min} = 16.48$ KN/m^3
$e_{min} = 0.373$ $e_{max} = 0.564$

Table 6.2 Summarized laboratory test results for the silt layer, intercepted at a depth of 3.65 m

Soil Classification (USCS, ASTM D2487 and D422)

ML - low plasticity silt

Atterberg Limits (ASTM D4318)

Liquid Limit - 40

Plastic Limit - 25

Water content - 28.5%

Plasticity Index - 15

Table 6.3 Test sequence, charge type, weight and depth of explosive for the six detonations fired during the test program.

Test number	Date July, 1987	Depth of charge placement (meters)	Type of Explosive	Charge mass (kilograms)
1	14th	3.5	blasting cap	0.0045
2	15th	3.5	Primacord	0.0453
3	15th	3.0	Tovex	0.091
4	15th	3.0	Tovex	0.453
5	16th	2.8	Tovex	2.264
6	16th	3.0-3.5	Tovex	9.103

VII. ANALYSIS OF SHOCK AND EXPLOSIVE INDUCED LIQUEFACTION

This chapter presents our empirical, analytical and theoretical models to predict liquefaction.

a. Empirical

As given in Chapters II and III, several empirical equations have been proposed to predict explosive induced porewater pressure increases and liquefaction. The major ones are presented below:

$$PPR = 1.65 + 0.64 \ln (W^{1/3}/R) \qquad \text{Eq. 2.1}$$

$$PPR = 16.3 (\Sigma\varepsilon_{pk})^{0.331} (\sigma_o')^{-0.308} (D_R)^{-.179} \qquad \text{Eq. 2.9}$$

$$R_{max} = 2.5 W^{1/3} \text{ for PPR} = 1 \qquad \text{Eq. 2.2}$$

$$R_{max} = k_1 W^{1/3} \text{ for PPR} = 1 \qquad \text{Eq. 2.3}$$

where PPR is the pore pressure ratio defined in Equation 3.4, W is the charge mass in kg, R is the radial distance from the charge in m, ε_{pk} is the peak compressive strain in percent, σ_o' is the effective stress in kPa and D_R is relative density in percent. Our field explosive tests on placed sand (Chapter V) and our field explosive tests on in-situ sand (Chapter VI) result in the following empirical equations:

$$PPR = 30073 \left(\frac{R}{wi}\right)^{-0.342} \text{ planar for } D_r=89\% \qquad \text{Eq. 5.1}$$

$$PPR = 1.15 \left(\frac{R}{W^{1/3}}\right)^{-0.25} \text{ spherical for } D_r=89\% \qquad \text{Eq. 5.5}$$

$$PPR = 57.2 \left(\frac{R}{W^{1/3}}\right)^{-1.87} \text{ spherical for } D_r=50\% \qquad \text{Eq. 5.7}$$

$$PPR = 117 \left(\frac{R}{W^{1/3}}\right)^{-2.3} \text{ spherical for } D_r=1\% \quad \text{Eq. 5.9}$$

$$PPR = 4.8 \left(R/W^{1/3}\right)^{-1.48} \text{ spherical for } D_r=90\% \text{ Eq. 6.4}$$

$$PPR = 2.38 \left(\varepsilon_{pk}\right)^{0.331} \text{ spherical for } D_r=90\% \quad \text{Eq. 6.5}$$

B. Analytical

Analytical methods to model explosive induced porewater pressure increases and liquefaction in the two-phase water saturated sands have been developed by Veyera (1985), Charlie et al. (1987), and Awad (1988). These models utilize Biot's (1956, 1962) theory solved numerically by either the finite element method or the finite difference method. Because of the steep wave front and the high velocity of stress wave propagation in water saturated soil, very small time steps and small element size are required for numerical stability, convergence and accuracy (Zienkiewicz and Bettess, 1982). For one-dimensional modeling, this does not present major computational problems but two- and three-dimensional modeling requires very large computer memory and considerable computer time. For example, Awad's (1988) axi-symmetric finite element model takes over 60 minutes to run on a CDC/205^R super computer.

Although these analytical models have had only limited verification, these analytical models have predicted explosive induced porewater pressure increases and liquefaction of water saturated cohesionless soils.

C. Theoretical

Bretz (1988) developed a closed form solution to theoretically predict radial and tangential strain and stress due to the detonation of

spherical charges in water saturated soil. The method models water saturated soil as an elastic water-solid mixture having zero shear strength and assuming that the soil particle contact can be ignored. Assuming that the soil skeleton follows the same strain path as the mixture, linear and non-linear stress-strain characteristics of the soil skeleton can be followed both during the loading and unloading phase. The method closely matches the results of field explosive tests on saturated sands reported by Bretz (1988). The basic equations utilized by Bretz (1988) are:

$$B_M = \frac{(1 + e)\, B_s\, B_w}{B_s\, e + B_w} \quad \text{(Wood Equation)} \quad \text{Eq. 8.1}$$

where B_M is the bulk modulus of the mixture; B_s and B_w are bulk moduli of the granules and water, respectively; and e is the void ratio.

$$\sigma_r = \frac{E}{(1 + \mu)(1 - 2\mu)} \left[(1 - \mu) \frac{\partial u}{\partial r} + 2\mu \frac{u}{r}\right] \quad \text{Eq. 8.2}$$

$$\sigma_r = \frac{E}{(1 + \mu)(1 - 2\mu)} \left[\mu \frac{\partial u}{\partial r} + \frac{u}{r}\right] \quad \text{Eq. 8.3}$$

where σ_r and σ_t are radial and tangential stresses, μ is Poisson's ratio; u is radial displacement; r is radius at which u occurs; and E is modulus of elasticity.

$$c_v = \frac{\partial^2 u_e}{\partial z^2} = \frac{\partial u_e}{\partial t} \quad \text{Eq. 8.4}$$

where c_v is the coefficient of consolidation; u_e is excess porewater pressure; z is a coordinate in the verticle direction, and t is time. This equation is the consolidation equation, and it was used with a finite difference solution to calculate excess porewater pressure after passage of the dynamic stress wave, i.e., in the t + 1 regime. Since soils are

multiphase materials, the soil skeleton is inelastic and excess porewater pressure dissipation occurs with time, a true closed form theoretical model for multiphase soil would be very complex and may be impossible to formulate. Theoretical modeling of the soil particle contacts to better understand the nonlinearity of granular material is needed.

VIII. SUMMARY

Our field, laboratory and theoretical research indicate that the destruction potential of an explosion may be greatly magnified if detonated in water saturated granular soils. While blast-induced liquefaction may not necessarily damage a facility structurally, it may render it unusable. Empirical models are given that can be used to estimate liquefaction potential as a function of density, effective stress and applied compressive strain. One of the models uses an empirical scaling law for explosive loadings to predict the extent of porewater pressure increases in the field from buried, contained charges in saturated soils. A numerical analysis that considers the saturated soil as a two-phase medium is presented. The analysis accounts for the nonlinear, inelastic behavior of the soil skeleton and has shown that liquefaction is dependent upon the constrained modulus of the soil skeleton. Results agree with the experimental observations of peak and long-term porewater pressure responses.

The results of our study indicate the following.

1. Liquefaction can be induced by single and multiple blasts.
2. Liquefaction can be induced at distances much greater than those associated with structural damage.
3. Long term increases in residual porewater pressures can be induced by compressive shock wave loadings when the peak particle velocity exceeds 0.075 m/s.
4. Liquefaction can be induced in loose saturated sand by a single compressive shock wave when the peak particle velocity exceeds 0.75 m/s.

5. Soils at higher initial effective stress and higher initial relative density require more energy to produce liquefaction.
6. Destruction potential of an explosive charge may be greatly magnified if detonated in water-saturated soils.
7. Liquefaction occurs because of compressive strain induced by the compression stress wave, but liquefaction occurs after the stress wave passes.
8. Liquefaction occurs because loading-unloading of the porewater is elastic but the soil skeleton is not.

An explosive detonated in a soil having a high liquefaction potential could cause damage disproportionate to the energy released. Documented occurrence of blast-induced liquefaction is available in the open literature. Although considerable work remains to be done in projecting this information into a comprehensive method of predicting liquefaction for actual or hypothetical blasts, the data indicate that residual porewater pressure increases should not occur in soils subject to strains of less than 0.005 percent. Transient and quasi-static tests indicate that residual porewater pressure increases and liquefaction are not strain-rate sensitive for sand but are strain-rate sensitive for silt.

IX. REFERENCES

Allard, D.J., (1988), M.S. Thesis, Dept. of Civil Engineering, Colorado State University, Fort Collins, Colorado, in preparation.

Chouicha, M.A., (1987), "Shock Induced Liquefaction Potential of Sand and Gravel," M.S. Thesis, Department of Civil Engineering, Colorado State University, Fort Collins, Colorado, Fall, 127 p.

Arya, A.S, Nandakumaran, P., Puri, V.K. and Mukerjee, S., (1978), "Verification of Liquefaction Potential by Field Blast Tests," 2nd International Conference on Microzonation for Safer Construction, American Society of Civil Engineers (ASCE) Earthquake Eng., Vol. 1, San Francisco, California, Nov. 26-Dec. 1, pp. 865-869.

Awad, A.A., (1988), Ph.D. Thesis, Dept. of Civil Engineering, Colorado State University, Fort Collins, Colorado, in preparation.

Banister, J.R., and Ellett, D.M., (1974), "Pore Pressure Enhancements Observed on Rio Blanco", Sandia National Laboratories, Report No. SLA-74-0328, Albuquerque, N.M., Aug., 47 p.

Banister, J.R., Pyke, R. Ellett, D.M., and Winters, L., (1976), "In-Situ Pore Pressure Measurements at Rio Blanco", Journal of the Geotechnical Engineering Division, American Society of Civil Engineers (ASCE), Vol. 102, No. GT10, Oct., pp. 1073-1091.

Biot, M.A., (1956), "Theory of Propagation of Elastic Waves in a Fluid Saturated Porous Solid, I. Low-Frequency Range and II. Higher Frequency Range," Journal Acoustical Society of America, Vol. 28, No. 2, March, pp. 168-191.

Biot, M.A., (1962), "Mechanics of Deformation and Acoustic Propagation in Porous Media," Journal of Applied Physics, Vol. 33, No. 4, pp. 1482-1498.

Blouin, S., (1978), "Liquefaction Evidence Observed in Various Explosive Events", Int. Workshop on Blast-Induced Liquefaction, Organized by Dames & Moore, London, U.S. Air Force Office of Scientific Research (AFOSR), Maidenhead, U.K., Sept., pp. 95-110.

Blouin, S.E. and Shinn, K.J., (1983), "Explosion Induced Liquefaction", U.S. Air Force Office of Scientific Research (AFOSR) Contract: F49620-81-C-0014, Applied Research Associates, Inc., New England Division, South Royalton, Vermont, September, 227 p.

Bolton, J.M., (1988), "Undrained Confined Compression Behavior of Saturated Sand and Silt," M.S. Thesis, Department of Civil Engineering, Colorado State University, Fort Collins, Colorado.

Bretz, T.E., (1988), Ph.D. Thesis, Dept. of Civil Engineering, Colorado State University, Fort Collins, Colorado, in preparation.

Carnes, B.L., (1981), "The Influence of a Shallow Water Table on Cratering", Technical Report SL-81-6, US Army Corps of Engineers, Waterways Experiment Station, Vicksburg, Miss., September, 122 p.

Castro, G. and Poulos, S.J., (1977), "Factors Affecting Liquefaction and Cyclic Mobility," Journal of the Geotechnical Engineering Division, ASCE, Vol. 103, No. GT6, pp. 501-506.

Charlie, W.A., (1978), "The Dial Pack Event", Int. Workshop on Blast-Induced Liquefaction, Dames and Moore, AFOSR, Maidenhead, U.K. Sept. 17-19, pp. 149-165.

Charlie, W.A. and Veyera, G., (1985), "Explosive Induced Porewater Pressure Increases". 11th Int. Conf. on Soil Mechanics and Foundation Engineering, San Francisco, California, Vol. 2, August, pp. 997-1000.

Charlie, W.A., Mansouri, T., and Ries, E., (1981), "Predicting Liquefaction Induced by Buried Charges", 10th Int. Conf. on Soil Mechanics and Foundation Engineering, Stockholm, Sweden, June, Vol. 1, pp. 77-80.

Charlie, W.A., Shinn, J., Melzer, L.S., Martin, J.P. and Blouin, S.E., (1980), "Blast-Induced Liquefaction Phenomenon and Evaluation," Int. Symposium on Soils under Cyclic and Transient Loading, Swansea, United Kingdom, January, pp. 533-542.

Charlie, W.A., Doehring, D.O. and Veyera, G.E., (1987), "An APL Function for Modeling P-Wave-Induced Porewater Pressure," COGS Computer Contributions, Computer Oriented Geological Society, Vol. 3, No. 3/4, pp. 123-127.

Charlie, W.A., Veyera, G.E., Doehring, D.O. and Abt, S.R., (1985), "Blast Induced Liquefaction Potential and Transient Porewater Pressure Response of Saturated Sands," Final Report, Research Grant No. AFOSR-80-0260, Air Force Office of Scientific Research, Colorado State University, Oct., 198 p.

Charlie, W.A., Veyera, G.E., and Muzzy, M.W., (1982), "Shock Induced Soil Liquefaction - Test Facility Development," 28th International Instrumentation Symposium, Instrument Society of America, Las Vegas, Nevada, pp. 45-49.

Committee on Earthquake Engineering, (1985), "Liquefaction of Soils during Earthquakes," National Academy Press, Washington, D.C., pp. 20-30.

Committee on Soil Dynamics of the Geotechnical Engineering Division, American Society of Civil Engineers, (1978), "Definition of Terms Related to Liquefaction," Journal of the Geotechnical Engineering Division, American of Civil Engineers, Vol. 104, No. GT 9, September, pp. 1197-1200.

Cole, R.H., (1948), Underwater Explosions, Princeton University Press, (reprinted by Dover Publications in 1965), Princeton, N.J., 437 p.

Crawford, R.E, Higgins, C.J. and Bultmann, E.A., (1974), The Air Force Manual for Design and Analysis of Hardened Structures, Air force Systems Command, Kirtland kAir Force Base, Albuquerque, New Mexico, July, 1118 p.

Damitio, C., (1978), "Field Experience on Blast-Induced Liquefaction", Int. Workshop on Blast-Induced Liquefaction, Dames and Moore, AFOSR, Maidenhead, U.K., Sept. 17-29, pp. 137-148.

Dill, R.F., (1967), "Effects of Explosive Loading on the Strength of Sea-Floor Sands" Marine Geotechnique, University of Illinois Press, Chicago, pp. 291-302.

Dowding, C.H., and Hryciw, R.D., (1986), "A Laboratory Study of Blast Densification of Saturated Sand", Journal of Geotechnical Engineering, ASCE, Vol. 112, No. 2, Feb., pp. 187-199.

Drake, J., (1978), "Results of some Experiments Conducted Primarily for the Purpose of Understanding the Influence of Water Table Depth on the Size and Extent of Craters". Int. Workshop on Blast-Induced Liquefaction, Dames and Moore, AFOSR, Maidenhead, U.K., Sept. 17-19, pp. 250-266.

Drake, J. L. and Ingram, L. F., (1981), "Predictions of the Airblast and Ground Motions Resulting from Explosive Removal of the Birds Point-New Madrid Fuze Plug Levee", Miscellaneous Paper: SL-81-30, U.S. Army Corps of Engineers, Waterways Experiment Station, Vicksburg, Mississippi, November, 23 p.

Drake, J.L. and Little, C.D., (1983), "Ground Shock from Penetrating Conventional Weapons," 1st Symposium of Non-Nuclear Munitions with Structures, U.S. Air Force Academy, Colorado, May, pp. 1-6.

Florin, V.A., and Ivanov, P.L., (1961), "Liquefaction of Saturated Sandy Soils", 5th Int. Conf. on Soil Mechanics and Foundation Engineering, Vol. 1, Paris, France, July 17-22, pp. 107-111.

Fragaszy, R.J., and Voss, M.E., (1986), "Undrained Compression Behavior of Sand", Journal of Geotechnical Engineering, ASCE, Vol. 112, No. 3, Mar., pp. 334-347.

Fragaszy, R.J., Voss, M.E., Schmidt, R.M. and Holsapple, K.A., (1983), "Laboratory and Centrifuge Modeling of Blast-Induced Liquefaction," 8th Int. Symposium on Military Application of Blast Simulation, Spiez, Switzerland, proceedings II, pp. III.5-1 to III.5-20.

Gilbert, P.A., (1976), "Case Histories of Liquefaction Failures," Miscellaneous Paper S-76-4, U.S. Army Corps of Engineers Waterways Experiment Station, Vicksburg, Mississippi, April.

Hassen, H.A. (1988), Ph.D. Thesis, Dept. of Civil Engineering, Colorado State University, Fort Collins, Colorado, in preparation.

Hendron, A.J., (1963), "The Behavior of Sand in One-Dimensional Compression," Ph.D. Thesis, Dept. of Civil Engineering, University of Illinois at Urbana.

Hubert, M.E., (1986), "Shock Loading of Water Saturated Eniwetok Coral Sand", M.S. Thesis, Department of Civil Engineering, Colorado State University, Fort Collins, Colorado, Fall, 159 p.

Ivanov, P.L., (1967), "Compaction of Noncohesive Soils by Explosions". Izdatel'stvo Literatury Po Stroitel'stvu, Leningrad, U.S.S.R., Translated by the Indian National Scientific Documentation Center, New Delhi, India; Published for the U.S. Department of the Interior, Bureau of Reclamation and National Science Foundation, Washington, D.C., 211 p.

Ivanov, P.L., Sinitsyn, A.P. and Musaelyan, A.A., (1981), "Characteristics of Soils at Cyclic and Shock Loads," 10th Int. Conf. on Soil Mechanics and Foundation Engineering, Stockholm, Sweden, Vol. 3, June, pp. 239-243.

Jacobs, P.J., (1988), "Blast-Induced Liquefaction of an Alluvial Sand Deposit," M.S. Thesis, Dept. of Civil Engineering, Colorado State Univ., Ft. Collins, Colorado, 228 p.

Jaramillo, E.E. and Pozega, R.E., (1974), "Middle Gust Free Field Data Analysis," Defense Nuclear Agency, Air Force Weapons Laboratory Report No. AFWL-TR-73-251, April.

Jones, G.H.S., (1976), "Complex Craters in Alluvium," Proc. Symp. on Planetary Cratering Mechanics, U.S. Geologic Survey, Geologic Div., Branch of Astrogeologic Studies, Flagstaff, Arizona, Sept., pp. 163-182.

Kim, K.J., and Blouin, S.E., (1984), "Response of Saturated Porous Nonlinear Materials to Dynamic Loadings", Air Force Office of Scientific Research, Contract No. F49620-81-C-0014, Applied Research Assoc. Inc., South Royalton, Vermont, 99 p.

Klohn, E.J., Garga, V.K. and Shukin, W., (1981), "Densification of Sand Tailings by Blasting", 10th Int. Conf. on Soil Mechanics and Foundation Engineering, Vol 3., Stockholm, Sweden, June, pp. 725-730.

Kok, L., (1977), "The Effect of Blasting in Water-Saturated Sands", 5th Int. Symposium on Military Applications of Blast Simulation, Stockholm, Sweden, May, pp. 7:6:1-7:6:10.

Kok, L., (1978a), "Some Empirical Prediction on Blast-Induced Liquefaction", Int. Workshop on Blast-Induced Liquefaction, Dames and Moore, AFOSR, Maidenhead, U.K., Sept., pp. 408-424.

Kok, L., (1978b), "Some Dutch Laboratory and Field Results on Blast-Induced Liquefaction", Int. Workshop on Blast-Induced Liquefaction, Dames and Moore, Maidenhead, U.K., AFOSR, Sept., pp. 71-94.

Kok, L., (1978c), "Explosion - Densification and Vertical Drainage as Soil Consolidation Techniques for Harbour Building", Proc. 7th international Harbour Congress, Antwerp, Belgium, pp. 1.04/1-7.

Kolsky, H., (1963), Stress Waves in Solids, Dover, New York, New York, 213 p. 213

Kummeneje, O. and Eide, O., (1961), "Investigation of Loose Sand Deposits by Blasting", 5th Int. Conf. on Soil Mechanics and Foundation Engineering, Vol. 1, Paris, France, July, pp. 491-497.

Kurzeme M., (1971), "Liquefaction of Saturated Granular Soils", 1st Australia-New Zealand Conference on Geomechanics, Australian Geomechanics Society, Melbourne, Australia, Vol.1, August 9-13, pp. 45-53.

Ladd, R.S., (1978), "Preparing Test Specimens Using Undercompaction", American Society for Testing and Materials Geotechnical Testing Journal, American Society for Testing and Materials, Philadelphia, Pennsylvania, Vol. 1, No.1, March, pp. 16-23.

Lambe, W.T. and Whitman, R.V., (1969), Soils Mechanics, John Wiley and Sons, New York, 553 p.

Langley, N.P., Smith, C.R., and Pfefferle, W., (1972), "Dial Pack Event, Soil Pore Pressure and Shear Strength Test", Aerospace Report No. TOR-0172-(S2970-20)-1, Space and Missile Systems Organization, Air Force Command, California, 139 p.

Lee, K.L., Morrison, R.A. and Haley, S.C., (1969a), "A Note on the Pore Pressure Parameter B", 7th Int. Conf. of Soil Mechanics and Foundation Engineering, Mexico, Vol. 1, pp. 231- 238.

Lee, K.L., Seed, B.H. and Dunlop, P., (1969b), "Effect of Transient Loading on the Strength of Sand", 7th Int. Conf. of Soil Mechanics and Foundation Engineering, Mexico, Vol. 1, pp. 239-246.

Long, J.H., Ries, E.R. and Michalopoulos, A.P., (1981), "Potential for Liquefaction Due to Construction Blasting", Int. Conf. on Recent Advances in Geotechnical Earthquake Engineering and Soil Dynamics, St. Louis, Missouri, Vol. 1, April-May, pp. 191-194.

Lyakhov, G.M., (1961), "Shock Waves in the Ground and the Dilution of Water Saturated Sand", Source: Zhurnal Prikladnoy Mekhaniki i. Tckhricheskoy, Fiziki, Moscow, USSR, Vol. 1, pp. 38-46.

Marti, J., (1978), "Blast-Induced Liquefaction of Materials," Report No. AFOSR-TR-78-3, Dames and Moore, London, U.K., Technical Report to AFOSR, Bolling Air Force Base, Wash., D.C.

Mason, H., and Walter, D., (1968), "An Exploratory Study to Assess The Magnitude of OCD Foundation Problems". Office of Civil Defense. Contract No. 12646 (6300A-590) California, 125 p.

McCracken, J. (1978), "Introductory Remarks," Int. Workshop on Blast-Induced Liquefaction," Dames and Moore, London, AFOSR, Maidenhead, U.K., Sept., pp. 9-11.

Melzer, L.S., (1978), "Blast-Induced Liquefaction of Materials", Nuclear Technology Digest, AFWL-TR-78-110, Air Force Weapons Lab., Kirkland Air Force Base, Albuquerque, New Mexico, August, pp. 21-38.

Mitchell, J.K. and Katti, R.K., (1981), "Soil Improvement - State-of-the-Art Report (preliminary)", 10th Int. Conf. on Soil Mechanics and Foundation Engineering, Stockholm, Sweden, June, pp. 261-317.

Muzzy, M.W., (1983), "Cyclic Triaxial Behavior of Monterey No. 0 and 0/30 Sands," M.S. Thesis, Dept. of Civil Engineering, Colorado State Univ., Fort Collins, Colorado, 142 p.

Nordyke, M.D., (1976), "Nuclear Cratering Experiments: United States and Soviet Union", Impact and Explosion Cratering, Proc. of Symposium on Planetary Cratering Mechanics, Flagstaff, Arizona, Sept., also in Impact and Explosive Cratering, (1977), Roddy, D.J., Pepin, R.O. and Merrill, R.B., Editors, Pergamon Press, New York, pp. 103-124.

Obermeyer J.R., (1980), "Monitoring Uranium Tailing Dams during Blasting Program", Symposium on Uranium Mill Tailings Management, Dept. of Civil Eng., Colorado State University, Ft. Collins, Colorado, Nov., pp. 513-527.

Perry, E.B., (1972), "Movement of Variable Density Inclusions in Wet Sand under Blast Loading", Misc. Paper S-72-37, U.S. Army Waterways Experiment Station, Vicksburg, Miss., 59 p.

Prakash, S., (1981), Soil Dynamics, McGraw Hill Book Co., New York, pp. 320-328.

Prakash, S. and Gupta, M.K., (1970), "Blast Tests at Tenughat Dam Site", Journal of the Southeast Asian Society of Soil Engineering, Vol. 1, No. 1., June, pp. 41-50.

Puchkov, S.V., (1962), "Correlation Between the Velocity of Seismic Oscillations of Particles and the Liquefaction Phenomenon of Water Saturated Sand", Problems of Engineering Seismology, Issue No. 6, Edited by Prof. S.V. Medvedev, Translated from Russian by Consultants Bureau, New York, pp. 92-94.

Queiroz, L.A., Oliveira, H.G., and Nazario, F.A., (1967), "Foundation Treatment of Rio Casca III Dam", 9th Int. Congress on Large Dams, Istanbul, Turkey, Vol. 1, Sept., pp. 321-333.

Richart, F., Hall, J. and Woods, R.D., (1970), Vibrations of Soils and Foundations, Prentice-Hall, Englewood Cliffs, New Jersey.

Rischbieter, F., (1977), "Soil Liquefaction-A Survey of Research", Proc. 5th International Symposium on Military Application of Blast Simulation, Stockholm, Sweden, May, pp. 7:1:1-7:1:24.

Rischbieter, F., (1978) "Liquefaction Tests on Re-filled, Partly Saturated Soil", Int. Workshop on Blast-Induced Liquefaction, Dames and Moore, AFOSR, Maidenhead, U.K.,September, pp. 65-70.

Rischbieter, F., Corvin P., Metz, K. and Schaepermeier, E., (1977), "Studies of Soil Liquefaction by Shock Wave Loading", 5th Int. Symposium on Military Application of Blast Simulation, Stockholm, Sweden, May, pp. 7:4:1-7:4:12.

Roddy, D.J., (1976), "Large-Scale Impact and Explosion Craters: Comparisons of Morphological and Structural Analogs", Proc. Symposium on Planetary Cratering Mechanics, Flagstaff, Arizona, September, also in Impact and Explosion Cratering, (1977), Roddy, D.J., Pepin, R.O. and Merrill, R.B., editors, Pergamon Press, New York, pp. 185-246.

Rwebyogo, F.J., (1987), "Time-Dependent Cone Penetration Resistance of a Disturbed Natural Sand Deposit," M.S. Thesis, Dept. of Civil Engineering, Colorado State Univ., Fort Collins, Colorado, Fall, 100 p.

Sanders, S.G., (1982), "Assessment of the Liquefaction Hazards Resulting from Explosive Removal of the Bird's Point New-Madrid Fuze Plug Levee", Misc. Paper No. GL-82-5, U.S. Army Corps of Engineering Waterways Experiment Station, Vicksburg, Mississippi, April, 32 p.

Schaepermeier, M.E., (1978a), "A Semi-Empirical Method for the Prediction of the Stability of Buried Shelters by Groundshocks-Induced Liquefaction", Int. Workshop on Blast-Induced Liquefaction, Dames and Moore, AFOSR, Maidenhead, U.K., Sept., pp. 401-407.

Schaepermeier, M.E., (1978b), "Liquefaction Induced by Compressional Waves", Int. Workshop of Blast-Induced Liquefaction, Dames and Moore, AFOSR, Maidenhead, U.K., Sept., pp. 57-64.

Schaepermeier, M.E., (1978c), "Soil Liquefaction Field Test in Meppen Proving Ground, 1978, Synoptic Paper", 6th Int. Symposium on Military Applications of Blast Simulation, Cahors, France, p. 7.4.1-5.

Schaepermeier, M.E., (1978d), "Soil Liquefaction Field Test in Meppen Proving Ground, 1978, Structure Response", 6th Int. Symposium on Military Applications of Blast Simulation, Cahors, France, pp. 7.5.1-27.

Schmidt, R.M., Fragaszy, R.J. and Holsapple, K.A., (1981), "Centrifuge Modeling of Soil Liquefaction due to Airblast", 7th Int. Symposium on Military Application of Blast Simulation, Alberta, Canada, July, Vol. 3, pp. 4.2-1 to 4.2-18.

Schure, L.A., (1988), M.S. Thesis, Dept. of Civil Engineering, Colorado State University, Fort Collins, Colorado, in preparation.

Seed, H.B., (1976), "Evaluation of Soil Liquefaction Effects on Level Ground During Earthquakes," Liquefaction Problems in Geotechnical Engineering, ASCE Preprint 2752, ASCE, New York, pp. 1-104.

Skempton, A.W., (1954), "The Pore-Pressure Coefficients A and B", Geotechnique, Vol. 4, pp. 143-147.

Solymar, Z., Iloabachie, B., Gupta, R. and Williams, L., (1984), "Earth Foundation Treatment at Jebba Dam Site", Journal of Geotechnical Engineering, American Society of Civil Engineers, Vol. 110, No. 10, Oct., pp. 1415-1430.

Studer, J., and Hunziker, E., (1977), "Experimental Investigation on Liquefaction of Saturated Sand Under Shock Loading". 5th Int. Symposium on Military Appl of Blast-Induced Liquefaction, Stockholm, Sweden, pp. 7:2, 1-19.

Studer, J. and Kok, L., (1980), "Blast-Induced Excess Porewater Pressure and Liquefaction Experience and Application." Int. Symposium on Soils under Cyclic and Transient Loading, Swansea, U.K., January, pp. 581-593.

Studer, J., Kok, L. and Trense, R.W., (1978), "Soil Liquefaction Field Test - Meppen Proving Ground 1978 Free Field Response", 6th Int. Symposium on Military Applications of Blast Simulation, Cahors, France, pp. 7.31-48.

Studer, J., (1978), "Laboratory and Field Shock Tube Tests," Int. Workshop on Blast-Induced Liquefaction, Dames and Moore, AFOSR, Maidenhead, U.K., Sept., pp. 167-187.

Studer, J. and Kok, L., (1980), "Blast-Induced Excess Porewater Pressures and Liquefaction: Experience and Application," Int. Symposium on Soils Under Cyclic and Transient Loading, Swansea, United Kingdom, January 7-11, pp. 581-593.

Studer, J. and Prater, E.G., (1977), "An Experimental and Analytical Study of the Liquefaction of Saturated Sands Under Blast Loads," Int. Conf. on Numerical Methods in Soil and Rock Mechanics, Karsruhe, Germany, Vol. 2, September 5-16, pp. 217-238.

Terzaghi, K., (1956), "Varieties of Submarine Slope Failures". Proc. of the 8th Texas Conference on Soil Mechanics and Foundation Engineering, Bureau of Engineering and Foundation Research, University of Texas, Austin, Texas, September, pp. 24 and 39.

Timoshenko, S.P. and Goodier, J.W., (1970), Theory of Elasticity, McGraw-Hill, New York, 567 p.

Trense, R.W., (1977), "Soil Liquefaction - New Results from Dutch Tests". 5th Int. Symposium on Military Application of Blast Simulation, Stockholm, Sweden, May, pp. 7:5/1-6.

True, D.G., (1969), "Dynamic Pore Pressure Propagation in Sand", Technical Report R-610, Naval Civil Engineering Laboratory, Port Hueneme, California, 45 p.

Van Der Kogel, H., Van Loon-Engels, C.H. and Ruygrok, P.A., (1981) "Wave Propagation in Porous Media, Shock Tube Experiments", 10th Int. Conf. on Soil Mechanics and Foundation Engineering, Stockholm, Sweden, Vol 3., June, pp. 253-256.

Veyera, G.E., (1985), "Transient Porewater Pressure Response and Liquefaction in a Saturated Sand", Doctoral Dissertation, Department of Civil Engineering, Colorado State University, Fort Collins, Colorado, Fall, 198 p.

Veyera, G.E. and Charlie, W.A., (1984), "Shock Induced Porewater Pressure Increases in Soil," Int. Symposium on Dynamic Soil Structure Interaction, Univ. of Minnesota, Minneapolis, Minnesota, Sept.

Yamamura, K. and Koga, Y., (1974), "Estimation of Liquefaction Potential by Means of Explosion Test", Proc. of the 6th Joint Panel Conference of U.S. - Japan Cooperative Program in Natural Resources, National Bureau of Standards, Washington, D.C., Vol. 76, May. pp. III-38-51.

Zienkiewicz, O.C. and Bettess, P., (1982), "Soils and other Saturated Media Under Transient and Dynamic Conditions," in Pande, G.N. and Zienkiewicz, O.C., eds., Soils Under Cyclic and Transient Loading, John Wiley and Sons, New York, pp. 1-6.

page left blank

APPENDIX A

LABORATORY SHOCK TESTS ON SAND

APPENDIX A.1. MONTEREY NO. 0/30 QUARTZ BEACH SAND

1. Skeleton Stress-Strain Curves

Static one-dimensional, confined, compression tests (Hendron, 1963; Whitman et al., 1964) were performed on air dry samples of Monterey No. 0/30 sand. The results of tests were used to obtain stress-strain information for the soil skeleton and to determine the constrained modulus of the skeleton to be used in calculating the theoretical porewater pressure response (C-parameter) and for modeling of the residual porewater pressure. To simulate the initial stress conditions in the experimental investigation, a corresponding initial effective stress was applied to each sample. The compressive strain values were referenced to the initial applied stress. Each sample was loaded and unloaded in increments two times to develop the stress-strain relationship for the soil skeleton. From these results, a constrained modulus for loading and unloading was determined.

Samples were tested at relative densities of 40 and 80 percent. Each sample was tested at initial effective stresses of 86 kPa and 690 kPa. The skeleton stress-strain curves for Monterey No. 0/30 sand are shown in Figures A.2 through A.5. The results show that the soil skeleton stiffness increases with increasing initial effective stress and density. Hysteresis between the loading and unloading curves decreases with increasing initial effective stress and density.

2. Static C-Parameter Response

Before loading of each sample, the porewater pressure response was checked to determine the degree of saturation. This was done by

increasing the confining pressure on the sample and monitoring the sample's porewater pressure response without drainage. The ratio of the sample porewater pressure response to the increase in confining pressure is termed the "C-parameter" (Lambe and Whitman, 1969) for a one-dimensional confined, compressive loading of a saturated soil with undrained conditions. A ratio of one indicates a saturated sample and values less than one indicates that the sample is not saturated or has a stiff soil skeleton. For an initial effective stress of 86 kPa, a ratio of one was consistently obtained. However, a C-parameter of less than one was obtained for higher initial effective stresses. Since the preparation and saturation process was identical for each sample, it was assumed that the porewater pressure ratios obtained indicated of a saturated condition. An examination of the compressive stress wave propagation velocity through samples verified this assumption. The measured compressive stress wave velocities were close to 1,500 meters per second in all samples investigated. This is the value that would be expected for saturated conditions.

Throughout the experimental investigation it was noted that the porewater pressure ratio varied in a predictable manner with variations in effective stress and relative density (Figure A.6). In considering this observation and those previously discussed, it is believed that the porewater pressure ratio response noted can be attributed to changes in the soil skeleton stiffness which increases with increasing initial relative density and effective stress. Accordingly, all samples were considered to be saturated.

3. Pressure-Time Histories

The pressure-time histories represent the porewater pressure transducer responses to applied shock loadings as function of time. They include both the peak and long-term response for the confining pressure and the sample porewater pressure. Selected pressure-time histories, representative of the behavior observed in this experimental investigation, are shown in Figures A.7 and A.8. A summary of numerical results from the pressure-time histories of all samples investigated is given in Tables A.2 through A.12.

Figure A.7 shows the experimental result for the "40%" relative density series at an effective stress of 172 kPa. Figure A.8 shows the experimental result for the "80%" relative density series at an effective stress of 172 kPa. The confining pressure and sample porewater pressure responses have been plotted together on each figure. The "series" designation for relative density has been used to group together data having approximately the same relative density. The designations include data that is within 10 percent greater than the series number (including the series number). For example, a "40%" series designation would include all data for a relative density from 40 percent to 49 percent.

The pressure-time histories are indicative of the system response during and after loading. On each figure, the traces of the confining pressure and sample porewater pressure follow each other closely in their response trends. The two curves are slightly offset from one another in the time domain due to the relative locations of each transducer. The sample peak porewater pressure is greater than the applied stress peak values for each impact.

In all cases, the confining pressure transducer response returned to its original baseline value once the compressive stress wave energy had dissipated. The confining pressure should return to its original value if the system is not allowed to drain. The residual excess porewater pressure indicated by the sample transducer, was above its original baseline value after each loading and continued to increase with each successive impact. The response of the sample porewater transducer was as expected since an increase in the residual excess porewater pressure should be maintained for undrained conditions. Liquefaction occurs when the residual excess porewater equals the effective stress which is also when the back pressure plus the residual excess porewater pressure equals the confining pressure.

The information from the pressure-time history records was used for the analysis of data presented in Tables A.2 through A.12. The porewater pressure response was evaluated as a function of initial effective stress, initial sample density, peak compressive strain.

APPENDIX A.2. TYNDALL QUARTZ BEACH SAND

1. Static Compression Tests on the Soil Skeleton

Static compression tests were not run on these samples.

2. Static C-Parameter Response

The saturation process was easily accomplished and the C-parameter was .92, .88 and .77 for relative densities of 55, 63 and 73 percent.

APPENDIX A.3. POUDRE VALLEY GRANITIC SAND

1. Skeleton Stress-Strain Curves

Samples of air dry soil were tested at initial relative densities of 20, 40, 60 and 80 percent. The skeleton stress-strain curves are shown in Chapter V.

2. Static C-Parameter Response

The C parameter varied between 0.95 for loose samples under a low effective stress to 0.5 for dense samples under a high effective stress. Compression wave velocity through the sample of approximately 1,500 m/sec confirmed that the sample was saturated.

3. Shock Induced Settlement

In Figure A.11, the settlement ratio is plotted versus the initial relative density.

APPENDIX A.4. POUDRE VALLEY GRANITIC FINE SAND AND GRAVEL

1. Skeleton Stress-Strain Curves

Static compression tests were not run on these samples.

2. Static C-Parameter Response

The static C-parameter ranged from 0.85 to 0.81 for the sand and from 0.98 to 0.89 for the gravel.

APPENDIX A.5. ENIWETOK CORAL BEACH SAND

One-dimensional static compression tests were performed on dry samples of Eniwetok coral sand to evaluate the stress-strain behavior of the soil skeleton and to estimate its crushing potential. The samples, at 40 and 80 percent relative density with an initial low and high confining pressure (150 and 517 kPa) were loaded and unloaded incrementally twice to generate the stress-strain relationship of the soil skeleton. Figures A.15 to A.20 show the variation in stress-strain for each test. The low density, low effective stress test is more compressible than the high density, high effective stress test.

In Figures A.15 and A.16, for low effective stresses, crushing of the particles can be recognized by the reverse curvature of the stress-strain curve (Lambe and Whitman, 1969). The result of these coral sand compression tests show a definite concave trend toward the strain axis on the loading path. Popping sounds could be heard during loading indicating also a moderate amount of particle fracturing.

2. Static C-Parameter Response

For all tests, the C-parameter value was less than one (Figure A.21). For low effective stress and low relative density tests, the porewater pressure response was usually higher than for the tests with denser sands and higher effective stresses. This difference may be attributed to the changes in soil skeleton stiffness since the compressibility of a soil skeleton will decrease with increases in effective stress and in relative density (Lee et al., 1969). Veyera (1985) reported similar porewater pressure response was recorded for

saturated dense sands. Accordingly, most tests were considered saturated. Secondary porosity of the individual sand grain, where the air may not have been totally removed and system compliance may also explain the lower C-parameter. Measured compression wave velocities of 1500 meters per second or greater through the sample indicate full saturation.

3. Shock Induced Settlement

Shock induced settlement as a function of relative density is given in Figure A.17

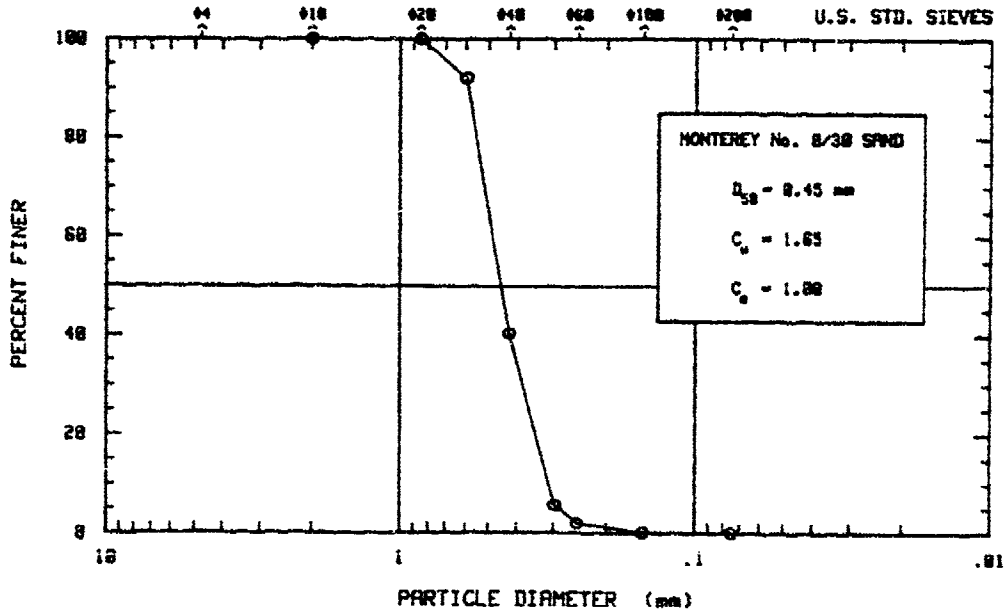

Figure A.1 Grain size distribution for Monterey No. 0/30 sand (Muzzy,1983; Charlie et al.,1984).

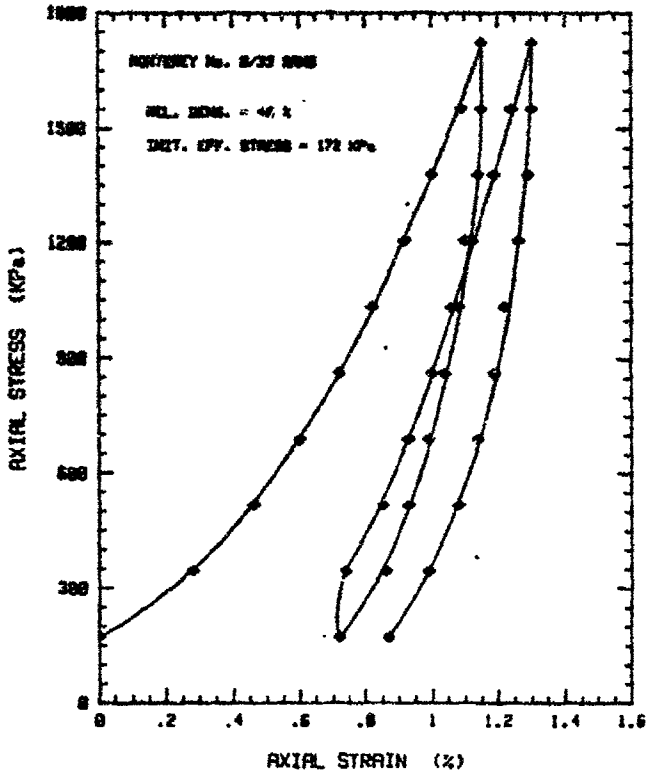

Figure A.2 Skeleton stress-strain curve for Monterey No. 0/30 sand at D_r = 40% and σ_o' = 172 kPa.

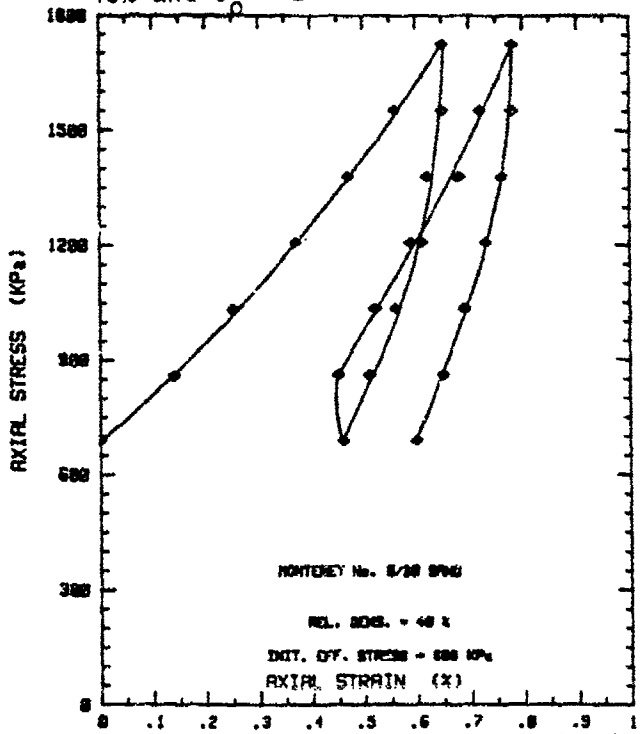

Figure A.3 Skeleton stress-strain curve for Monterey No. 0/30 sand at D_r = 40% and σ_o' = 690 kPa.

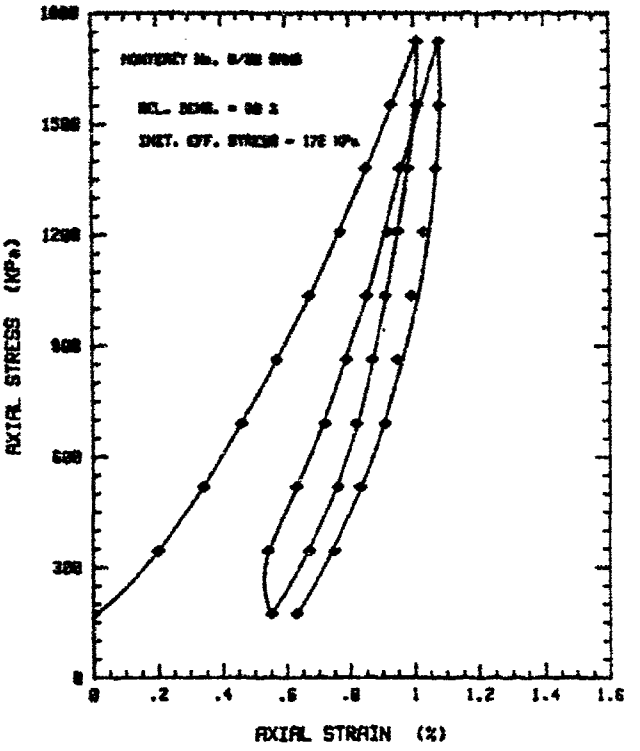

Figure A.4 Skeleton stress-strain curve for Monterey No. 0/30 sand at D_r = 80% and σ_o' = 172 kPa.

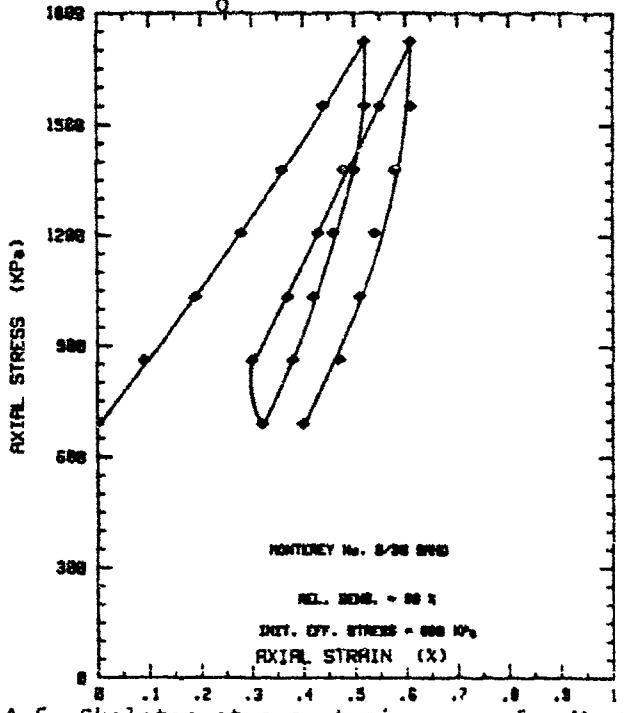

Figure A.5 Skeleton stress-strain curve for Monterey No. 0/30 sand at D_r = 80% and σ_o' = 690 kPa.

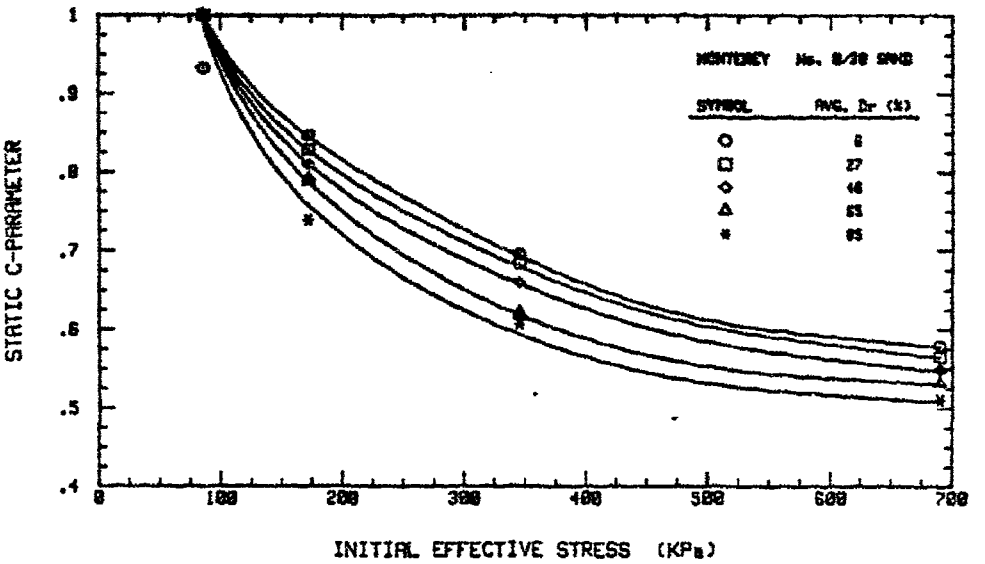

Figure A.6 Static C-Parameter response as a function of effective stress for Monterey No. 0/30 sand.

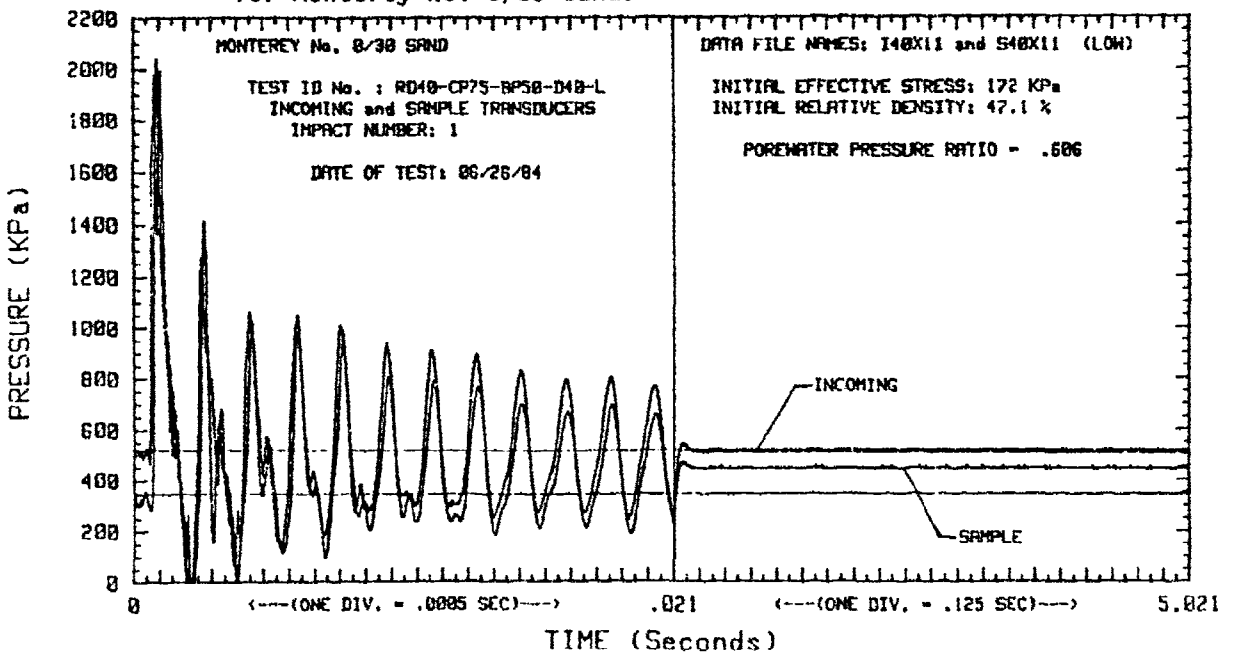

Figure A.7 Pressure-time histories for D_r = "40%" series and σ'_o = 172 kPa (low impact stress-first impact), Monterey No. 0/30 Sand.

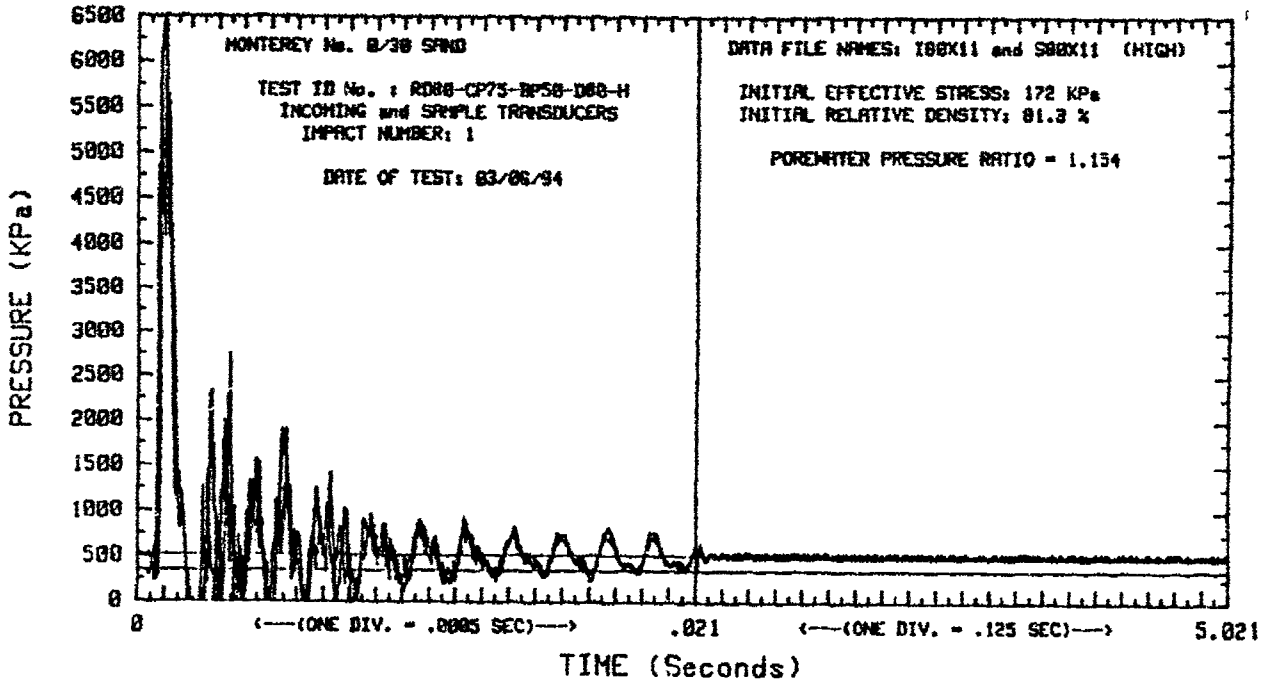

Figure A.8 Pressure-time histories for D_r = "80%" series and σ'_o kPa (high impact stress-first impact), Monterey No. 0/30 sand.

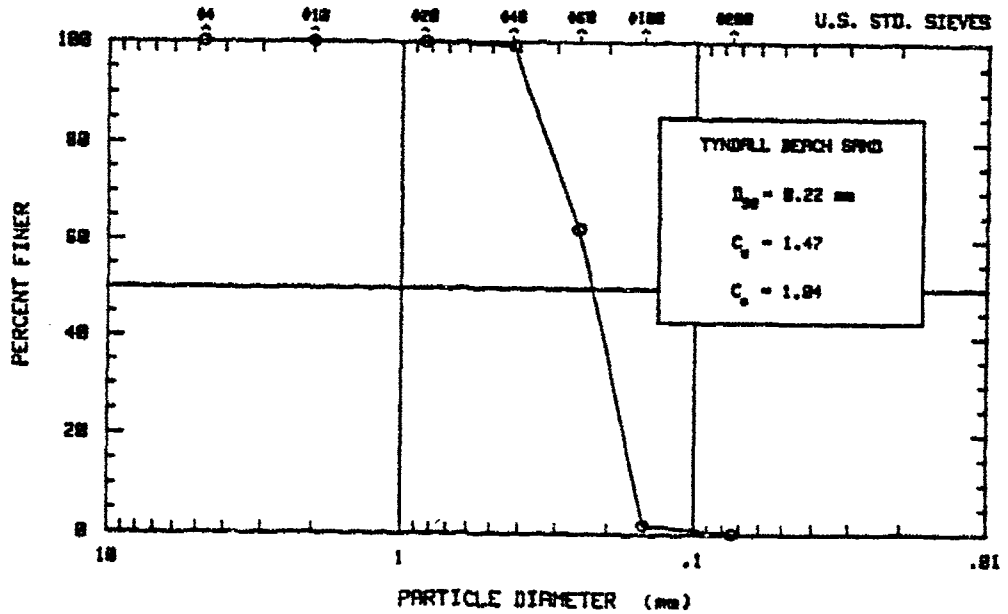

Figure A.9 Grain size distribution of Tyndall Beach sand.

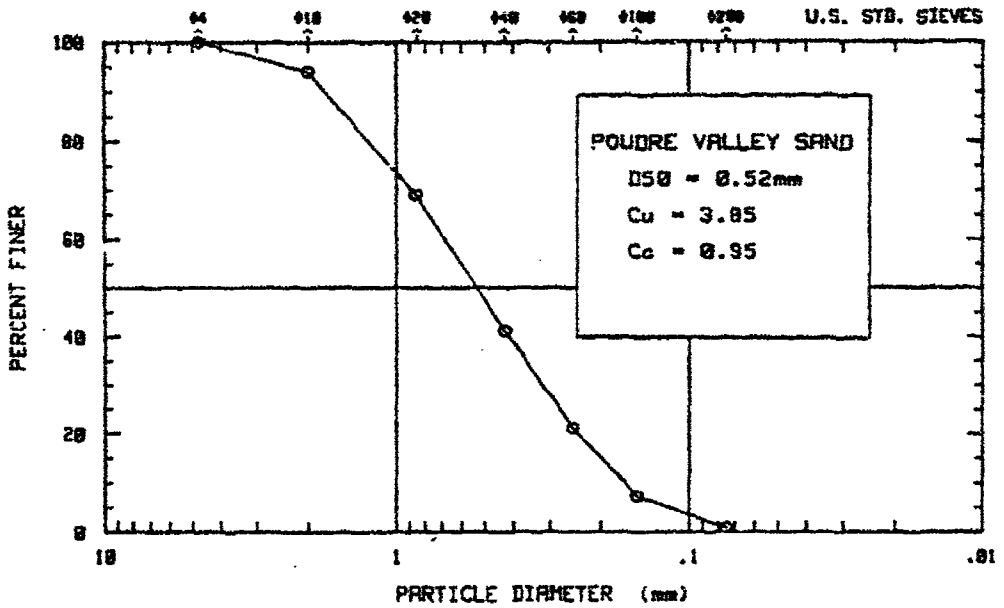

Figure A.10 Grain size distribution of Poudre Valley sand.

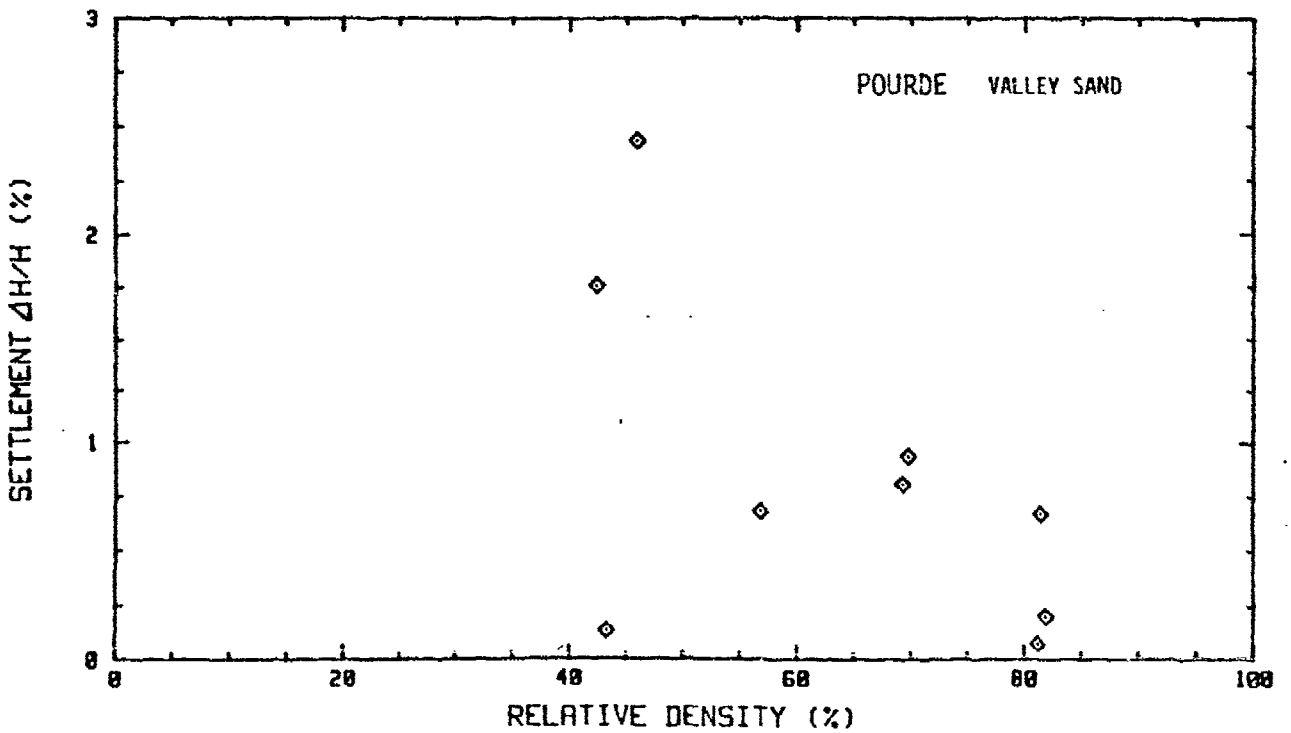

Figure A.11 Settlement ratio for Poudre Valley Sand.

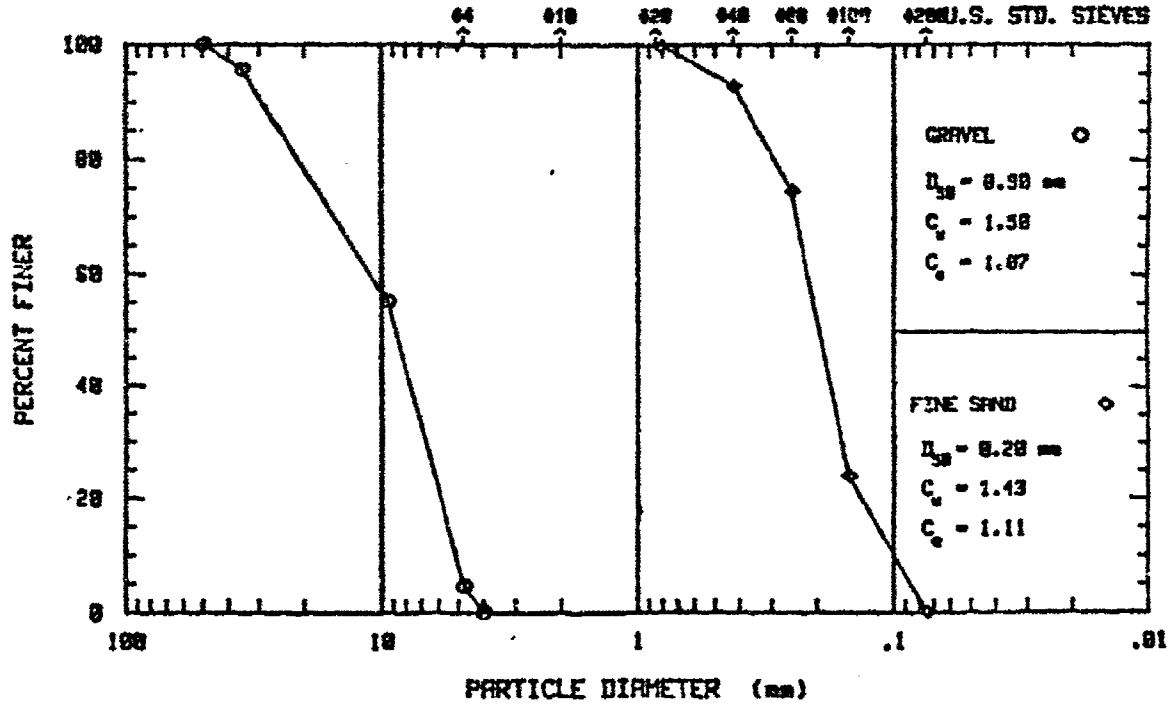

Figure A.12 Grain size distribution for the fine sand and gravel.

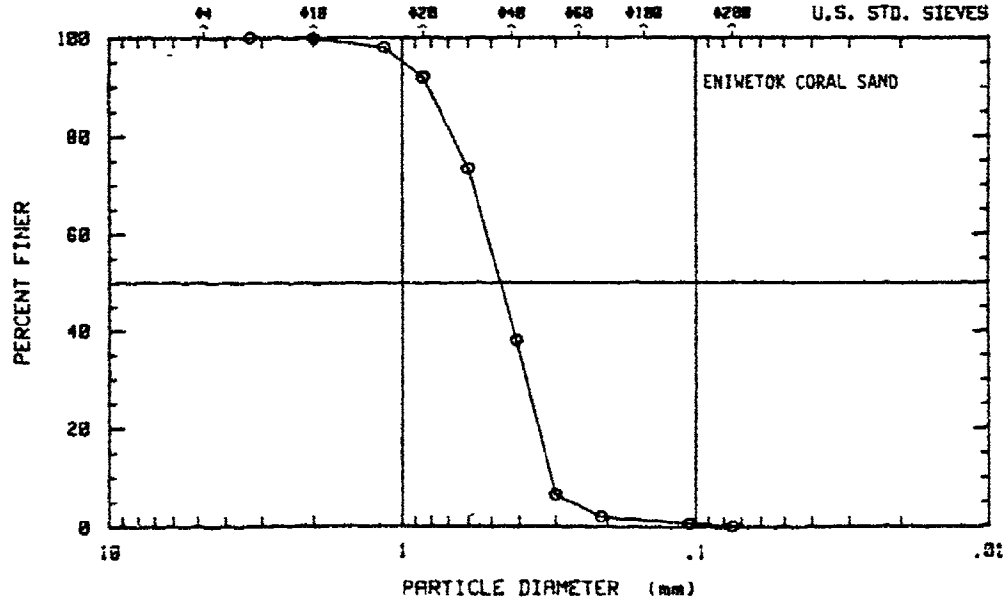

Figure A.13 Grain size distribution for the Eniwetok coral sand.

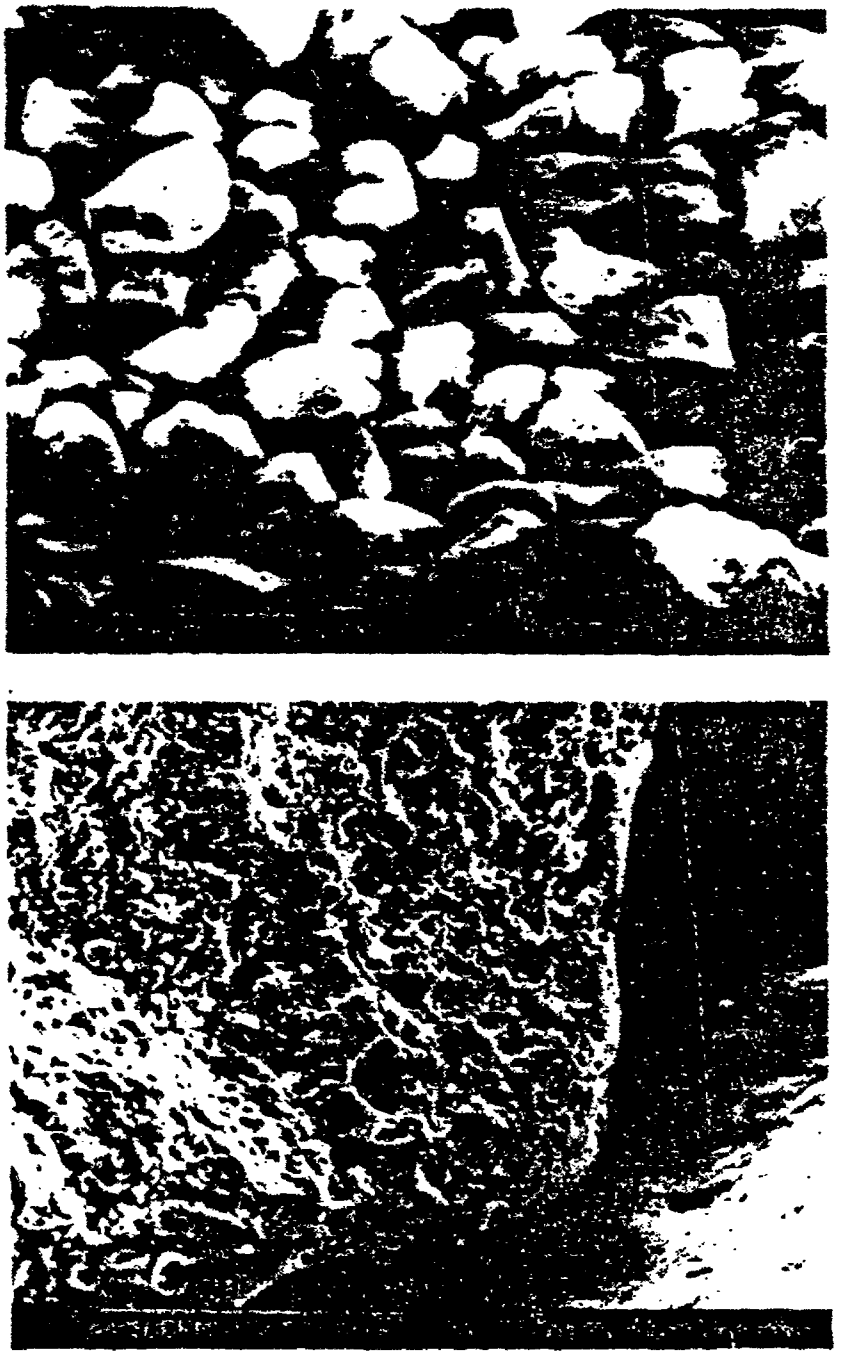

Figure A.14 Photomicrographs of the Eniwetok coral sand grains.

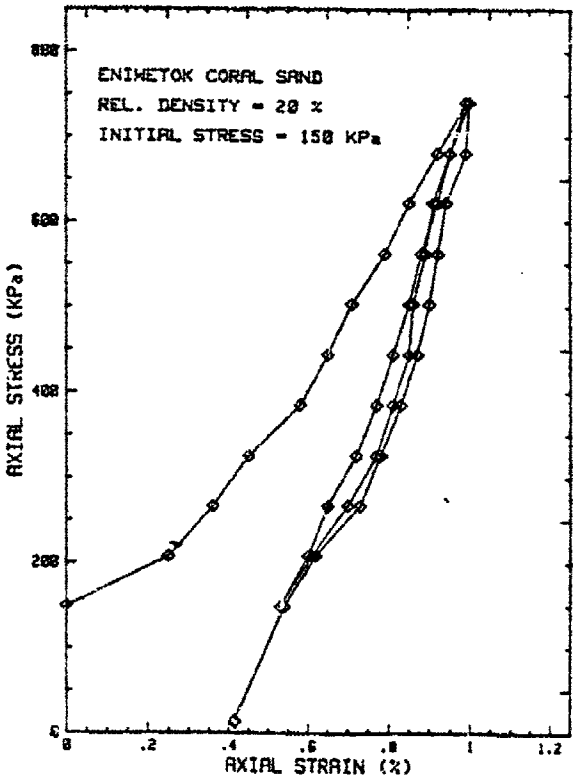

Figure A.15 Skeleton stress-strain curve for Eniwetok coral sand at D_r = 20% and σ'_o = 150 kPa.

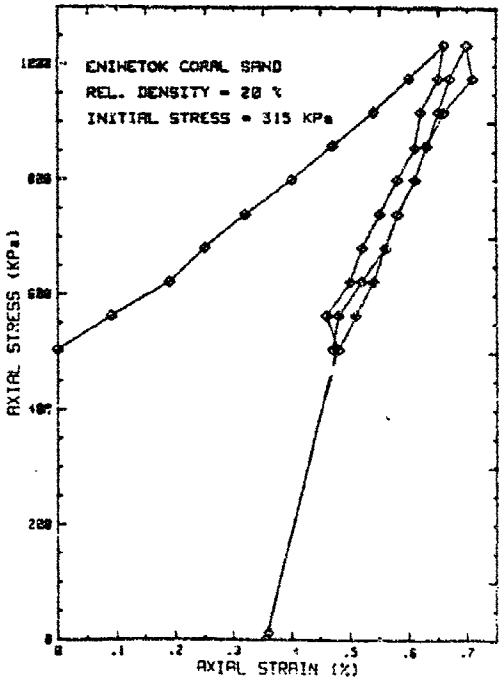

Figure A.16 Skeleton stress-strain curve for Eniwetok coral sand at D_r = 20% and σ'_o = 517 kPa.

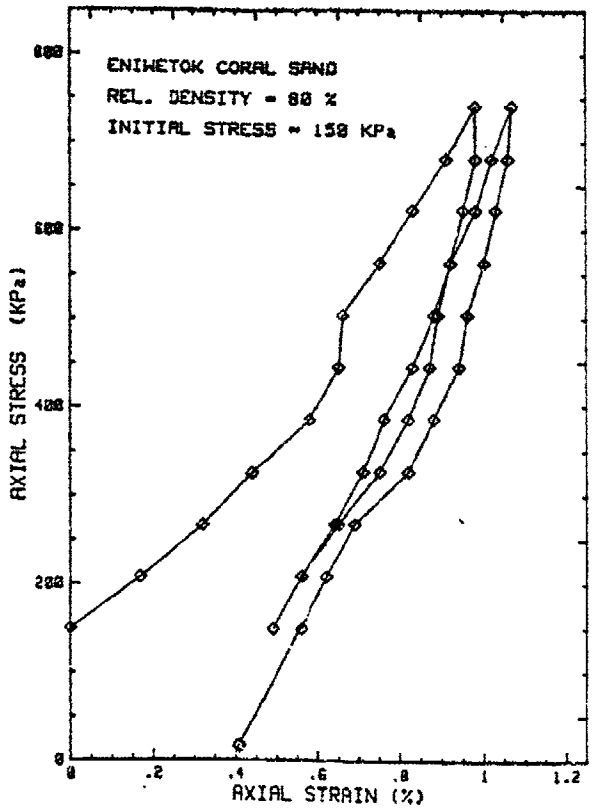

Figure A.17 Skeleton stress-strain curve for Eniwetok coral sand at D_r = 80% and σ'_o = 150 kPa.

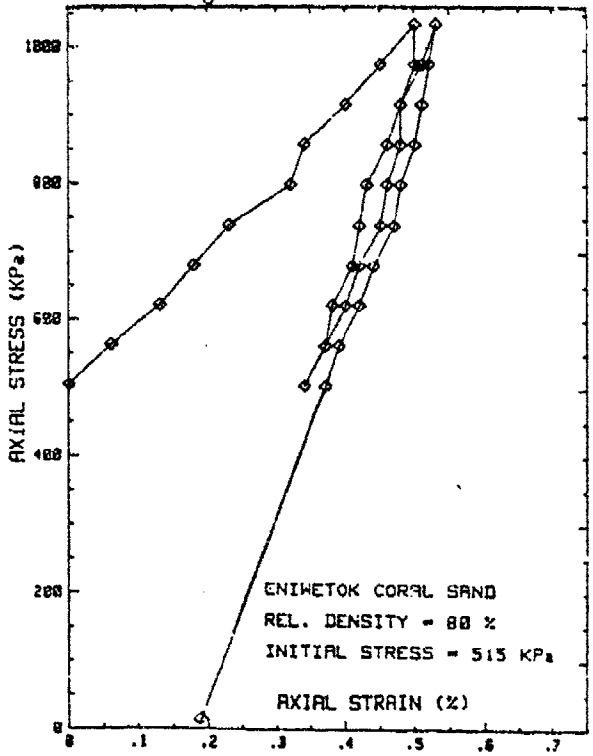

Figure A.18 Skeleton stress-strain curve for Eniwetok coral sand at D_r = 80% and σ'_o = 517 kPa.

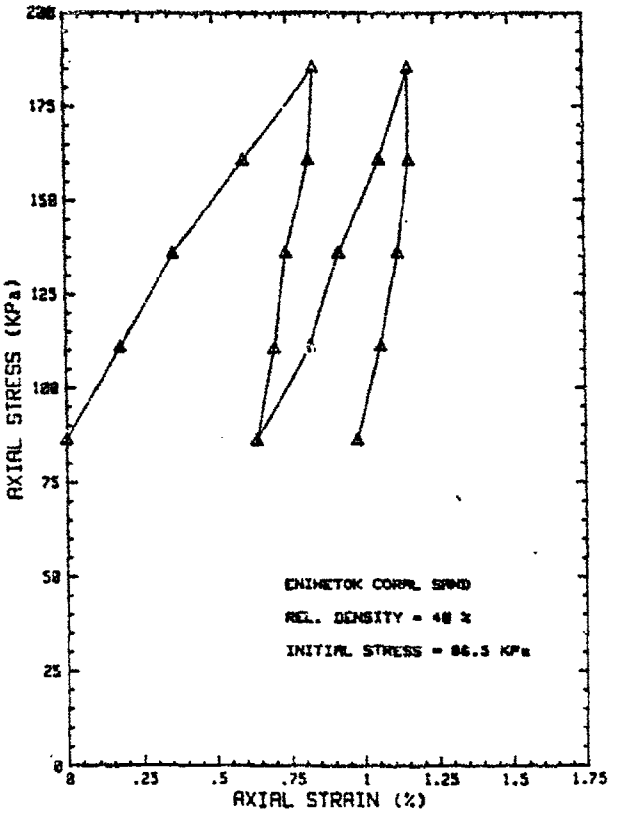

Figure A.19 Skeleton stress-strain curve for Eniwetok coral sand at D_r = 40% and σ_o' = 86.5 kPa.

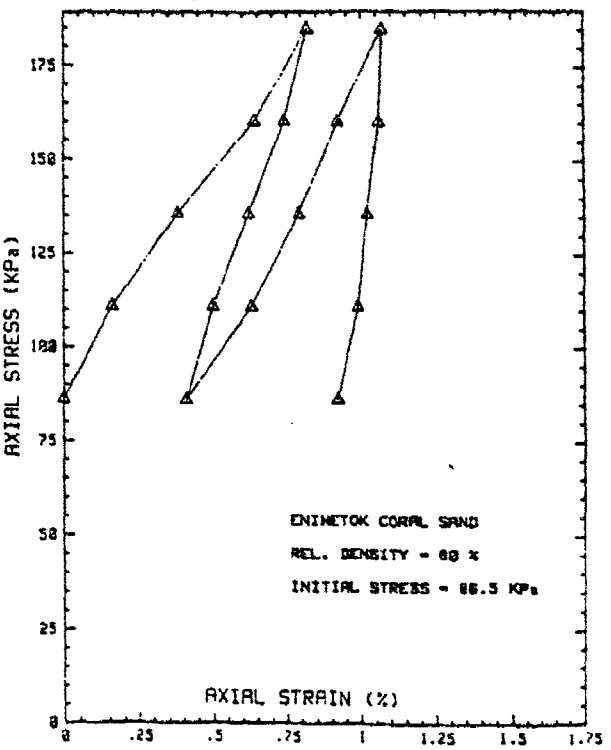

Figure A. 20 Skeleton stress-strain curve for Eniwetok coral sand at D_r = 80% and σ_o' = 86.5 kPa.

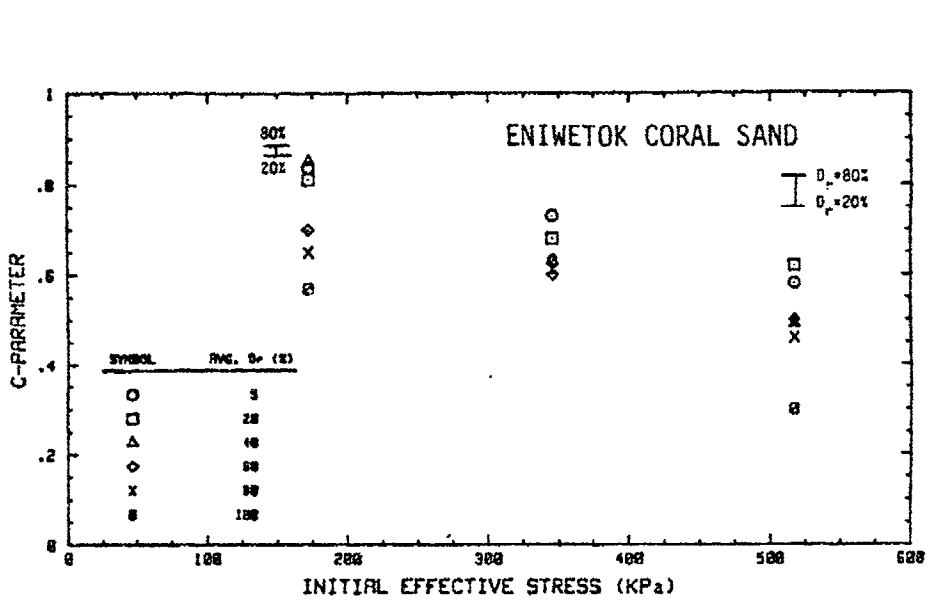

Figure A.21 Static C-Parameter response as a function of the effective stress for Eniwetok coral sand.

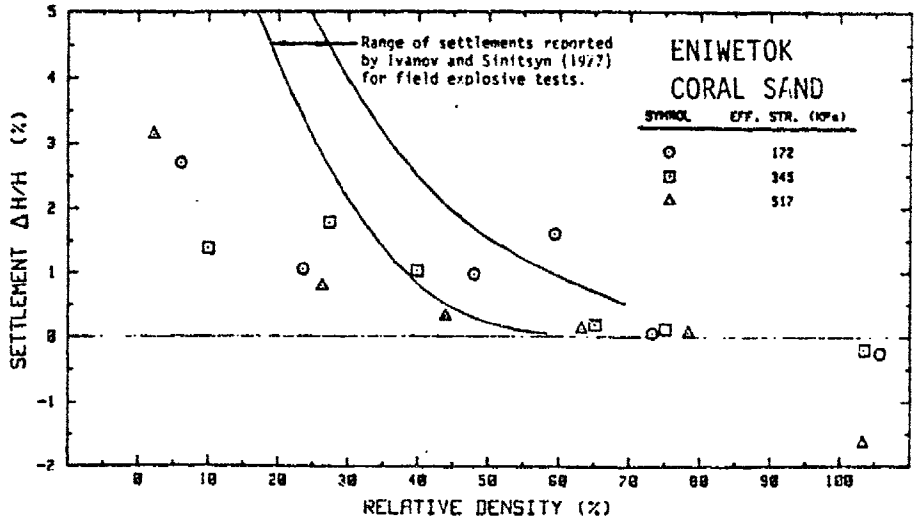

Figure A.22 Settlement ratio for each test versus initial relative density.

Table A.1 Physical Properties of Monterey No. 0/30 Sand
(Muzzy, 1983; Charlie et al., 1984)

USCS Classification	SP
Specific Gravity	2.65
Particle Size Data:	
D_{10}	0.29 mm
D_{30}	0.38 mm
D_{50}	0.45 mm
C_u (1)	1.65
C_c (2)	1.00
% Passing #100 Sieve (3)	0.05 %
Relative Density Test Data:	
Dry Unit Weight:	
Maximum	1700 Kg/M^3
Minimum	1470 Kg/M^3
Void Ratio:	
Maximum	0.803
Minimum	0.563

Note: (1) C_u = coefficient of uniformity

(2) C_c = coefficient of curvature

(3) U.S. Standard Sieve Size

Table A.2 Peak Porewater Pressures and Peak Compressive Strains for Monterey No. 0/30 Sand for Low Impact Stress Loading and D_r = "0%" Series

Test I.D.	σ'_o (KPa)	D_r (%)	Impact	u_{pk} (1) (KPa)	ε_{pk} (2) (%)	PPR (1)
S00I*	86	10.0	1	272	.00606	.329
			2	118	.00263	.457
			3	235	.00524	.743
			4	108	.00241	.735
			5	335	.00747	1.078
			6	145	.00323	1.134
S00I1	172	4.6	1	461	.01030	.774
			2	217	.00485	.902
			3	362	.00808	1.114
			4	443	.00990	1.220
			5	643	.01435	1.215
			6	588	.01314	1.219
S00I2	345	7.5	1	1222	.02734	.557
			2	588	.01316	.614
			3	670	.01498	.740
			4	244	.00546	.742
			5	516	.01154	.848
			6	917	.02052	.956
S00I4	690	7.5	1	81	.00182	.020
			2	543	.01214	.211
			3	208	.00466	.225
			4	670	.01498	.341
			5	561	.01256	.378
			6	2786	.06232	.873

Note: (1) Measured
(2) Calculated

Table A.3 Peak Porewater Pressures and Peak Compressive Strains for Monterey No. 0/30 Sand for Low Impact Stress Loading and D_r = "20%" Series

Test I.D.	σ'_o (kPa)	D_r (%)	Impact	u_{pk} (1) (kPa)	ε_{pk} (2) (%)	PPR (1)
S20X*	86	29.2	1	353	.00764	.116
			2	516	.01116	.467
			3	316	.00685	.565
			4	362	.00783	.635
			5	634	.01371	.576
			6	379	.00821	.634
S20X1	172	27.9	1	524	.01136	.105
			2	416	.00903	.423
			3	452	.00981	.740
			4	469	.01017	.743
			5	226	.00490	.849
			6	452	.00981	.889
S20X2	345	29.6	1	661	.01429	.229
			2	489	.01057	.117
			3	1048	.02267	.132
			4	570	.01233	.213
			5	1276	.02760	.536
			6	914	.01977	.609
S20X4	690	28.8	1	380	.00823	.185
			2	441	.00956	.181
			3	425	.00921	.278
			4	543	.01175	.384
			5	516	.01117	.422
			6	272	.00588	.423

Note: (1) Measured
(2) Calculated

Table A.4 Peak Porewater Pressures and Peak Compressive Strains for Monterey No. 0/30 Sand for Low Impact Stress Loading and D_r = "40%" Series

Test I.D.	σ'_o (KPa)	D_r (%)	Impact	u_{pk} (1) (KPa)	ϵ_{pk} (2) (%)	PPR (1)
S40I*	86	46.7	1	517	.01087	.421
			2	398	.00836	.567
			3	448	.00942	.527
			4	769	.01617	.898
			5	706	.01484	1.064
			6	996	.02093	1.222
S40I1	172	47.1	1	1692	.03554	.606
			2	353	.00742	.656
			3	416	.00875	.695
			4	1140	.02396	.881
			5	407	.00856	.935
			6	443	.00931	.996
S40I2	345	45.9	1	543	.01142	.062
			2	480	.01010	.114
			3	3061	.06444	.531
			4	751	.01581	.562
			5	878	.01848	.572
			6	2006	.04224	.691
S40I4	690	46.7	1	724	.01522	.345
			2	136	.00286	.347
			3	597	.01255	.447
			4	570	.01199	.488
			5	760	.01597	.527
			6	525	.01103	.551

Note: (1) Measured
(2) Calculated

Table A.5 Peak Porewater Pressures and Peak Compressive Strains for Monterey No. 0/30 Sand for Low Impact Stress Loading and D_r = "60%" Series (First Set)

Test I.D.	σ'_o (KPa)	D_r (%)	Impact	u_{pk} (1) (KPa)	ε_{pk} (2) (%)	PPR (1)
S60X*	86		*****	No Data Retrieved		*****
S60X1	172	66.7	1	941	.01908	.164
			2	3592	.07281	.336
			3	796	.01614	.408
			4	796	.01614	.457
			5	896	.01815	.525
			6	480	.00973	.495
S60X2	345	67.5	1	652	.01319	.216
			2	823	.01666	.346
			3	335	.00678	.346
			4	832	.01684	.409
			5	751	.01520	.399
			6	4220	.08540	.560
S60X4	690	65.4	1	543	.01103	.335
			2	965	.01961	.369
			3	534	.01084	.458
			4	263	.00534	.439
			5	697	.01416	.495
			6	1339	.02721	.610

Table A.6 Peak Porewater Pressures and Peak Compressive Strains for Monterey No. 0/30 Sand for Low Impact Stress Loading and D_r = "60%" Series (Second Set)

Test I.D.	σ'_o (KPa)	D_r (%)	Impact	u_{pk} (1) (KPa)	ε_{pk} (2) (%)	PPR (1)
S60X*	86	67.5	1	349	.00767	.464
			2	190	.00385	.606
			3	63	.00128	.562
			4	308	.00622	.747
			5	352	.00712	.741
			6	398	.00805	1.021
S60X1	172	67.1	1	380	.00769	.165
			2	244	.00494	.263
			3	498	.01008	.370
			4	724	.01466	.411
			5	652	.01320	.478
			6	643	.01302	.527
S60X2	345	66.3	1	290	.00587	.117
			2	724	.01469	.298
			3	416	.00845	.357
			4	507	.01028	.345
			5	950	.01927	.397
			6	1077	.02185	.504
S60X4	690	65.8	1	480	.00974	.185
			2	325	.00661	.208
			3	434	.00882	.225
			4	1149	.02333	.354
			5	1031	.02094	.410
			6	No Data Recorded this Impact		

Note: (1) Measured
(2) Calculated

Table A.7 Peak Porewater Pressures and Peak Compressive Strains for Monterey No. 0/30 Sand for Low Impact Stress Loading and D_r = "80%" Series

Test I.D.	σ'_o (KPa)	D_r (%)	Impact	u_{pk} (1) (KPa)	ε_{pk} (2) (%)	PPR (1)
S80I*	86	85.8	1	796	.01554	.636
			2	914	.01784	.890
			3	561	.01095	.932
			4	1240	.02418	.960
			5	1575	.03072	1.060
			6	1057	.02066	1.073
S80I1	172	87.9	1	950	.01845	.532
			2	805	.01564	.619
			3	2151	.04178	.798
			4	579	.01125	.850
			5	878	.01705	.902
			6	878	.01705	.938
S80I2	345	85.4	1	697	.01361	.364
			2	715	.01396	.424
			3	914	.01785	.468
			4	643	.01255	.476
			5	733	.01431	.532
			6	661	.01290	.511
S80I4	690	86.3	1	715	.01394	.331
			2	416	.00812	.358
			3	597	.01164	.399
			4	389	.00758	.408
			5	470	.00917	.435
			6	461	.00899	.411

Table A.8 Peak Porewater Pressures and Peak Compressive Strains for Monterey No. 0/30 Sand for High Impact Stress Loading and D_r = "0%" Series

Test I.D.	σ'_o (KPa)	D_r (%)	Impact	u_{pk} (1) (KPa)	ε_{pk} (2) (%)	PPR (1)
S00I1	172	4.6	1	5711	.12832	.662
			2	6674	.14997	.664
			3	6730	.15121	.664
			4	6219	.13974	.600
S00I2	345	3.8	1	6585	.14813	1.077
			2	6757	.15201	1.593
			3	6985	.15713	1.276
			4	5400	.12148	1.310
S00I4	690	3.8	1	2912	.06532	1.007
			2	2601	.05835	.994
			3	4693	.10527	.994
			4	4807	.10780	1.068

Note: (1) Measured
(2) Calculated

– No loadings were done for σ'_o = 86 KPa

Table A.9 Peak Porewater Pressures and Peak Compressive Strains for Monterey No. 0/30 Sand for High Impact Stress Loading and D_r = "20%" Series

Test I.D.	σ'_o (KPa)	D_r (%)	Impact	u_{pk} (1) (KPa)	ε_{pk} (2) (%)	PPR (1)
S20X1	172	23.8	1	3817	.08332	1.015
			2	4580	.09999	.994
			3	5033	.10986	.994
			4	4750	.10369	.994
S20X2	345	27.5	1	5400	.11719	.994
			2	5655	.12271	.994
			3	5768	.12517	.828
			4	3421	.07425	.837
S20X4	690	22.1	1	5768	.12624	1.035
			2	6274	.13733	1.035
			3	6247	.13673	.994
			4	5089	.11139	.994

Note: (1) Measured
(2) Calculated

- No loadings were done for σ'_o = 86 KPa

Table A.10 Peak Porewater Pressures and Peak Compressive Strains for Monterey No. 0/30 Sand for High Impact Stress Loading and D_r = "40%" Series

Test I.D.	σ'_o (KPa)	D_r (%)	Impact	u_{pk} (1) (KPa)	ε_{pk} (2) (%)	PPR (1)
S40X1	172	44.2	1	4524	.09550	.504
			2	6647	.14032	.829
			3	6902	.14571	.829
			4	6619	.13974	.871
S40X2	345	46.7	1	4693	.09866	.834
			2	3676	.07727	.919
			3	4015	.08440	.929
			4	4269	.08974	.928
S40X4	690	46.7	1	3845	.08083	.787
			2	5570	.11708	.911
			3	4976	.10460	.952
			4	7212	.15160	1.076

Note: (1) Measured
(2) Calculated

- No loadings were done for σ'_o = 86 KPa

Table A.11 Peak Porewater Pressures and Peak Compressive Strains for Monterey No. 0/30 Sand for High Impact Stress Loading and D_r = "60%" Series

Test I.D.	σ'_o (KPa)	D_r (%)	Impact	u_{pk} (1) (KPa)	ϵ_{pk} (2) (%)	PPR (1)
S60X1	172	61.1	1	4156	.08504	.834
			2	5711	.11686	1.166
			3	3421	.07000	1.166
			4	4326	.08851	1.143
S60X2	345	64.2	1	6022	.12265	.662
			2	5117	.10421	.745
			3	5598	.11401	.909
			4	6019	.12259	.994
S60X4	690	62.5	1	5894	.12245	.624
			2	5681	.11607	.704
			3	5771	.11790	.787
			4	5599	.11438	.787

Note: (1) Measured
(2) Calculated

- No loadings were done for σ'_o = 86 KPa

Table A.12 Peak Porewater Pressures and Peak Compressive Strains for Monterey No. 0/30 Sand for High Impact Stress Loading and D_r = "80%" Series

Test I.D.	σ'_o (KPa)	D_r (%)	Impact	u_{pk} (1) (KPa)	ϵ_{pk} (2) (%)	PPR (1)
S60X1	172	81.3	1	6867	.13525	1.154
			2	4185	.08241	1.104
			3	5824	.11470	1.196
			4	6929	.13647	1.230
S60X2	345	83.3	1	8198	.16076	.332
			2	6985	.13697	.497
			3	7040	.13805	.564
			4	8453	.16576	.581
S60X4	690	83.8	1	5966	.11688	.627
			2	5737	.11240	.745
			3	5737	.11240	.794
			4	8371	.16400	.911

Note: (1) Measured
(2) Calculated

- No loadings were done for σ'_o = 86 KPa

Table A.13 Experimental Porewater Pressure Ratio Predictor Models

	Model	R^2 (%)	S
(a)	$PPR = (11.76)\left[\frac{(\Sigma \varepsilon_{pk})(VDP)}{\sigma_o'}\right]^{.278}$	55.0	.206
(b)	$PPR = (16.93)\left[\frac{\Sigma \varepsilon_{pk}}{(\sigma_o')(D_r)}\right]^{.277}$	61.1	.193
(c)	$PPR = (9.41)(\Sigma \varepsilon_{pk})^{.315}(\frac{VDP}{\sigma_o'})^{-.238}$	57.6	.207
(d)	$PPR = (12.71)(\Sigma \varepsilon_{pk})^{.325}(\sigma_o' D_r)^{-.232}$	63.8	.191
(e)	$PPR = (11.39)(\Sigma \varepsilon_{pk})^{.321}(\sigma_o')^{-.305}(VDP)^{.149}$	59.8	.205
(f)	$PPR = (16.30)(\Sigma \varepsilon_{pk})^{.331}(\sigma_o')^{-.308}(D_r)^{-.179}$	65.9	.187

Note:
- ε_{pk} and D_r are in percent
- σ_o' is in kPa
- D_r = relative density
- VDP = Volume Decrease Potential = $e - e_{min}$
- e = void ratio = volume of voids/volume of solids

R^2 = the coefficient of determination
S = the standard error of estimate

Table A.14 Tyndall Florida Beach Sand Characteristics and Tests Performed

Florida Beach Sand Characteristics

G_s = 2.65 (quartz)
B (modulus) = 30680 MPa (quartz)
γ_{min} = 1290 kg/m³
(method by Kolbuszewski, 1948)
γ_{max} = 1724 kg/m³
(method by Kolbuszewski, 1948)

USCS Classification SP Particle Size

D_{10} = 0.17 mm
D_{30} = 0.21 mm
D_{50} = 0.22 mm
D_{60} = 0.31 mm
Cu = 1.47
Cc = 1.04

Shock Test Parameters

C-parameter = .77 to .92
Cannon pressure = 45.5 to 50.0 KPa

Tests Performed

Relative Density = 50%, 60%, 70%
Effective stress = 345 KPa (50 psi)

Table A.15 Results of Tests Performed on Tyndall Beach Sand

Test ID	σ_o' (kPa)	D_r (%)	Impact	u_{pk} (kPa)	ε_{pk} (%)	PPR
50/50	345	54.7	1	995	.0214	.038
			2	973	.0210	.392
			3	3438	.0743	.899
			4	1945	.0420	.965
			5	2375	.0512	.929
			6	4478	.0968	.965
60/50	345	62.6	1	1040	.0232	.526
			2	3822	.0852	.993
			3	135	.0030	.993
			4	4139	.0923	.992
			5	498	.0111	1.022
			6	4207	.0938	1.016
70/50	345	72.8	1	68	.0014	.016
			2	1674	.0349	.203
			3	498	.0103	.251
			4	4455	.0922	.325
			5	588	.0122	.732
			6	1809	.0377	.834

Table A.16 Poudre Valley Sand Characteristics and Tests Performed

Poudre Valley Sand Characteristics

G_s = 2.68
γ_{min} = 1490 kg/m³ (93.0 pcf)
γ_{max} = 1860 kg/m³ (116.3 pcf)

USCS Classification SP Particle Size

D_{10} = 0.18 mm
D_{30} = 0.25 mm
D_{50} = 0.52 mm
D_{80} = 1.2 mm
Cu = 3.85
Cc = 0.95

Shock Test Parameters

C-parameter = .5 to .9
Cannon pressure = 45.5 to 49.6 KPa

Tests Performed (9 tests)

Relative density (D_r) = 20%, 40%, 60%, 80%
Effective stress (σ_o') = 86 KPa and 172 KPa (12.5 and 25 Psi)

One test at 80% D_r and 517 KPa (75Psi) ø
No test was performed for a relative density of 100%

Table A.17 Results of Tests Performed on Saturated Poudre Valley Sands

Test ID	σ_o' (KPa)	D_r (%)	Impact	u_{pk} (KPa)	ϵ_{pk} (%)	PPR
20/12.5	86	26.6	1	1193	.025	.798
			2	1220	.025	1.061
			3	1827	.038	1.060
			4	3523	.075	1.298
20/25	172	27.	1	2599	.055	.670
			2	3523	.075	.673
			3	3730	.079	.691
			4	1537	.070	.931
40/12.5	86	46.8	1	1241	.025	.788
			2	2261	.045	.924
			3	1103	.022	1.002
			4	2868	.058	1.062
40/25	172	42.9	1	136	.002	.108
			2	1103	.022	.801
			3	1220	.025	1.061
			4	1289	.026	1.126

Table A.17 Continued

Test ID	σ_o' (KPa)	D_r (%)	Impact	u_{pk} (KPa)	ϵ_{pk} (%)	PPR
60/12.5	86	66.5	1	179	.003	.080
			2	226	.004	.272
			3	1310	.024	.878
			4	1333	.025	1.042
60/25	172	65.5	1	2640	.050	.331
			2	1310	.024	.353
			3	1379	.026	.380
			4	723	.018	.529
80/12.5	86	81.1	1	2420	.043	.789
			2	2054	.036	.796
			3	1537	.027	.796
			4	1537	.027	.827
80/25	172	81.1	1	2889	.051	.536
			2	2389	.051	.674
			3	68	.001	.680
			4	2641	.047	.801
80/75	517	80.9	1	2620	.046	.663
			2	2551	.045	.766
			3	2710	.048	.855
			4	2620	.046	.915
			5	2303	.041	.958
			6	2847	.050	.955

Table A.18 Physical Properties of the Poudre Valley Fine Sand and Gravel Material

		Fine sand	Gravel
USCS Classification		SP	GP
Specific Gravity		2.68	2.68
Particle Size Data:			
	D_{10}	0.10 mm	5.00 mm
	D_{30}	0.18 mm	6.80 mm
	D_{50}	0.20 mm	8.90 mm
	D_{60}	0.23 mm	12.00 mm
	C_u(1)	1.43	1.50
	C_c(2)	1.11	1.07
Relative Density Test Data			
Dry Unit Weight:			
Maximum		1655 kg/m^3	1676 Kg/m^3
Minimum		1458 kg/m^3	1527 Kg/m^3
Void Ratio:			
Maximum		0.838	0.757
Minimum		0.619	0.599

Table A.19 Peak Porewater Pressures and Peak Compressive Strains for the Poudre Valley Fine Sand, D_r = "30%" Series

Test I.D	σ_o' kPa	Dr %	Impact	u_{pk}(1) kPa	ϵ_{pk}(2) %	ppR(3)
C-parameter = 0.85						
S133	207	37.4	1	68	.00159	.111
			2	203	.00479	.331
			3	792	.01864	.781
			4	588	.01385	.897
			5	57	.00054	.914
			6	1040	.02450	1.105
C-parameter = 0.81						
S135	345	35.8	1	543	.01282	.398
			2	316	.00748	.596
			3	181	.00427	.663
			4	159	.00375	.730
			5	203	.00481	.796
			6	272	.00642	.928

Note: (1) Measured
(2) Calculated
(3) Calculated

Table A.20 Peak Porewater Pressures and Peak Compressive Strains for the Poudre Valley Fine Sand, D_r = "70%" Series

Test I.D	σ_o' (kPa)	D_r (%)	Impact	u_{pk}(1) (kPa)	ϵ_{pk}(2) (%)	PPR(3)
C-parameter = 0.82						
S173	207	77.3	1	452	.00976	.333
			2	475	.01025	.539
			3	475	.01025	.664
			4	203	.00439	.672
			5	1357	.02929	.995
			6	113	.00244	.995
C-parameter = 0.81						
S175	345	77.3	1	701	.01507	.467
			2	543	.01167	.530
			3	1018	.02188	.666
			4	1018	.02188	.795
			5	995	.02139	.860
			6	1176	.02529	.951

Table A.21 Peak Porewater Pressures and Peak Compressive Strains for the Poudre Valley Gravel Material, D_r = "30%" Series

Test I.D	σ_o' (kPa)	D_r (%)	Impact	u_{pk}(1) (kPa)	ϵ_{pk}(2) (%)	PPR(3)
C-parameter = .98						
S233	207	39.7	1	757	.01700	.556
			2	181	.00411	.652
			3	339	.00772	.667
			4	521	.01185	.819
			5	973	.00411	1.043
			6	950	.02215	1.108
C-parameter = .94						
S235	345	38.4	1	1086	.02481	.662
			2	724	.01654	.728
			3	1131	.02583	.861
			4	678	.01550	.927
			5	1154	.02635	.993
			6	701	.01602	.993

Table A.22 Peak Porewater Pressures and Peak Compressive Strains for the Poudre Valley Gravel Material, D_r = "70%" Series

Test I.D	σ_o' (kPa)	D_r (%)	Impact	u_{pk}(1) (kPa)	ϵ_{pk}(2) (%)	PPR(3)
C-parameter = .93						
S273	207	78.6	1	498	.01054	.374
			2	152	.00309	.452
			3	639	.01366	.635
			4	769	.01628	.721
			5	1131	.02394	.992
			6	860	.01820	1.028
C-parameter = .89						
S275	345	78.4	1	1063	.02237	.513
			2	113	.00238	.596
			3	1040	.02189	.729
			4	882	.01855	.788
			5	1131	.02379	.862
			6	1402	.02950	.994

Table A.23 Physical Properties of the Eniwetok Coral Sand

USCS Classification		SP
Specific Gravity		2.80
Particle Size		
D_{10}		.32 mm
D_{30}		.43 mm
D_{50}		.48 mm
D_{60}		.65 mm
Coefficient of Uniformity	C_u	1.66
Coefficient of Curvature	C_c	1.09
Relative Density (dry unit weight)		
Maximum		1705 kg/m³
Minimum		1509 kg/m³
Void Ratio		
Minimum		.609
Maximum		.818
Bulk Modulus of $CaCO_3$ (Calcite) *		67500 MPa
Bulk Modulus of $CaCO_3$ (Aragonite)**		70000 MPa

Note: * from Goodman (1976)
** from Clark (1966)

Table A.24 Peak Porewater Pressure and Peak Compressive Strain for Eniwetok Coral Sand, D_r = "0%" Series

Test #	σ_o' (KPa)	D_r (%)	Impact	u_{pk}[1] (KPa)	ε_{pk}[2] (%)	PPR[3]
S-00/25	172	6.1	1	22.75	.0004	.030
			2	701.22	.0182	1.100
			3	339.23	.0077	1.088
			4	1017.70	.0231	1.070
			5	565.39	.0128	1.063
			6	1583.09	.0358	1.190
S-00/50	345	10.0	1	0.00	.0010	.000
			2	180.65	.0040	.203
			3	113.08	.0025	.260
			4	339.23	.0076	.453
			5	90.32	.0020	.457
			6	791.54	.0179	.676
S-00/75	517	2.2	1	3008.29	.0684	1.015
			2	2284.31	.0519	1.104
			3	3460.60	.0788	1.104
			4	3008.29	.0685	1.104
			5	3777.08	.0860	1.104
			6	2985.53	.0680	1.104

Table A.25 Peak Porewater Pressure and Peak Compressive Strain for Eniwetok Coral Sand, D_r = "20%" Series

Test #	σ_o' (KPa)	D_r (%)	Impact	u_{pk}[1] (KPa)	ε_{pk}[2] (%)	PPR[3]
S-20/25	172	23.5	1	0.50	.0001	.001
			2	1900.26	.0422	.977
			3	1854,75	.0411	.947
			4	1130.78	.0251	.954
			5	1877.51	.0416	.923
			6	950.13	.0211	.929
S-20/50	345	27.2	1	2329.82	.0514	.986
			2	1379.69	.0304	.970
			3	2329.82	.0514	.934
			4	2239.50	.0495	.928
			5	3483.35	.0769	.935
			6	3958.42	.0873	.952
S-20/75	517	26.2	1	2374.64	.0524	.851
			2	1741.68	.0385	1.008
			3	1176.29	.0260	1.101
			4	1442.90	.0539	1.148
			5	1153.53	.0254	1.144
			6	1425.20	.0315	1.136

Table A.26 Peak Porewater Pressure and Peak Compressive Strain for Eniwetok Coral Sand, D_r = "40%" Series

Test #	σ_0' (KPa)	D_r (%)	Impact	u_{pk}[1] (KPa)	ϵ_{pk}[2] (%)	PPR[3]
S-40/25	172	47.8	1	542.64	.0117	.442
			2	1312.12	.0281	.662
			3	610.90	.0132	.794
			4	814.30	.0174	.795
			5	1221.10	.0262	.933
			6	814.30	.0174	1.032
S-40/50	345	39.7	1	1289.36	.0280	.596
			2	2578.73	.0559	.927
			3	3415.09	.0740	1.059
			4	837.05	.0181	1.059
			5	3799.83	.0824	1.062
			6	950.13	.0206	1.059
S-40/75	517	43.8	1	316.48	.0074	.180
			2	2691.80	.0580	.748
			3	1017.70	.0220	.795
			4	2736.62	.0590	.883
			5	3211.69	.0693	.971
			6	2352.57	.0507	.971

Table A.27 Peak Porewater Pressure and Peak Compressive Strain for Eniwetok Coral Sand, D_r = "60%" Series

Test #	σ_0' (KPa)	D_r (%)	Impact	u_{pk}[1] (KPa)	ϵ_{pk}[2] (%)	PPR[3]
S-60/25	172	59.7	1	2261.56	.0476	.929
			2	1741.68	.0367	.929
			3	994.95	.0209	.927
			4	791.55	.0167	.920
			5	2917.96	.0614	.929
			6	2374.64	.0499	.928
S-60/50	345	65.0	1	3528.86	.0738	.201
			2	3302.01	.0690	.411
			3	3935.67	.0823	.464
			4	4184.57	.0875	.502
			5	4048.74	.0846	.465
			6	3234.44	.0676	.464
S-60/75	517	63.1	1	3437.85	.0704	.785
			2	2872.46	.0603	.873
			3	3257.20	.0682	.917
			4	3550.92	.0744	.969
			5	4184.57	.0877	1.002
			6	2601.48	.0545	1.047

Table A.28 Peak Porewater Pressure and Peak Compressive Strain for Eniwetok Coral Sand, D_r = "80%" Series

Test #	σ_o' (KPa)	D_r (%)	Impact	u_{pk}[1] (KPa)	ϵ_{pk}[2] (%)	PPR[3]
S-80/25	172	73.1	1	45.07	.0010	.259
			2	1221.10	.0252	.511
			3	2080.91	.0429	.673
			4	3096.54	.0640	.882
			5	7.96	.0004	.920
			6	2239.50	.0462	.927
S-80/50	345	75.0	1	3279.95	.0675	.463
			2	4546.56	.0935	.582
			3	90.24	.0018	.592
			4	3890.15	.0800	.556
			5	4478.30	.0921	.530
			6	4365.22	.0898	.529
S-80/75	517	78.3	1	3257.20	.0666	.839
			2	1922.33	.0394	.923
			3	3008.29	.0615	.971
			4	3302.01	.0676	.971
			5	2261.56	.0463	1.021
			6	2307.07	.0473	1.044

Table A. 29 Peak Porewater Pressure and Peak Compressive Strain for Eniwetok Coral Sand, D_r = "100%" Series

Test #	σ_o' (KPa)	D_r (%)	Impact	u_{pk}[1] (KPa)	ϵ_{pk}[2] (%)	PPR[3]
S-100/25	172	105.7	1	1990.59	.0389	.706
			2	2261.56	.0442	1.266
			3	2714.56	.0530	1.037
			4	2397.39	.0468	.811
			5	2442.90	.0767	.811
			6	2374.64	.0463	.802
S-100/50	345	103.5	1	67.57	.0013	.067
			2	859.80	.0168	.395
			3	4433.48	.0869	.664
			4	1605.84	.0315	.724
			5	1130.78	.0221	.730
			6	2261.56	.0441	.775
S-100/75	517	103.5	1	1130.78	.0221	.593
			2	1877.51	.0367	.576
			3	2080.91	.0408	.684
			4	1425.20	.0279	.629
			5	1153.53	.0226	.663
			6	3279.95	.0643	.685

Note: [1] Measured
[2] Calculated
[3] Calculated

page left blank

APPENDIX B

OVERVIEW OF RESEARCH GRANT

BLAST INDUCED LIQUEFACTION OF SOILS
LABORATORY AND FIELD TESTS

RESEARCH GRANT AFOSR-85-0172

WAYNE A. CHARLIE, Ph.D., P.E.
PRINCIPAL INVESTIGATOR
COLORADO STATE UNIVERSITY

JULY 25, 1988

B.1 RESEARCH OBJECTIVES

The primary objective of our research was to systematically evaluate the behavior of saturated granular soils subjected to shock and explosive loadings. Secondary objectives included developing experimental, empirical, analytical and theoretical methods to better understand and evaluate blast induced liquefaction.

B.2 SIGNIFICANT ACCOMPLISHMENTS

Our development of laboratory shock and field explosive facilities are major accomplishments. These facilities have the capability of being upgraded for higher stress levels and for conducting different types of transient tests on saturated and unsaturated soils. The current testing of level soil deposits can be expanded to sloping ground, soil-structure interaction, and pile foundation response. The experimental testing has allowed us to develop empirical models and to start to develop and evaluate theoretical and analytical models. Our research demonstrates that the destruction potential of an explosion may be greatly magnified if detonated in water saturated granular soils. While blast-induced liquefaction may not necessarily damage a facility structurally, it may render it unusable. Blast-induced liquefaction can cause late time decreases in the soil's shear strength that produces damage disproportionate to the amount of explosive used and ground motions inconsistent with previous experience.

The results of our study indicate the following.

1. Liquefaction can be induced by single and multiple explosive induced compressive wave loadings.

2. Liquefaction can be induced at distances from explosions much greater than those associated with structural damage.
3. Fairly long term increases in residual porewater pressures can be induced by compressive shock wave loadings when the peak particle velocity exceeds 0.075 m/s or the peak strain exceeds 0.005 percent.
4. Liquefaction can be induced in loose saturated sands by a single compressive shock wave when the peak particle velocity exceeds 0.75 m/s or the peak strain exceeds 0.05 percent.
5. Soils at higher initial effective stress and higher initial relative density require more energy to produce liquefaction.
6. Liquefaction occurs as a result of compressive strain induced by the compression stress wave, but liquefaction occurs during unloading and after the stress wave passes.
7. Liquefaction occurs because loading-unloading of the porewater is elastic and reversible, but loading-unloading of the soil skeleton is not an elastic-reversible process.

B.3 WRITTEN PUBLICATIONS

1. REFEREED JOURNALS AND BOOKS

Charlie, W.A., Mansouri, T.A., and Ries, E.R., "Predicting Liquefaction Induced by Buried Charges", Int. Society for Soil Mech. and Fdn. Engineering, Vol. 2, No. 10, June 1981.

Charlie, W.A., Muzzy, M.W., Tiedemann, D.A., and Doehring, D.O., "Cyclic Triaxial Behavior of Monterey Number 0 and Number 0/30 Sands", Geotechnical Testing Journal, ASTM, Vol. 7, No. 4, Dec. 1984.

Charlie, W.A. and Veyera, G.E., "Explosive Induced Porewater Pressure Increases," Int. Society for Soil Mech. and Fdn. Engineering, Vol. 1, No. 11, Aug. 1985.

Charlie, W.A., Veyera, G.E., and Abt, S.R., "Predicting Blast Induced Porewater Pressure Increases in Soils: A Review", Int. Journal for Civil Engineering for Practicing and Design Engineers, Pergamon Press, Vol. 4, No. 4, April 1985.

Charlie, W.A., Veyera, G.E., Bretz, T.E. and Allard, D.J., "Shock Induced Porewater Pressure Increases in Water Saturated Soils", Shock and Vibration Bulletin, Vol. 1, No. 57, Oct., 1986.

Charlie, W.A., Hassen, H., Doehring, D.O. and Hubert, M.E., "Microcomputers in Shock Testing of Water Saturated Sands", Shock and Vibration Bulletin, Vol. 1, No. 57, Oct., 1986.

Charlie, W.A., Doehring, D.O. and Veyera, G.E., "An APL Function for Modeling P-Wave Induced Porewater Pressure," Computer Oriented Geological Society, Journal of Computer Contributions, Vol. 3, Nos. 34, December, 1987.

Charlie, W.A., and Ross, C.A., "Compression Wave Propagation in Unsaturated Soils," Geotechnical Testing Journal, ASTM, (in review).

Charlie, W.A., Doehring, D.O., and Veyera, G.E., "Development of an Apparatus to Evaluate Shock-Induced Liquefaction," Geotechnical Testing Journal, ASTM (in review).

Ross, C.A., Thompson, P.Y., Charlie, W.A. and Doehring, D.O., "Transmission of Pressure Waves in Partially Saturated Soils," Society for Experimental Mechanics, Journal of Experimental Mechanics, (accepted - in press).

Veyera, G.E. and Charlie, W.A. "Liquefaction of Shock Loaded Saturated Sand," Soil Dynamics and Liquefaction, Ed. by A.S. Cakmak, Developments in Geotechnical Engineering, No. 42, Elsevier, 1987.

2. REFEREED PROCEEDINGS

Charlie, W.A., Shinn, J., and Melzer, S., "Blast Induced Soil Liquefaction", U.S. National Conference on Earthquake Engineering, Stanford University, Stanford, California, August 1979.

Charlie, W.A., Shinn, J., Melzer, S., and Martin, J., "Blast Induced Soil Liquefaction - Phenomena and Evaluation", Int. Sym. on Soils Under Cyclic and Transient Loads, Univ. College of Swansea, Swansea, United Kingdom, January 1980.

Charlie, W.A., Veyera, G.E., and Muzzy, M.W., "Shock Induced Soil Liquefaction: Test Facility Development", Aerospace Industries Division and Test Measurements Division, Instrument Society of America, 28th Inter. Inst. Symposium, Las Vegas, Nevada, May 1982.

Charlie, W.A., Abt, S.R. and Veyera, G.E., "Dynamic Pore Pressure Response of Saturated Soil Under Shock Loading", Proc. of the Second Symposium on the Interaction of Non-Nuclear Munitions with Structures, Panama City Beach, Florida, April 1985.

Charlie, W.A., Doehring, D.O., Durnford, D.S. and Hubert, M., "Compressional Wave-Induced Liquefaction of Carbonate Sand", (Abs.), The Geological Society of America, Section Meeting, Hilo, Hawaii, May 1987.

Charlie, W.A., Doehring, D.O. and Lewis, W., "Explosive Induced Damage Potential to Earthfill Dams and Embankments", Proc. of the 13th Annual Conf. on Explosives and Blasting Techniques, Society of Explosive Engineers, Miami, Florida, February 1987.

Charlie, W.A., Doehring, D.O, and Veyera, G.E., "An APL Function for Modeling P-Wave Induced Liquefaction," Conf. on Computer-Aided Methods and Modeling in Geology and Engineering, Denver GeoTech 87, October 1987.

Charlie, W.A., Doehring, D.O. and Veyera, G.E., "Investigation of Compressional Wave-Induced Liquefaction", (Abs.), The Geological Society of America, Annual Meeting, Orlando, Florida, October 1985.

Charlie, W.A., Doehring, D.O. and Veyera, G.E., "Liquefaction of Water Saturated Granular Materials," (Abs.), Focussed Session on Granular Materials, American Physical Society, New Orleans, LA, March 1988.

Charlie, W.A., Veyera, G.E., Abt, S.R. and Patrone, H.D., "Blast Induced Soil Liquefaction: State-of-the-Art", The First Symposium on the Interaction of Non-Nuclear Munitions with Structures", U. S. Air Force Academy, Colorado Springs, Colorado, May 1983.

Charlie, W.A., Veyera, G.E., and Muzzy, M.W., "Explosive Compaction of Soil: Test Facility Development", Underground Technology Research Council, Ground Strengthening Committee's Research Workshop on Deep Compaction, ASCE Fall Convention, New Orleans, LA, Oct. 1982.

Ross, C.A., Thompson, P.Y., Charlie, W.A. and Doehring, D.O., "Transmission of Pressure Waves in Partially Saturated Soils," Proc. of the 1987 Fall Conf. on Dynamic Failure, Society of Experimental Mechanics, Oct. 1987.

Veyera, G.E., and Charlie, W.A., "Shock Induced Porewater Pressure Increases in Soils", Int. Symposium on Dynamic Soil Structure Interaction, Univ. of Minnesota, Minneapolis, Minnesota, Sept. 1984.

Veyera, G.E. and Charlie, W.A., "Liquefaction of Shock Loaded Saturated Sand", Proc. of the 3rd Inter. Conf. on Soil Dynamics and Earthquake Engineering, Princeton, N.J., June 1987.

B.4 PRESENTATIONS ON AFOSR RESEARCH

1. "Earthquake Engineering and Soil Dynamics", ASCE Geotechnical Division Specialty Conference, Pasadena, California, June 1978.

2. "International Workshop as a Means for Selecting an Approach to Blast Induced Liquefaction", U.S. Air Force and Dames and Moore, Maidenhead, United Kingdom, September 1978.

3. "Second U.S. National Conference on Earthquake Engineering", Stanford University, Stanford, California, August 1979.

4. "ASTM Symposium on Laboratory Shear Strength of Soil and Rock", ASTM D-18, Chicago, Illinois, June 1980.

5. "International Conference on Recent Advances in Geotechnical Earthquake Engineering and Soil Dynamics", University of Missouri, St. Louis, Missouri, April 1981.

6. "Instrument Society of America's 28th International Instrument Symposium", ISA, Las Vegas, Nevada, May 1982.

7. "AFOSR Workshop on Shock Induced Liquefaction", U.S. Air Force Office of Scientific Research, Washington, D.C., Sept. 1982.

8. "ASCE 1982 Fall National Convention", ASCE, New Orleans, LA, Oct. 1982.

9. "The First Symposium on the Interaction of Non-Nuclear Munitions with Structures", U.S. Air Force Office of Scientific Research, Colorado Springs, Colorado, May 1983.

10. "X International Conference on Soil Mechanics and Foundation Engineering", Stockholm, Sweden, June 1981.

11. "XI International Conference on Soil Mechanics and Foundation Engineering", San Francisco, California, 1985.

12. "2nd Symposium on the Interaction of Non-Nuclear Munitions with Structures", Panama City Beach, Florida, April 1985.

13. "International Symposium on Dynamic Soil-Structure Interaction", Minneapolis, Minnesota, September 1984.

14. "Geological Society of America's Annual Meeting", Orlando, Florida, October 1985.

15. "Geological Society of America's Annual Meeting", San Antonio, Texas, November 1986.

16. "57th Shock and Vibration Symposium", New Orleans, October 1986.

17. "Geologic Society of America's Western Regional Conference," Hilo, Hawaii, May 1987.

18. "NSF Workshop on Geotechnical Engineering Research at U.S. Universities," Houston, Texas, March 1987.

19. "AFOSR Research Meeting," Boston, Massachusetts, 1987.

20. "Society of Explosives Engineers, Colorado Chapter," Denver, Colorado, April, 1988.

B.5 PROFESSIONAL PERSONNEL (ASSOCIATED WITH THIS RESEARCH)

1. Principal Investigator

Wayne A. Charlie, Ph.D., P.E.
Associate Professor of Civil Engineering
Geotechnical Engineering Program Leader
Colorado State University

2. Research Associates and Research Advisors

D.O. Doehring, Ph.D.
Professor of Earth Resources
Colorado State University

G.E. Veyera, Ph.D., P.E.
Assistant Professor of Civil Enginering
Drexel University
(formerly CRT, Inc., New Mexico)

D.S. Durnford, Ph.D., P.E.
Assistant Professor of Civil, Agricultural and Chemical Engineering
Colorado State University
(formerly Cornell University)

E. Rinehart, Ph.D.
DNA Washington, D.C.
(formerly CRT, Inc. and AFWL)

S.E. Blouin, Ph.D.
Applied Research Assoc., Inc., Vermont

B.6 GRADUATE STUDENTS (ASSOCIATED WITH THIS RESEARCH)

Ph.D. Degrees

G.E. Veyera, Ph.D. received 1985 (laboratory shock)
T. Bretz, Ph.D. expected 1988 (field explosive)
H. Hassen, Ph.D. expected 1988 (field explosive)
A. Awad, Ph.D. expected 1988 (theoretical)

M.S. Degrees

M.A. Hubert, M.S. received 1986 (laboratory shock)*
M.W. Muzzy, M.S. received 1983 (laboratory cyclic)*
M.E. Al-Gassimi, M.S. received 1986 (in-situ testing)
Y.P. Chen, M.S. received 1985 (laboratory cyclic)
M.S. Khattak, M.S. received 1986 (coral sand review)
C. Amine, M.S. received 1987 (laboratory shock)
J. Bolton, M.S. received 1988 (laboratory-silt)*
B. Butler, M.S. expected 1988 (in-situ testing)*
P. Jacobs, M.S. received 1988 (field explosive)*
A. Jewell, M.S. expected 1989 (theoretical)
C. Johnson, M.S. expected 1989 (laboratory shock)
W. Lewis, M.S. expected 1988 (field explosive)*
S. Pierce, M.S. expected 1989 (laboratory shock)
L. Schure, M.S. expected 1988 (field explosive)*
C. Scott, M.S. expected 1989 (in-situ testing)
D. Allard, M.S. expected 1988 (field explosive)

*received AFOSR funding

B.7 CONSULTATIONS TO GOVERNMENT AGENCIES

DNA (blast-induced liquefaction)
AFWL (blast-induced liquefaction)
AFESC (blast-induced liquefaction)
ONR (blast-induced liquefaction)
WES (blasting near dams)
Bureau of Reclamation (blasting near dams)
Bureau of Mines (blasting near dams)

8.8 NEW DISCOVERIES AND INVENTIONS

We have observed and recorded blast-induced liquefaction in laboratory shock tests and field explosive tests. Empirical, analytical and theoretical methods to predict and better understand shock induced porewater pressure have been developed and evaluated. We have discovered that peak strain controls development of residual porewater pressure and that liquefaction occurs upon unloading. Loading rate is not important in generation of residual porewater pressure in sands but is important for silty soils.

We have applied for a patent for a piezovane developed to evaluate the potential for blast-induced liquefaction leading to large soil strains (RTC Disclosure No. 044-D144-88).